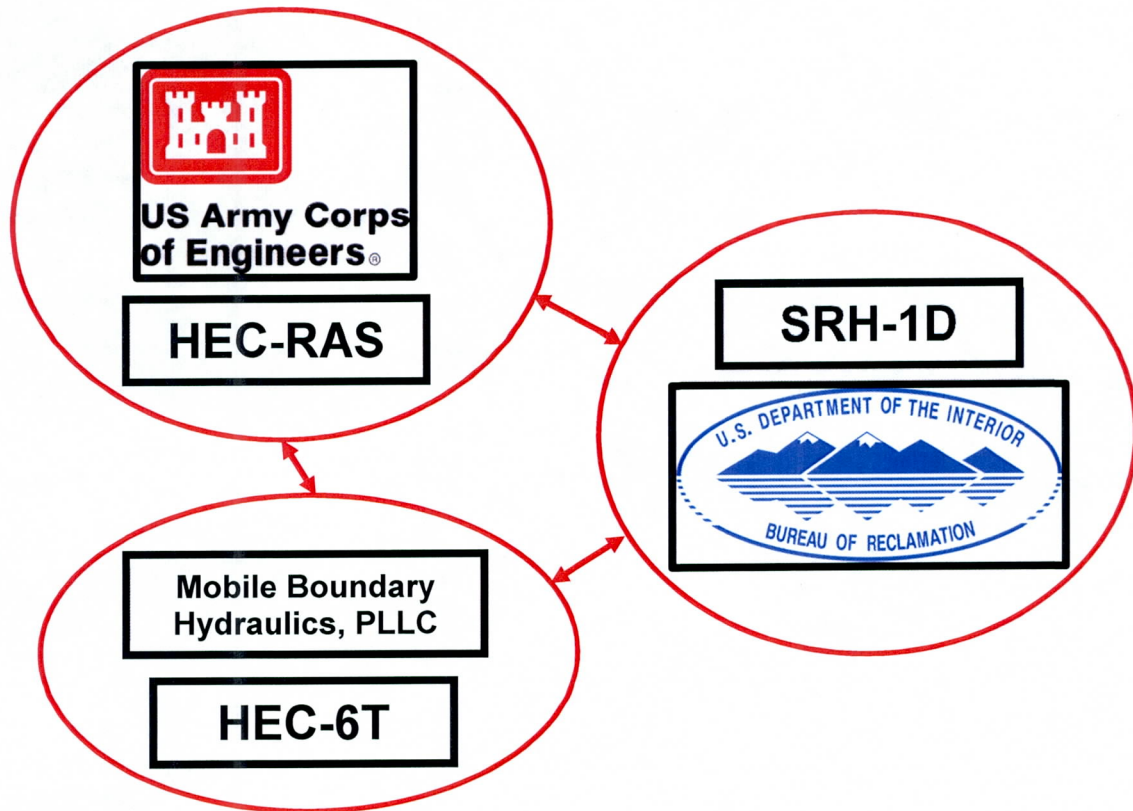


Sediment Transport Tool

Sediment Transport Model Comparison

Contract Number: FCD 2010C027 Assignment #4



Prepared for:
Flood Control District of Maricopa County
2801 West Durango Street
Phoenix, AZ 85009

Prepared by:
WEST Consultants, Inc.
8950 S 52nd Street
Suite 210
Tempe, AZ 85284

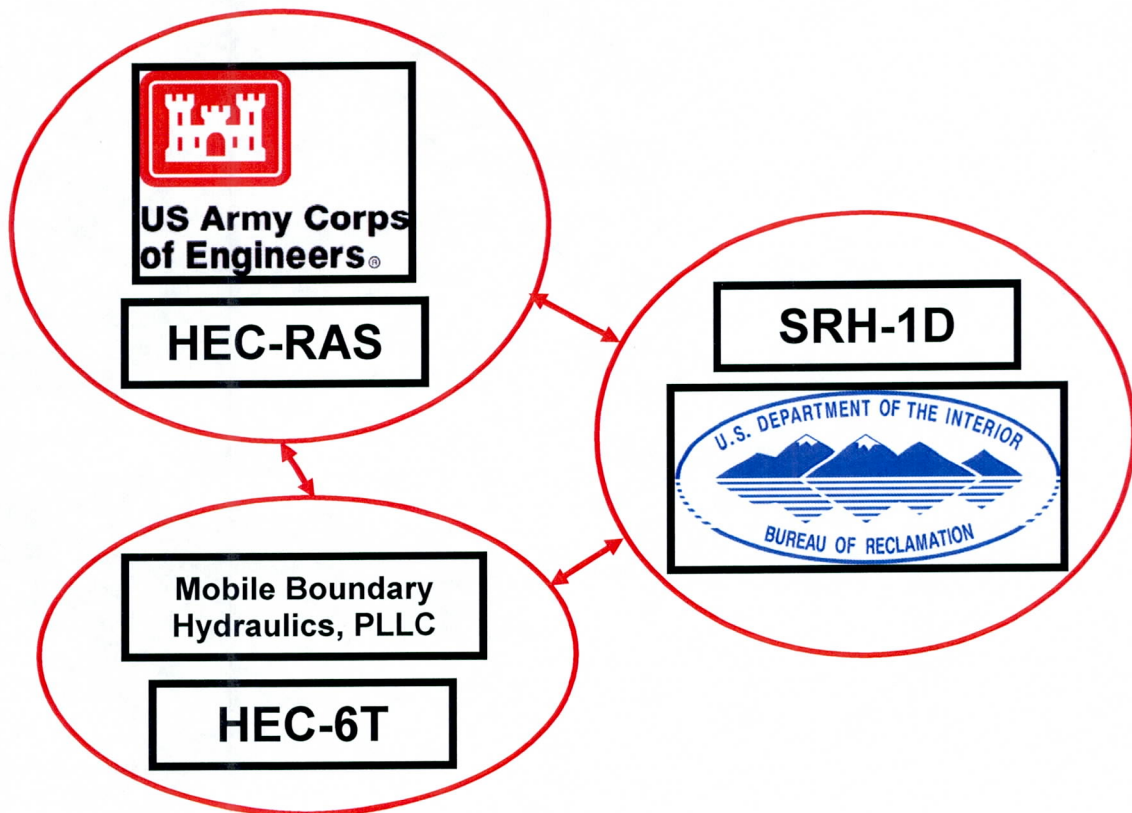
August 2011



Sediment Transport Tool

Sediment Transport Model Comparison

Contract Number: FCD 2010C027 Assignment #4



Prepared for:
Flood Control District of Maricopa County
2801 West Durango Street
Phoenix, AZ 85009

Prepared by:
WEST Consultants, Inc.
8950 S 52nd Street
Suite 210
Tempe, AZ 85284

August 2011



Expires 3/31/2014

Table of Contents



1	Introduction.....	1-1
1.1	Purpose.....	1-1
1.2	Previous Reports.....	1-2
1.3	Datum.....	1-3
1.4	Sediment Transport Models.....	1-3
1.4.1	HEC-RAS.....	1-3
1.4.2	HEC-6T.....	1-4
1.4.3	SRH-1D.....	1-4
2	Sediment Transport Modeling Comparison in the Field: The Salt-Gila River System	2-1
2.1	Introduction.....	2-1
2.2	Hydraulics.....	2-2
2.2.1	Model Geometry.....	2-2
2.2.2	Bridge Geometry for the Base Models.....	2-3
2.2.3	Sand and Gravel Mining Pit Geometry for the Ultimate Pit Models.....	2-3
2.3	Hydrology.....	2-7
2.4	Sediment Data.....	2-8
2.4.1	Bed Material.....	2-8
2.4.2	Inflowing Sediment Load.....	2-9
2.5	Sediment Transport Modeling Considerations.....	2-11
2.5.1	Moveable Bed Limits.....	2-11
2.5.2	Sediment Transport Functions.....	2-11
2.6	Results.....	2-12
2.6.1	Results of the Model Comparison Runs using HEC-RAS, HEC-6T, and SRH-1D..	2-13
2.6.2	Results of the Base Condition Models using HEC-RAS and HEC-6T.....	2-18
2.6.3	Results of the Ultimate Pit Models using HEC-RAS and HEC-6T.....	2-20
3	Sediment Transport Modeling for the Test Cases.....	3-1
3.1	Introduction.....	3-1
3.2	Independent Variables.....	3-1
3.2.1	Cross-Section Geometry.....	3-1
3.2.2	Sediment Transport Functions.....	3-1
3.2.3	Flow Rates.....	3-2
3.2.4	Downstream Boundary Conditions.....	3-2
3.2.5	Bed Gradations.....	3-3
3.2.6	Sediment Inflow.....	3-4
3.3	Final Design.....	3-4
3.4	Results.....	3-6
3.4.1	Data Transformation.....	3-7
3.4.2	Descriptive Statistics.....	3-7
3.4.3	MANOVA Analysis Results.....	3-8

3.5	Scour Effects.....	3-11
3.5.1	Overall.....	3-11
3.5.2	Main Effects.....	3-11
3.5.3	Interaction Effects.....	3-12
3.6	Deposition Effects.....	3-13
3.6.1	Overall.....	3-13
3.6.2	Main Effects.....	3-14
3.6.3	Interaction Effects.....	3-14
3.7	Comparison of Test Case Modeling Output to Brownlie’s Dataset	3-15
4	Conclusions and Recommendations	4-1
4.1	Conclusions.....	4-1
4.2	Recommendations on the Application of the Study Results.....	4-2
4.3	Recommendations for Future Research Based on the Study	4-5
5	References.....	5-1
	Appendix A: Final Bed Sediment Samples from GSRP utilized in the Sediment Transport Modeling, and the WEST Technical Memorandum to the District Summarizing Data Collection	A-1
	Appendix B: Sediment transport functions available in common 1-dimensional sediment transport models.....	B-1
	Appendix C: Profile Output for the Model Comparison Runs in HEC-RAS, HEC-6T, and SRH-1D.....	C-1
	Appendix D: Profile Output for the Base Condition Model Runs in HEC-RAS and HEC-6T ..	D-1
	Appendix E: Profile Output for the Ultimate Pit Model Runs in HEC-RAS and HEC-6T	E-1
	Appendix F: Case Study Data.....	F-1
	Appendix G: FCDMC Final Review Comment Technical Memorandum	G-1

List of Tables

Table 2-1. Bridges added to the two base condition sediment transport models.....	2-3
Table 2-2. 100-year hydrographs (cfs).....	2-7
Table 2-3. Inflowing sediment load rating curve and gradations for the Salt River.....	2-9
Table 2-4. Inflowing sediment load rating curve and gradations for the Upper Gila River.....	2-10
Table 2-5. Inflowing sediment load rating curve and gradations for the Agua Fria River.....	2-10
Table 2-6. Sediment transport functions common to the 1-dimensional sediment transport models.....	2-12
Table 2-7. RMSE values (feet) for various sediment transport functions within an individual model.....	2-13
Table 2-8. RMSE values (feet) for various sediment transport models for a given sediment transport function.....	2-14
Table 2-9. Average differences between the maximum scour values for each sediment transport function.....	2-14
Table 2-10. RMSE values (feet) for the two base condition sediment transport models versus one another and the “without bridges” condition.....	2-18
Table 2-11. Average differences between maximum scour for the base condition models.....	2-18
Table 2-12. RMSE values (feet) for the ultimate pit models.....	2-20
Table 2-13. Average differences between maximum scour for the ultimate pit models.....	2-20
Table 3-1. Hydraulic parameters from the datasets by which the transport functions were developed.....	3-2
Table 3-2. Bed sediment gradations based on the artificially sorted sand gradation from Vanoni (1975).....	3-4
Table 3-3. Inflowing sediment load rating curve and gradations for the test cases*.....	3-5
Table 3-4. Final comparison study design.....	3-5
Table 3-5. Test case descriptive statistics.....	3-8
Table 3-6. MANOVA testing results for the full test case database.....	3-9
Table 3-7. Scour ANOVA testing.....	3-11
Table 3-8. Deposition ANOVA testing.....	3-13
Table A-1 Summary of sediment samples in the Salt-Gila River System used for numerical sediment transport model development.....	A-1
Table B-1 Sediment transport functions available in common 1-dimensional sediment transport models.....	B-1
Table F-1 RMSE values for all of the case study runs transport models.....	F-1
Table F-2 Zero scour test case runs removed from the analysis.....	F-12
Table F-3 Zero deposition test case runs removed from the analysis.....	F-15

List of Figures

Figure 2-1. Study reach location figure for the sediment transport model comparison of the Salt-Lower Gila River System.....	2-5
Figure 2-2. Sand and gravel pit location figure for the ultimate pit sediment transport models of the Salt-Lower Gila River System	2-6
Figure 2-3. Maximum scour comparison for the Engelund-Hansen function	2-15
Figure 2-4. Maximum scour comparison for the Yang function	2-15
Figure 2-5. Maximum scour comparison for the Toffaleti function.....	2-16
Figure 2-6. Maximum aggradation comparison for the Engelund Hansen function	2-16
Figure 2-7. Maximum aggradation comparison for the Yang function	2-17
Figure 2-8. Maximum aggradation comparison for the Toffaleti function.....	2-17
Figure 2-9. Maximum scour comparison for the base condition models with bridges.....	2-19
Figure 2-10. Maximum aggradation comparison for the base condition models with bridges	2-19
Figure 2-11. Maximum scour comparison for the ultimate pit models	2-21
Figure 2-12. Maximum aggradation comparison for the ultimate pit models	2-21
Figure 3-1. Generalized gradations for artificially sorted sand and river sand (Vanoni, 1975)	3-3
Figure 3-2. Log ₁₀ transformed deposition normal fit.....	3-10
Figure 3-3. Log ₁₀ transformed scour normal fit.....	3-10
Figure 3-4. Scour main effects.....	3-11
Figure 3-5. Scour interaction effects.....	3-12
Figure 3-6. Deposition main effects.....	3-13
Figure 3-7. Deposition interaction effects	3-14
Figure 3-8. Minimum and maximum D ₅₀ values plotted against minimum and maximum sediment loadings from a subset of Brownlie's database	3-16
Figure 3-9. Minimum and maximum energy slope values plotted against minimum and maximum sediment loadings from a subset of Brownlie's database.....	3-16
Figure 3-10 Minimum and maximum water discharge values plotted against minimum and maximum sediment loadings from a subset of Brownlie's database.....	3-17
Figure 3-11 Results of all of the test case runs compared to minimum and maximum D50 values and sediment loadings from a subset of Brownlie's database	3-18
Figure 3-12 Results of all of the test case runs compared to minimum and maximum energy slope values and sediment loadings from a subset of Brownlie's database.....	3-18
Figure 3-13 Results of all of the test case runs compared to minimum and maximum water discharge values and sediment loadings from a subset of Brownlie's database.....	3-19
Figure 3-14 Results of the test case runs for S = 0.0005 and S = 0.001 compared to minimum and maximum D50 and sediment loadings from a subset of Brownlie's database	3-20
Figure 3-15 Results of the test case runs for S = 0.0005 and S = 0.001 compared to minimum and maximum energy slope values and sediment loadings from a subset of Brownlie's database	3-20
Figure 3-16 Results of the test case runs for S = 0.0005 and S = 0.001 compared to minimum and maximum water discharge values and sediment loadings from a subset of Brownlie's database.....	3-21

1 Introduction

1.1 Purpose

The Flood Control District of Maricopa County (District) retained WEST Consultants, Inc. (WEST) to compare various numerical sediment transport models for consistency in modeling results. This work is being performed under District Contract Number FCD 2010C027, Assignment Number 4. The WEST project number is FCDM001-004. The District Project Manager is Bing Zhao, Ph.D., P.E., and the District Project Engineer is Richard Waskowsky, P.E. The WEST personnel for this project are Brian Wahlin, Ph.D., P.E., D.WRE (Project Manager); Chuck Davis, P.E., CFM (Hydraulic Engineer); Brent Travis, Ph.D., P.E. (Hydraulic Engineer); Christy Warren, P.E. (Hydraulic Engineer); and Cameron Jenkins, CFM (Hydraulic Engineer).

WEST would like to acknowledge Bing Zhao and Richard Waskowsky from the District, both of who provided invaluable assistance during the course of this task in gathering data and responding to questions. Additionally, WEST would like to acknowledge the District for providing a unique and interesting opportunity to advance the body of knowledge regarding the science of numerical sediment transport modeling.

The first purpose of the engineering task under Assignment Number 4 was to collect and organize data in support of sediment transport modeling of the Gila River System from the confluence of the Salt and Gila Rivers to approximately 8,000 feet west of Arizona State Route (SR) 85. This data included the following:

- Gillespie mapping (2008) for the Salt and Gila Rivers between El Mirage Road and Palo Verde Road;
- Gila River sediment samples and location shape files from Gila River Sediment Program, Phase 1 - Bed Material Sampling Plan Memorandum, by Stantec (2009);
- HEC-6T models and supporting documentation from the Tres Rios (WEST, 2004); El Rio (Stantec, 2003); and Cotton Lane (R2D, 2006) sediment transport modeling studies; and
- Report and plans for the approved sand and gravel pit permits for the study reach.

These deliverables were collected, and a summary data collection technical memorandum was provided to the District on April 29, 2011. A table of the final sediment sampling locations derived from this memorandum can be found in Appendix A of this report, along with the entire technical memorandum.

The second task was to compare three common sediment transport models (HEC-6T, HEC-RAS Sediment Transport, and SRH-1D) for the Gila River System from the confluence of the Salt and Gila Rivers to approximately 8,000 feet west of Arizona SR 85 (approximately 21 miles). The input geometry and other sediment transport modeling parameterizations were derived from the new Gila River sediment samples (2009) and HEC-6T models from Tres Rios, El Rio, and Cotton Lane projects. The portion of this model downstream of Bullard Avenue was updated based on the Gillespie Mapping topography product provided by the District (2008). After

developing the inputs for these comparison models, three sediment transport equations commonly utilized by the District for sediment transport studies were chosen to be applied to each of the three models: Yang's total bed material load based on a stream power approach (1973, 1979, 1984); the Engelund-Hansen function for total bed material load (1967); and the Toffaleti function for total bed material load (1968). The only difference in the modeling inputs to each of the models was the selection of the sediment transport functions; all other modeling inputs were identical. Outputs from the various models for each sediment transport function were compared using a root mean squared error analysis of the maximum scour and deposition at each cross section throughout the simulation.

The third task was to develop two base sediment transport models (HEC-6T and HEC-RAS Sediment Transport) for the Gila River System based on the output of the modeling effort in task two above. Bridges were added to these models at several locations. A single sediment transport function was selected for these models: Yang's total bed material load based on a stream power approach (1973, 1979, 1984).

The fourth task was to add currently developed sand and gravel pits in the reach to the base models developed in task three. The ultimate pit depth and configurations were added to the cross-section data in the two base sediment transport models, and the geometry for the two models was altered identically to represent the pits.

The fifth and sixth tasks were to compare HEC-6T and HEC-RAS based on a controlled test case, and to compare the output of each of the modeling efforts above to the Brownlie data set (1981a). These tasks are discussed in greater detail below.

It should be noted that there are two other one-dimensional sediment transport models used commonly by the District: HEC-6 and FLUVIAL-12. These models were not considered in this study; however, at times, information is provided in this report regarding these models for comparison purposes.

This report update summarizes the results of each of the tasks of this assignment as described above.

1.2 Previous Reports

The three base sediment transport models developed for the Salt-Gila River System were based on several previous studies. Cross sectional alignments, model geometries, inflowing sediment loads, and existing HEC-6T sediment transport models were obtained from the following reports:

- *Cotton Lane Bridge/King Ranch Floodplain Redelineation: Gila River, Goodyear, Arizona* (R2D, 2006)
- *El Rio Watercourse Master Plan and Area Drainage Master Plan* (Stantec, 2003)
- *PED Hydraulic Design of Tres Rios North Levee, Maricopa County: Pre-Final Project Analysis* (WEST, 2004)

Bed sediment data for the entire study reach were obtained from the *Technical Memorandum: Gila River Sediment Program Phase I, Bed Material Sampling Plan* (Stantec, 2009). Updated topography for the study reach downstream of El Mirage Road was taken from the *Gillespie Area Drainage Master Plan Mapping* (DEA, 2009).

1.3 Datum

All geographic and spatial data used in this study were adjusted to a horizontal datum of North American Datum (NAD) 1983 HARN State Plane Arizona Central (FIPS 0202 International Feet) and a vertical datum of the North American Vertical Datum of 1988 (NAVD88).

1.4 Sediment Transport Models

1.4.1 HEC-RAS

HEC-RAS was developed by and periodically updated by the US Army Corps of Engineers at the Hydrologic Engineering Center. The latest version includes a sediment transport component which provides one-dimensional sediment transport/movable boundary calculations. Both scour and deposition is modeled. The feature is designed for moderate time periods; moderate time periods are defined generally as years, but applications of the sediment transport module can be applied to single flood events as well.

Grain size fraction is used to calculate sediment transport potential, and hence hydraulic sorting and armoring can be simulated. Other features include the ability to model a full network of streams, channel dredging, and encroachment alternatives. The user can select one of several different equations for the computation of sediment transport.

The primary purpose of the model is to simulate long-term trends of scour and deposition that might result from the effects of water discharge, river stage, and / or modifications to the channel geometry. This system can also be used to evaluate deposition in reservoirs, design channel geometry needed for riverine navigation requirements, predict the influence of dredging, and estimate scour during large flood events.

The sediment component of HEC-RAS represents the incorporation of the HEC-6 program directly into HEC-RAS. The sediment component was included into HEC-RAS in version 4.0 of the program. The version utilized for this project was version 4.1 released in January of 2010.

1.4.2 HEC-6T

HEC-6T is an enhancement of the U.S. Government Computer Program "Scour and Deposition in Rivers and Reservoirs (HEC-6)." HEC-6T is a proprietary program developed by William Thomas and owned by MBH Software, Inc. There are many features in HEC-6T that are not in the Library Version of HEC-6.

The most recent version of HEC-6T was acquired for this project, version 5.13.22. However, bugs were discovered in this code. WEST is currently working with William Thomas, the developer of HEC-6T, to determine the source of these bugs. Consequently, version 5.13.19 of HEC-6T was used to complete this work assignment. This version was released in 2004.

1.4.3 SRH-1D

SRH-1D (Sedimentation and River Hydraulics - One Dimension) is a one-dimensional mobile boundary hydraulic and sediment transport computer model that can be used for rivers and / or canals. It was developed by the US Bureau of Reclamation. Using cross-section based river data, the program can simulate steady or unsteady flows; internal boundary conditions; looped river networks; cohesive and / or non-cohesive sediment transport; and lateral inflows. It can also estimate sediment concentrations throughout a waterway given the applicable sediment inflows, bed material, hydrology, and hydraulics.

The most recent version of SRH-1D, a freeware program available on the USBR website, was acquired for this project, version 2.6. This version of the program was released in 2010.

2 Sediment Transport Modeling Comparison in the Field: The Salt-Gila River System

2.1 Introduction

This section will discuss the steps taken to develop sediment transport models of the Salt-Gila River system from approximately the 83rd Avenue alignment to approximately 7,500 feet west of AZ SR 85 (see location map in Figure 2-1). The models included for this portion of the study are defined below:

- (1) three commonly utilized 1-D sediment transport models (HEC-6T, HEC-RAS Sediment Transport, and SRH-1D) and three commonly utilized sediment transport functions for total bed material load (Yang, Engelund-Hansen, and Toffaleti functions);
- (2) two base sediment transport models (HEC-6T and HEC-RAS Sediment Transport) for the Gila River System based on the output of the previous modeling efforts (see Section 1.2) including bridges in the study reach and using a single sediment transport function: Yang's total bed material load based on a stream power approach (1973, 1979, 1984); and
- (3) two sediment transport models (HEC-6T and HEC-RAS Sediment Transport) representing the ultimate built-out condition for several sand and gravel mining pits in the reach based on the output of the previous modeling efforts (see Section 1.2).

The three models mentioned above correspond to tasks 2, 3, and 4 of this work order, respectively. Inputs to the models were identical; only the model or sediment transport function varied from one run to the next.

The steps taken to develop the input for each of these models were:

- (1) compiling the geometry data from hydraulic models from various sources into a single model for use in HEC-RAS, HEC-6T, and SRH-1D;
- (2) developing the inflowing 1% annual chance flood event hydrographs for the Salt, Gila, and Agua Fria Rivers in the study reach;
- (3) developing the appropriate sediment input data for the model including bed sediment data gradations and inflowing sediment loads and gradations; and
- (4) determining the appropriate numerical computation parameters for the sediment models such as moveable bed limits and channel bank stationing.

Since these inputs did not vary from one model to the next, each of these components of the sediment transport model development is discussed individually below. Following the discussion of the model inputs, the results for each of the sediment transport functions as applied in each of the sediment transport models is discussed.

2.2 Hydraulics

2.2.1 Model Geometry

Cross section locations from the El Rio Watercourse Master Plan (WMP) models were used to represent the downstream portion of the study from the downstream limit (cross section 178.61) to just downstream of Bullard Avenue (cross section 195.0). However, the cross section geometry from the El Rio WMP models was based on a combination of 1992 and 1993 topographic mapping. In order to represent existing conditions, the geometry for these cross sections was updated based on a topographic dataset collected in 2008, hereafter referred to as the Gillespie mapping.

Cross section locations from the Tres Rios Levee PED models (WEST, 2004) were used to represent the upstream portion of the study from Bullard Avenue (cross section 195.16) to the upstream end of the study (cross section 199.47). The cross section geometry from the Tres Rios Levee PED was based on a topographic dataset from 2001. Since the Tres Rios Levee PED HEC-6T model was a fully calibrated sediment transport model that had previously verified many parameters of numerical modeling associated with model geometry through sensitivity analysis such as moveable bed limits, ineffective flow areas, and bank stations, the geometry of this model overlapping the Gillespie topography was not updated based on the newer topographic information. Additionally, a brief comparison of the topography in the overlapping region indicated that the 2008 topography was slightly lower than the original 2001 topography, but the cross sectional geometries would not have reflected significant differences. A future effort could include verification of the sediment transport model by comparing the results of the Tres Rios Levee PED model run with the 2008 topography as a validation and verification modeling effort.

Bank stations were based on the two previous studies (El Rio WMP and Tres Rios Levee PED) and represent the low flow channel. Some minor adjustments were made to the bank stations at a few cross sections. Manning's n roughness values were taken directly from the two previous studies and were not altered in any way.

Ineffective flow areas obtained from the El Rio WMP and Tres Rios Levee PED hydraulic models were initially used for this study. Some adjustments were made to the ineffective flow areas based on engineering judgment. The Tres Rios Levee was included in this study as a levee/encroachment based on its location in the Tres Rios Levee PED model.

2.2.2 Bridge Geometry for the Base Models

For the two base condition models (HEC-RAS and HEC-6T) including the bridges, five bridges were added to the model geometries. The names and locations of these bridges are shown in Table 2-1 below. All bridge input data including geometry and bridge modeling approach were taken directly from the HEC-RAS models for the Tres Rios Levee PED and the El Rio Watercourse Master Plan.

Table 2-1. Bridges added to the two base condition sediment transport models

Bridge Name	River Station	No. of Piers	Source of Bridge Data
116th Avenue Bridge	119.19	17	Tres Rios Levee PED
Bullard Avenue Bridge	195.21	14	Tres Rios Levee PED
Estrella Parkway (Reems Rd)	194.205	17	El Rio WMP
Tuthill Road	188.055	14	El Rio WMP
AZ SR 85	180.025	21	El Rio WMP

The five bridges were input directly into the HEC-RAS model for the study reach. The bridge modeling approach for each used the highest energy answer resulting from the energy, momentum, and Yarnell equations. HEC-6T does not include the hydraulic equations specifically developed to estimate hydraulic losses through bridges that are included in HEC-RAS; therefore, the HEC-6T models were altered slightly to represent the hydraulics of these bridges. Consistent with standard methods, two additional cross sections were created in the HEC-6T models to represent each of the five bridges in the study reach. The two bridge cross sections included a combination of the ground geometry and the pier geometry to represent the upstream and downstream faces of the bridge. The bridge decks were not included in the HEC-6T data because the 1% annual chance flood event flows do not reach the low chord of any of the bridge decks in the study reach.

2.2.3 Sand and Gravel Mining Pit Geometry for the Ultimate Pit Models

Three gravel pits were added to the base model to represent the ultimate pit configuration in the study reach. Plans were provided by the District for gravel pits SG04-005, SG08-004, and FA01-043, which were georeferenced to determine the location of the gravel pits for the models. Corresponding cross sections were then modified based on the plans to represent the ultimate pit configuration. All three gravel pits were assumed to be in the active flow path of the river and within the moveable bed limits.

Gravel pit SG04-005 is located on the right side of the main channel of the Gila River between cross sections 191.19 and 191.48. Plans were provided referencing the National Geodetic Vertical Datum of 1929 (NGVD29) and were converted to the NAVD88 vertical datum for this study. The excavation depth of the pit is shown to be 40 feet, therefore an average bottom pit elevation of 842.1 ft NAVD88 was used for all four modified cross sections. The side slopes of the pit are shown to be 3H:1V, and the pit covers approximately 60 acres.

Gravel pit FA01-043 is located in the left overbank of the Gila River between cross sections 195.98 and 196.23. The pit is located behind a berm along the left side of the main channel. The majority of the gravel pit has been excavated based on the 2008 Gillespie topography and 2010 aerial photography. The four cross sections from river station 195.98 to 196.23 were modified to represent the ultimate pit configuration and depth. The plans were provided in NGVD29 vertical datum and were converted to the NAVD88 vertical datum for this study. The excavation depth of the pit was not specified on the plans; however, the side slopes were shown to be 3H:1V, and the width of the slope is approximately 150 feet. Therefore, the pit excavation depth is approximately 50 feet. An average bottom pit elevation of 870 ft NAVD88 was used for all four modified cross sections. The pit covers approximately 40 acres.

Gravel pit SG08-004 is located in the right overbank of the Gila River between cross sections 196.63 and 197.18. The pit is located behind a high berm that spans between cross sections 196.5 and 197.28. A total of 16 cross sections were modified to represent the ultimate pit configuration and the berm. The provided plans for this pit referenced the NAVD88 vertical datum; therefore, no adjustment was required to the pit contours from the plans to input this information into the model geometry. The pit was shown to have a bottom elevation of 820 feet with 3H:1V side slopes. The berm is approximately 140 feet wide with a top elevation of 930 feet. The pit covers approximately 55 acres.

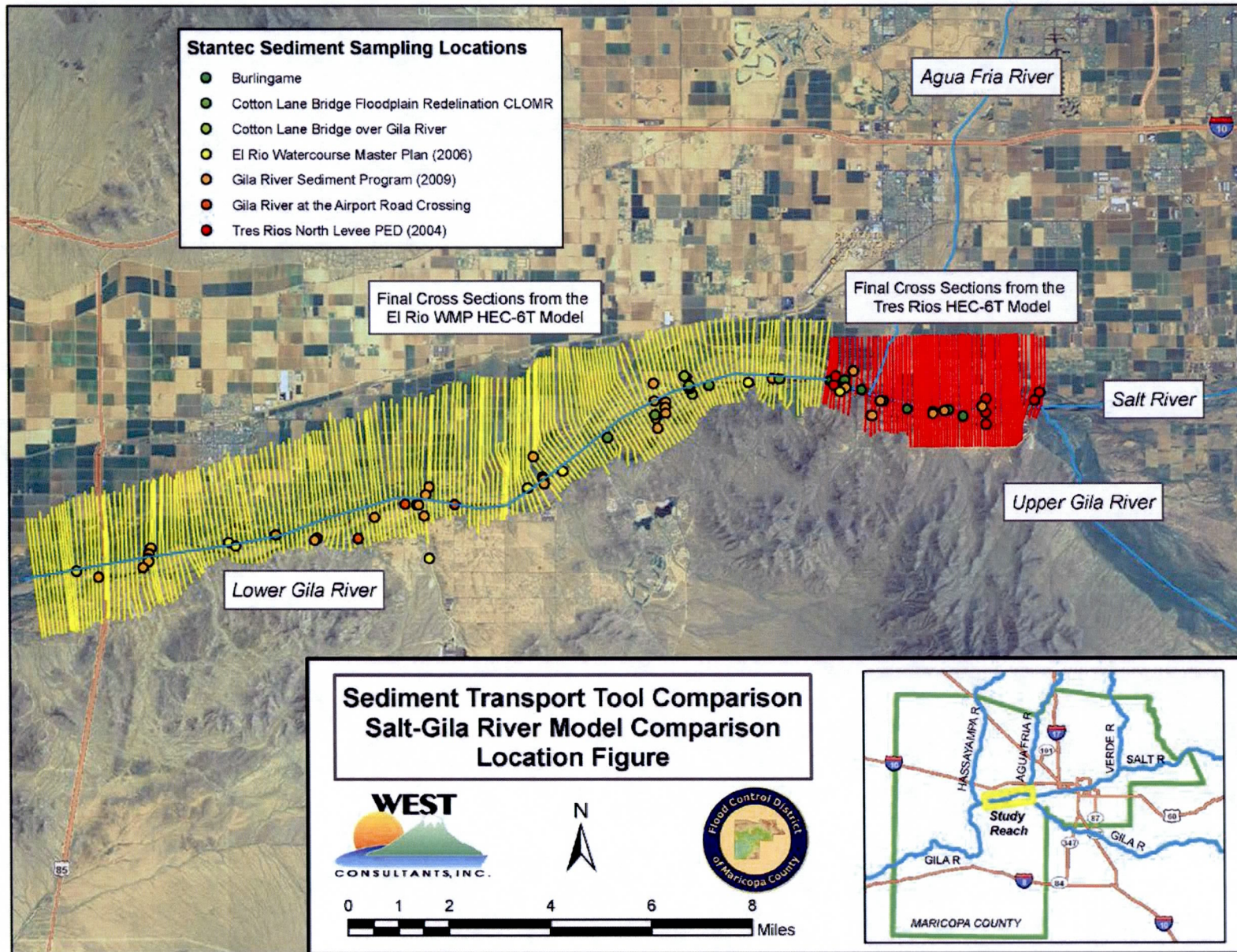


Figure 2-1. Study reach location figure for the sediment transport model comparison of the Salt-Lower Gila River System

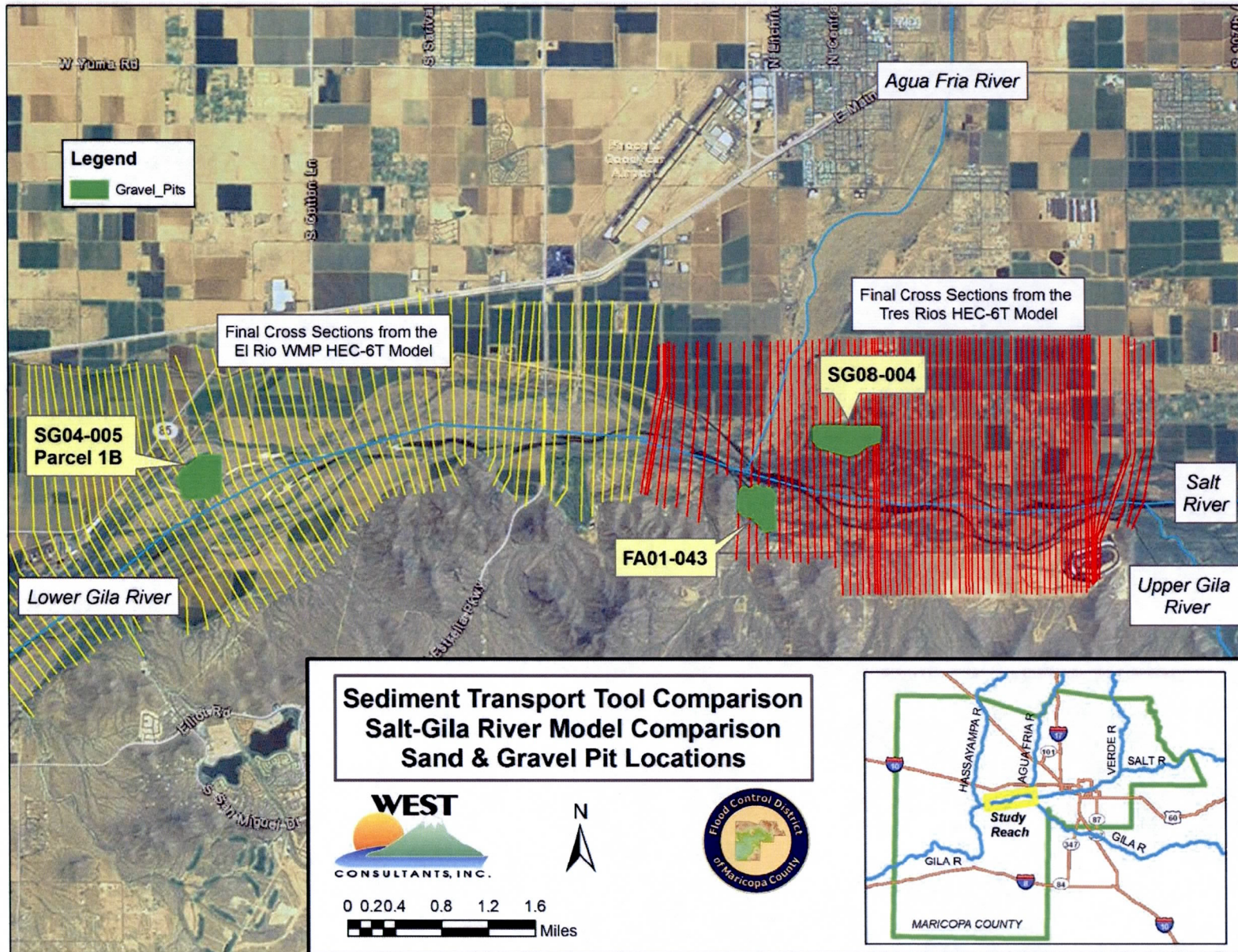


Figure 2-2. Sand and gravel pit location figure for the ultimate pit sediment transport models of the Salt-Lower Gila River System

2.3 Hydrology

The 100-year hydrograph provided in the El Rio WMP HEC-6T model was used for the modeling efforts for this study. The El Rio WMP HEC-6T model included the 100-year hydrographs for the Gila River and the Upper Gila River, but did not include flows for the Agua Fria River. The 100-year peak flow for the Agua Fria River was obtained from the Agua Fria Watercourse Master Plan (KHA, 2001). Unfortunately, a 12-day hydrograph was not available, so the 1-day hydrograph from the Master Plan was adjusted to span the 12 days necessary to complete the modeling effort. Specifically, this allowed the sediment input from the Agua Fria River to be introduced into the Gila River towards the beginning of the run. The 100-year hydrograph flow values used for modeling are shown in Table 2-2. The downstream boundary condition was based on the rating curve provided in the El Rio WMP HEC-6T model.

Table 2-2. 100-year hydrographs (cfs)

Day	Lower Gila River ¹	Agua Fria River ²	Middle Gila River (Lower Gila - Agua Fria)	Upper Gila River ¹	Salt River (Middle Gila - Upper Gila)
1	40,000	5,100	34,900	9,000	25,900
2	200,000	54,000	146,000	46,000	100,000
3	165,000	5,500	159,500	38,000	121,500
4	140,000	5,500	134,500	32,000	102,500
5	120,000	5,500	114,500	28,000	86,500
6	103,000	5,500	97,500	24,000	73,500
7	90,000	5,500	84,500	21,000	63,500
8	79,000	5,500	73,500	18,000	55,500
9	68,000	5,500	62,500	16,000	46,500
10	58,000	5,500	52,500	13,000	39,500
11	49,000	5,500	43,500	11,000	32,500
12	40,000	5,500	34,500	9,000	25,500

¹ Obtained from the El Rio WMP model

² Obtained from the Agua Fria Watercourse Master Plan report (KHA, 2001)

2.4 Sediment Data

2.4.1 Bed Material

Bed material input for the Gila River HEC-6T model was based on data from the Gila River Sediment Program (GRSP) developed by Stantec Consulting (Stantec, 2009) which compiled sediment data on the Gila River from AZ SR 85 crossing upstream 20 miles to the Salt River confluence. A total of 110 samples from seven sources were included in the GRSP and compiled into a geodatabase as listed below:

- Gila River Sediment Program, Stantec Consulting (59 samples)
- El Rio Watercourse Master Plan, Stantec Consulting (12 samples)
- Burlingame, Construction Inspection & Testing (8 samples)
- Gila River at Airport Road Crossing, Terracon (13 samples)
- Cotton Lane Bridge CLOMR, River Research and Design (4 samples)
- Cotton Lane Bridge Geotechnical and Foundation Report, Richer-Atkinson-McBee & Associates (7 samples)
- Tres Rios North Levee, Los Angeles Corps of Engineers (LACOE) (7 samples)

In addition to the sediment samples provided in the GRSP, the LACOE collected 15 more sediment samples for the Tres Rios North Levee project. These samples were also analyzed for use in the Gila River sediment transport models.

In the GRSP, Stantec classified each sample based on its size gradation characteristics where Type A defines predominantly silt and clay material, Type B defines predominantly sand material, and Type C defines predominantly gravel and cobble material. Samples classified as Type A represent the wash load and the active bed material and therefore; the Type A samples were discarded from use in the HEC-6T input. Stantec's conclusions stated that:

- (1) Type C is the dominant bed material for the Gila River from the confluence with the Salt River downstream to the Tuthill Bridge, and
- (2) Type B material occurs more frequently downstream of Tuthill Bridge.

Based on these conclusions, sediment samples with gradations classified as Type B (predominantly sand) were discarded for bed material input upstream of Tuthill Bridge and sediment samples with very coarse gradations (Type C) were looked at closely downstream of Tuthill Bridge.

The geodatabase provided a spatial reference of the sediment samples and WEST associated each sample to the nearest cross section from the sediment transport models. Some cross sections had more than one corresponding sediment sample that fit the proper material classification. When this occurred, those gradations were averaged.

The majority of sediment samples were taken at the surface (depth = 0 feet); however, some samples were taken in an excavated trench at depths up to 10 feet. For the purpose of determining the bed material input for the sediment transport models, surface samples were prioritized over samples at greater depths because the surface samples represent the bed material

that will initially be eroded. In some cases, the surface sample did not appear to provide a good representation of the bed material and a deeper sample was chosen.

Table 2-2 summarizes the corresponding cross section of each sediment sample along with the location of the sample relative to the main channel, the depth and material type of each sample, and the conclusion of which sample to use for bed material input for the sediment transport models.

2.4.2 Inflowing Sediment Load

The sediment inflow at the upstream end of this study was developed based on the results of an HEC-6T model developed for the Rio Salado Oeste (WEST, 2002). The sediment transport function used in the Rio Salado Oeste HEC-6T model was Toffaleti-Meyer-Peter Muller. A sediment rating curve was developed using the outgoing sediment load from the Rio Salado Oeste model as sediment inflow for this study, which is shown in Table 2-3. This sediment inflow is the same as that used at the upstream end of the Tres Rios Levee PED.

Table 2-3. Inflowing sediment load rating curve and gradations for the Salt River

Flow (cfs)	100	1,000	5,000	11,000	20,000	49,000	80,000	130,000	200,000	
Inflowing Sediment Load (tons/day)	200	740	4,350	13,000	38,915	120,550	275,000	505,000	884,000	
Gradations*	VFS	0.433	0.271	0.191	0.169	0.158	0.129	0.12	0.109	0.13
	FS	0.285	0.296	0.24	0.212	0.196	0.159	0.145	0.136	0.161
	MS	0.19	0.251	0.283	0.274	0.253	0.222	0.201	0.191	0.218
	CS	0.078	0.113	0.143	0.149	0.149	0.141	0.131	0.125	0.126
	VCS	0.011	0.055	0.085	0.093	0.097	0.091	0.087	0.079	0.071
	VFG	0.002	0.008	0.047	0.06	0.069	0.068	0.066	0.06	0.051
	FG	0.001	0.002	0.006	0.036	0.067	0.08	0.08	0.073	0.062
	MG	0	0.002	0.003	0.004	0.007	0.106	0.125	0.121	0.098
	CG	0	0.002	0.002	0.003	0.004	0.004	0.045	0.106	0.083

*VFS = very fine sand, FS = fine sand, MS = medium sand, CS = coarse sand, VCS = very coarse sand, VFG = very fine gravel, FG = fine gravel, MG = medium gravel, CG = coarse gravel

The Tres Rios Levee PED HEC-6T model was executed with the 100-year hydrograph for the Upper Gila River to obtain the outgoing sediment load for the Upper Gila River, which enters the Gila River at XS 199.38. The sediment transport function used in the Tres Rios Levee PED HEC-6T model was Toffaleti-Meyer-Peter Muller. A sediment rating curve was developed based on the outgoing sediment load and this was used as the sediment inflow for the Upper Gila River for this study, which is shown in Table 2-4.

Table 2-4. Inflowing sediment load rating curve and gradations for the Upper Gila River

Flow (cfs)	9,000	13,000	18,000	21,000	24,000	28,000	32,000	38,000	46,000	
Inflowing Sediment Load (tons/day)	6,514	7,282	11,953	14,123	16,020	20,679	24,263	24,683	34,988	
Gradations*	VFS	0.607	0.608	0.591	0.609	0.660	0.674	0.686	0.700	0.696
	FS	0.218	0.182	0.180	0.175	0.156	0.148	0.157	0.161	0.190
	MS	0.103	0.120	0.136	0.137	0.118	0.119	0.113	0.102	0.084
	CS	0.047	0.061	0.061	0.053	0.045	0.041	0.032	0.027	0.021
	VCS	0.018	0.023	0.024	0.020	0.016	0.014	0.010	0.008	0.006
	VFG	0.005	0.004	0.008	0.006	0.005	0.005	0.003	0.002	0.002
	FG	0.001	0.001	0.000	0.000	0.000	0.000	0.000	0.000	0.000
	MG	0.001	0.001	0.000	0.000	0.000	0.000	0.000	0.000	0.000
	CG	0.000	0.000	0.000	0.000	0.000	0.000	0.000	0.000	0.000

*VFS = very fine sand, FS = fine sand, MS = medium sand, CS = coarse sand, VCS = very coarse sand, VFG = very fine gravel, FG = fine gravel, MG = medium gravel, CG = coarse gravel

A HEC-6T model developed for the Agua Fria River, Sediment Trend Analysis (WEST, 2001) was used in conjunction with the 100-year hydrograph to determine the outgoing sediment load for the Agua Fria River, which enters the Gila River at XS 196.08. The sediment transport function used in the Agua Fria River HEC-6T model was Yang's stream power. A sediment rating curve was developed based on the outgoing sediment load and was used as the sediment inflow for the Agua Fria River for this study, which is shown in Table 2-5.

Table 2-5. Inflowing sediment load rating curve and gradations for the Agua Fria River

Flow (cfs)	5,100	5,500	5,800	9,000	20,000	30,000	44,000	52,000	54,000	
Inflowing Sediment Load (tons/day)	33,065	29,661	40,055	76,175	137,211	262,483	561,655	845,800	981,454	
Gradations*	VFS	0.306	0.013	0.148	0.142	0.034	0.048	0.118	0.085	0.063
	FS	0.372	0.189	0.356	0.225	0.297	0.311	0.312	0.307	0.326
	MS	0.211	0.386	0.350	0.358	0.420	0.412	0.374	0.364	0.386
	CS	0.081	0.301	0.107	0.199	0.185	0.171	0.147	0.182	0.171
	VCS	0.030	0.111	0.039	0.074	0.063	0.058	0.049	0.061	0.053
	VFG	0.000	0.000	0.000	0.000	0.000	0.000	0.000	0.000	0.000
	FG	0.000	0.000	0.000	0.001	0.000	0.000	0.000	0.000	0.000
	MG	0.000	0.000	0.000	0.000	0.000	0.000	0.000	0.000	0.000
	CG	0.000	0.000	0.000	0.000	0.000	0.000	0.000	0.000	0.000

*VFS = very fine sand, FS = fine sand, MS = medium sand, CS = coarse sand, VCS = very coarse sand, VFG = very fine gravel, FG = fine gravel, MG = medium gravel, CG = coarse gravel

2.5 Sediment Transport Modeling Considerations

2.5.1 Moveable Bed Limits

Moveable bed limits were defined to allow erosion and deposition within the active portion of the Gila River. For the upstream portion of the model, moveable bed limits that were defined in the Tres Rios Levee PED were initially used. Some adjustments were made to allow for erosion and deposition in portions of the channel that appeared to be active. For the downstream portion of the model, moveable bed limits were not defined in the El Rio WMP. Therefore, they were defined based on the high flow channel where erosion and deposition could occur. Cross sectional geometry and aerial imagery were also used.

For the ultimate pit model, the moveable bed limits were widened to include the area of the sand and gravel pits as well as the main channel.

2.5.2 Sediment Transport Functions

Three sediment transport functions were compared in this study: Toffaleti, Engelund-Hansen, and Yang. These sediment transport functions were chosen based on their widespread use in sediment transport modeling and the preference of the District.

There are 7 available sediment transport functions in the sediment module of HEC-RAS. These are Ackers and White (1973); Yang's stream power for sand (1973) and gravel (1984) grain sizes; Copeland's (1989) modification of Laursen's (1958) relationship; Engelund and Hansen (1967); Meyer-Peter and Müller (1948); Toffaleti (1968); and Wilcock (2001). Table 2-6 provides a comparison of the availability of six of these functions among the five identified numerical sediment transport models. From this table, it can be seen that two of the sediment transport functions available in HEC-RAS (Ackers and White and Yang's stream power for sand grain sizes) are available in all four of the other sediment transport models. Four sediment transport functions available in HEC-RAS (Copeland's modification of Laursen's relationship, Engelund and Hansen, Meyer-Peter and Müller, and Toffaleti) are available in at least two of the other sediment transport models. The final sediment transport function available in HEC-RAS (Wilcock's bedload function) is available in SRH-1D and HEC-6T; however, this function has been precluded from this scope of work due to the limited application of this transport function to river systems in Maricopa County. More detailed information and references for each of the transport functions available in all five of the identified numerical sediment transport models are provide in Table B-1 of Appendix B.

Table 2-6. Sediment transport functions common to the 1-dimensional sediment transport models

Numerical transport model	Available sediment transport functions *					
	A-W (BML)	L-C (BML)	E-H (BML for sand)	MPM (BL)	Toff (BML for sand)	Yang (BML)
HEC-RAS	•	•	•	•	•	•
HEC-6	•	•		•	•	• [†]
HEC-6T	•	•	•	•	•	• [†]
FLUVIAL-12	•		•	•		•
SRH-1D	•		•	• ^{††}		•

* *A-W = Ackers and White; L-C = Laursen-Copeland; E-H = Engelund-Hansen; MPM = Meyer-Peter and Müller, Toff = Toffaleti, Yang = Yang's stream power; BML = total bed-material load function; BL = bedload function*

[†] *In HEC-RAS, FLUVIAL-12, and SRH-1D, the Yang's sediment transport function includes Yang's 1973 equation for sands and Yang's 1984 equation for gravels. In HEC-6 and HEC-6T, the Yang's sediment transport function includes only the 1973 equation for sands.*

^{††} *In SRH-1D, the Meyer-Peter and Müller transport function includes the correction developed by Wong and Parker (2006). None of the other numerical sediment transport models include this correction in the Meyer-Peter and Müller transport function.*

2.6 Results

Comparisons of the various models were performed using the averaged RMSE calculation as shown below:

$$RMSE = \sqrt{\frac{\sum_{i=1}^n (X_i - Y_i)^2}{n}}$$

where n is the number of cross-sections for comparison, and X and Y are the elevation values of cross section i to be compared for two sediment transport models. X and Y could represent a number of different elevation variables including (1) maximum scour for the cross section throughout the simulation, (2) maximum aggradation for the cross section throughout the simulation, (3) thalweg elevation of the cross section at the end of the simulation period, or (4) average bed elevation of the cross section at the end of the simulation period.

Additionally, X and Y were compared for two primary scenarios including (1) different sediment transport functions calculated by the same numerical sediment transport model (i.e., X or Y represented an elevation output value for the Yang function, Toffaleti function, or Engelund-Hansen function depending on the scenario) or (2) the same sediment transport function calculated by different numerical sediment transport models (i.e., X or Y represented an elevation output value from HEC-6T, HEC-RAS, or SRH-1D depending on the scenario).

2.6.1 Results of the Model Comparison Runs using HEC-RAS, HEC-6T, and SRH-1D

After finalizing the models for the comparison runs for SRH-1D, HEC-6T, and HEC-RAS (see Section 2.2.1 above), the results of the models were compared to one another using the RMSE calculation. Table 2-7 and Table 2-8 show the results of these RMSE calculations. Additionally, Table 2-9 shows the average difference for the maximum aggradation to compare the magnitude difference between the various sediment transport models.

Figure 2-3, Figure 2-4, and Figure 2-5 compare the maximum scour for the different models and transport functions; likewise, Figure 2-6, Figure 2-7, and Figure 2-8 do the same for maximum aggradation. Because there is wide scatter, a moving average is shown for each model as well.

It is immediately apparent that the different models produce significantly different results. There is a general trend however: The HEC-6T model predicts the most scour, followed by SRH-1D and finally HEC-RAS which predicts the least scour. Additionally, HEC-RAS predicts less aggradation than either HEC-6T or SRH-1D. This is supported by the results in Table 2-9 as well; this table shows that the results from the HEC-6T model calculated a greater value for maximum scour on average than the other two models, and SRH-1D calculated a greater value for maximum scour on average than HEC-RAS. Final thalweg and average bed elevation plots of the entire study reach for the comparison runs can be found in Appendix C.

Table 2-7. RMSE values (feet) for various sediment transport functions within an individual model

Transport Functions Compared*	RMSE for Maximum Scour	RMSE for Maximum Aggradation	RMSE for Final Thalweg
SRH1D			
Engelund Hansen vs. Yang	0.77	0.36	0.92
HEC-6T			
Toffaleti vs. Engelund Hansen	1.91	2.65	2.09
Engelund Hansen vs. Yang	1.42	2.30	1.43
Yang vs. Toffaleti	0.91	1.01	1.43
HEC-RAS			
Toffaleti vs. Engelund Hansen	1.15	1.29	1.72
Engelund Hansen vs. Yang	0.63	1.19	1.48
Yang vs. Toffaleti	1.00	0.41	1.04

* Note that in HEC-RAS and SRH-1D, the Yang's sediment transport function includes Yang's 1973 equation for sands and Yang's 1984 equation for gravels. In HEC-6T, the Yang's sediment transport function includes only the 1973 equation for sands.

Table 2-8. RMSE values (feet) for various sediment transport models for a given sediment transport function

Models Compared	RMSE for Maximum Scour	RMSE for Maximum Aggradation	RMSE for Final Thalweg
<i>Toffaletti</i>			
HEC-6T vs. HEC-RAS	0.62	0.78	0.97
<i>Engelund Hansen</i>			
SRH-1D vs. HEC-6T	1.96	2.25	1.83
HEC-6T vs. HEC-RAS	1.79	2.29	1.34
HEC-RAS vs. SRH-1D	1.37	0.52	1.56
<i>Yang*</i>			
SRH-1D vs. HEC-6T	0.81	0.73	1.75
HEC-6T vs. HEC-RAS	0.91	1.09	1.51
HEC-RAS vs. SRH-1D	0.91	1.16	2.02

* Note that in HEC-RAS and SRH-1D, the Yang's sediment transport function includes Yang's 1973 equation for sands and Yang's 1984 equation for gravels. In HEC-6T, the Yang's sediment transport function includes only the 1973 equation for sands.

Table 2-9. Average differences between the maximum scour values for each sediment transport function

	<i>Toffaletti</i>	<i>Engelund Hansen</i>			<i>Yang</i>		
	<i>6T/RAS*</i>	<i>6T/RAS*</i>	<i>6T/SRH**</i>	<i>RAS/SRH***</i>	<i>6T/RAS*</i>	<i>6T/SRH**</i>	<i>RAS/SRH***</i>
Average	0.17	0.52	0.12	0.40	0.18	0.13	0.06
Count > 0 [†]	185	173	136	120	157	142	100
Count < 0 ^{††}	57	55	93	94	81	92	117
Count = 0 ^{†††}	17	31	30	45	21	25	42
Total count	259	259	259	259	259	259	259

* Positive value indicates that HEC-6T computed deeper maximum scour than HEC-RAS

** Positive value indicates that HEC-6T computed deeper maximum scour than SRH-1D

*** Positive value indicates that SRH-1D computed deeper maximum scour than HEC-RAS

[†] This row reports the number of cross sections in the model that had a positive value as defined for the transport functions being compared

^{††} This row reports the number of cross sections in the model that had a negative value as defined for the transport functions being compared

^{†††} This row reports the number of cross sections in the model that had the same amount of maximum scour for the transport functions being compared

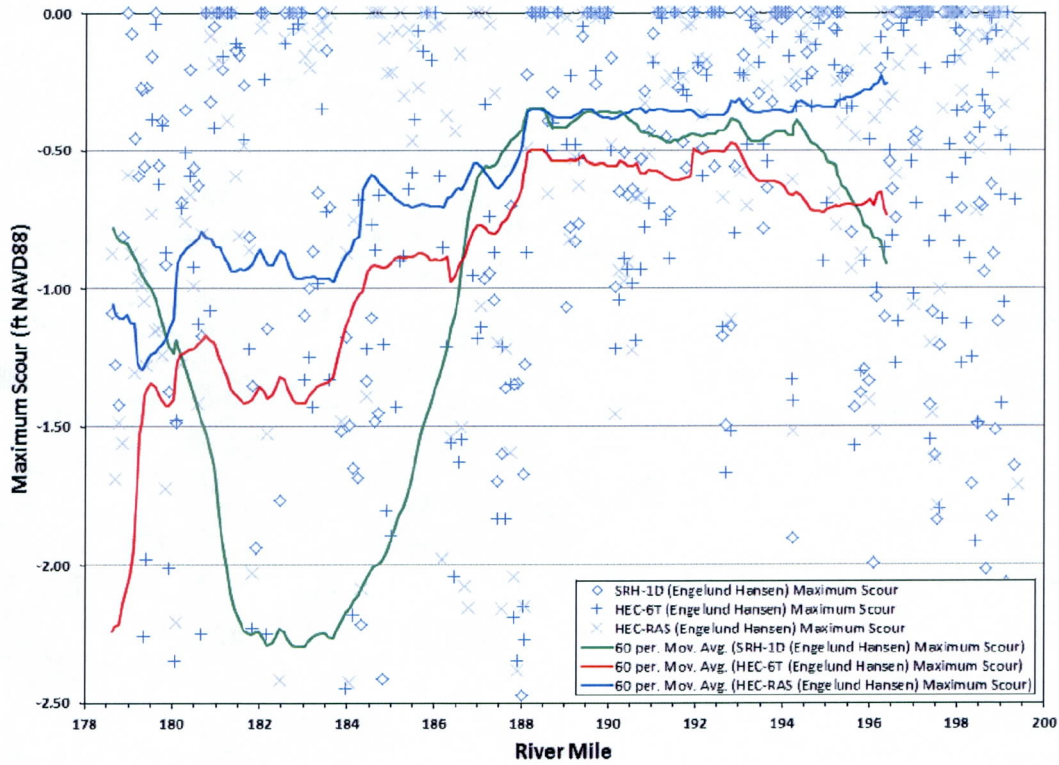


Figure 2-3. Maximum scour comparison for the Engelund-Hansen function

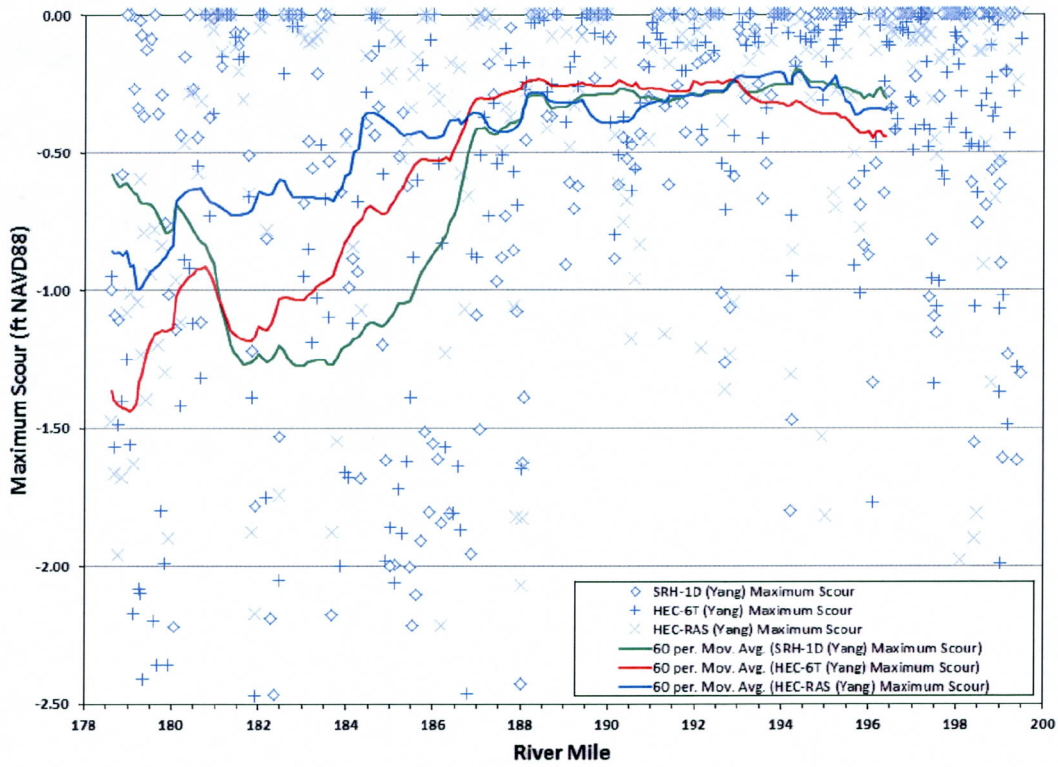


Figure 2-4. Maximum scour comparison for the Yang function

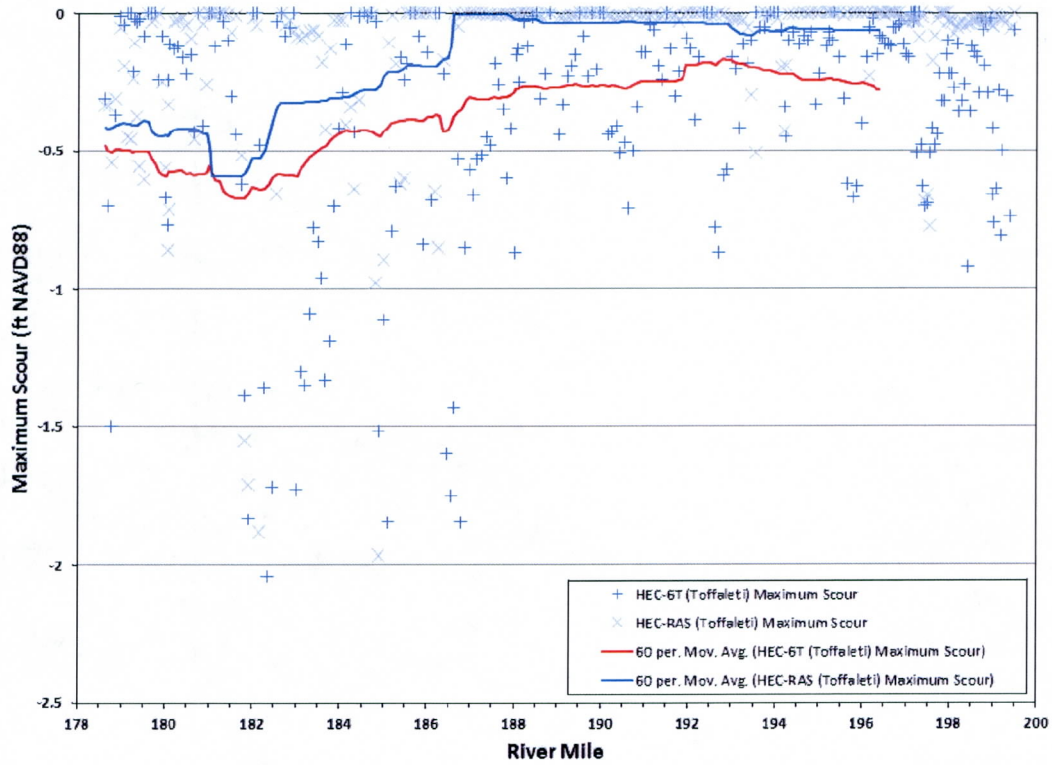


Figure 2-5. Maximum scour comparison for the Toffaleti function

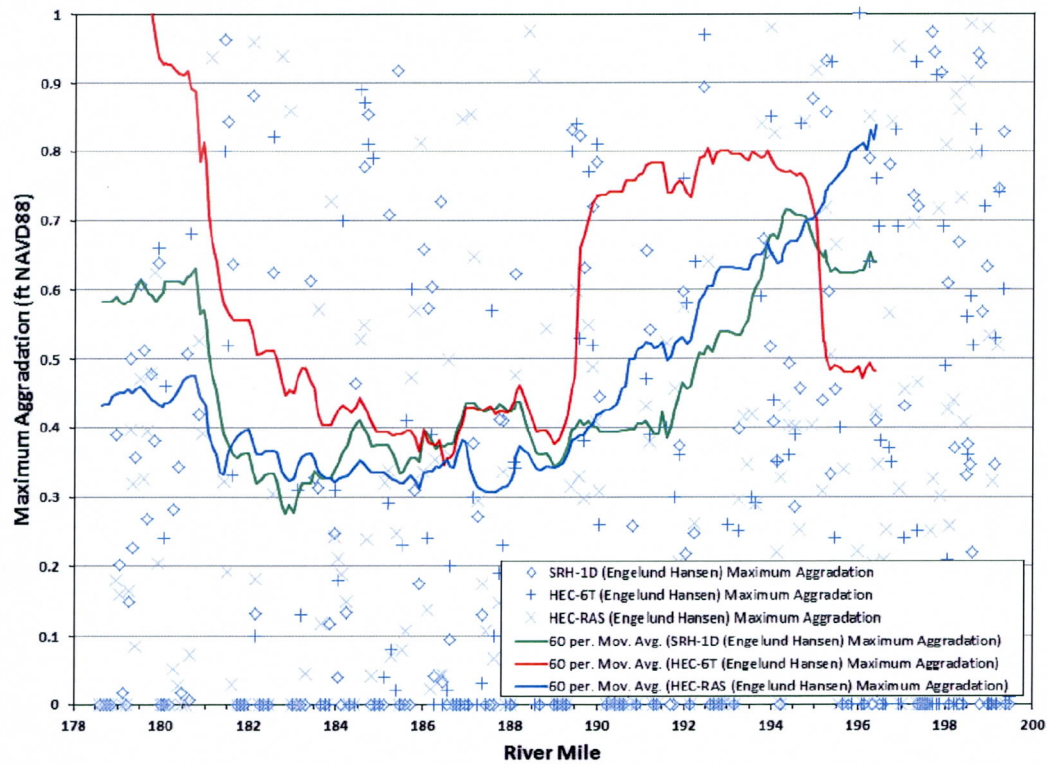


Figure 2-6. Maximum aggradation comparison for the Engelund Hansen function

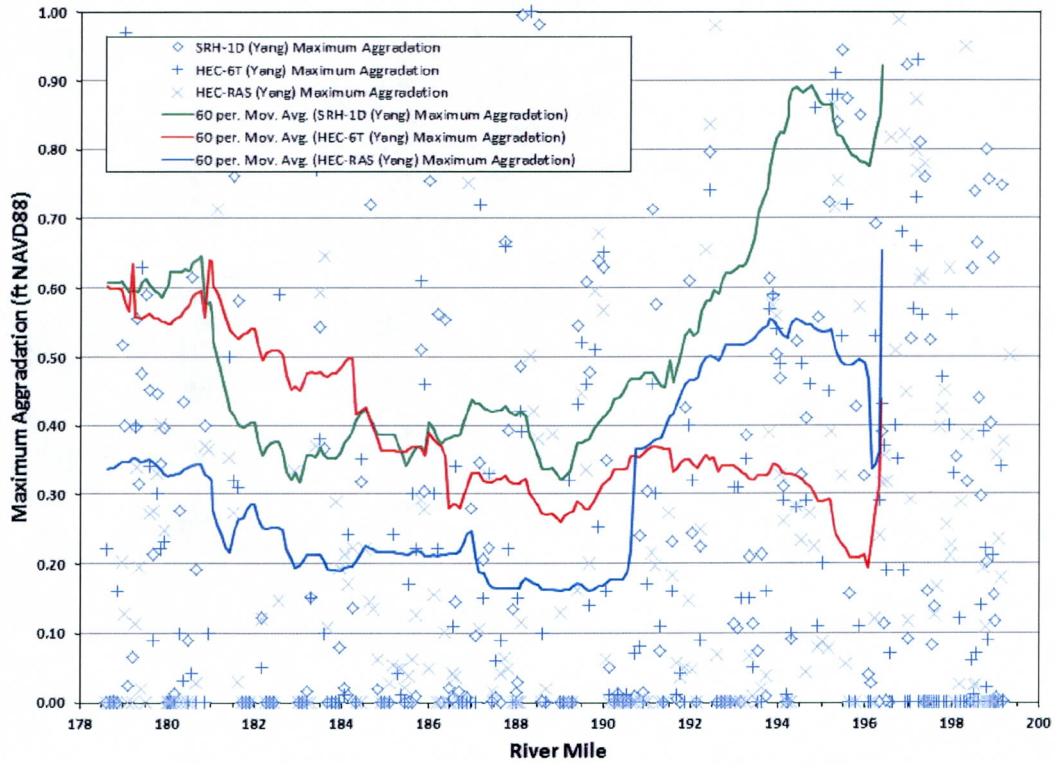


Figure 2-7. Maximum aggradation comparison for the Yang function

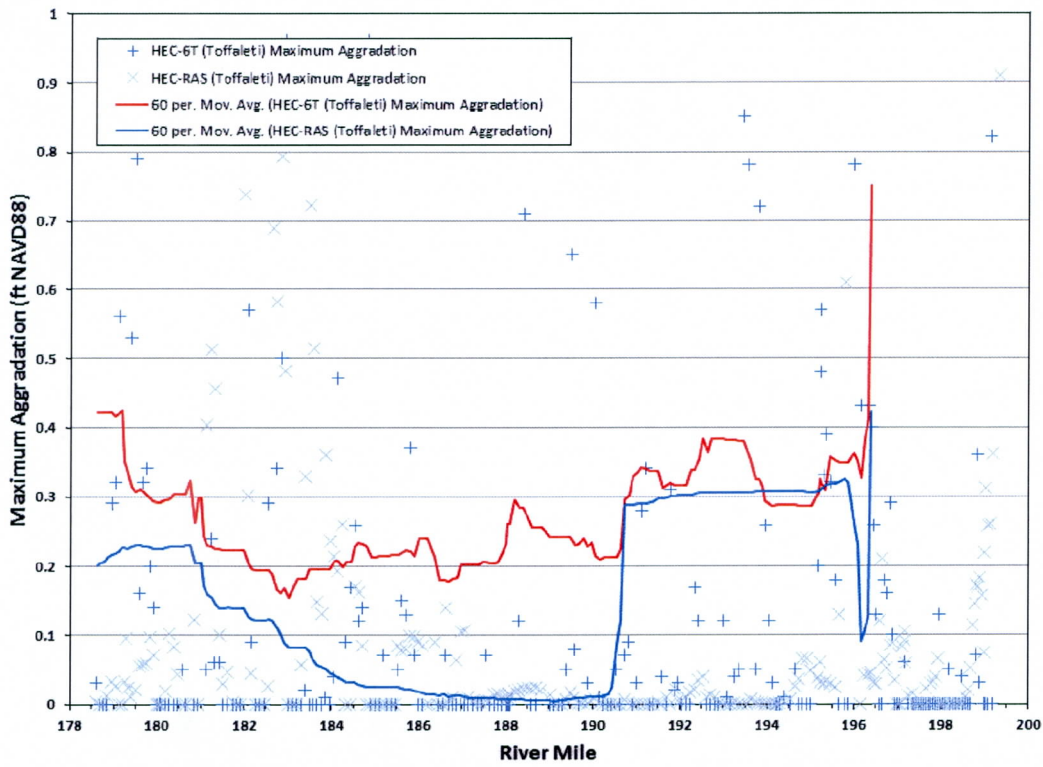


Figure 2-8. Maximum aggradation comparison for the Toffaleti function

2.6.2 Results of the Base Condition Models using HEC-RAS and HEC-6T

Consistent with the analysis method used for the comparison models comparison (2.6.1), the results of the base models run for HEC-6T and HEC-RAS were also compared using the RMSE calculation. Table 2-10 shows the results of these calculations, and Table 2-11 shows the average difference for the maximum aggradation in order to compare the magnitude difference between HEC-6T and HEC-RAS.

Figure 2-9 compares the maximum scour for the different models and transport functions, and Figure 2-10 does the same for maximum aggradation. Again, because there is wide scatter, a moving average is shown for the results of the two models as well.

Like the model comparison analysis, the HEC-6T model predicts more scour and aggradation than HEC-RAS. As shown in Table 2-11, the HEC-6T model calculated a greater value for maximum scour on average than HEC-RAS. Final thalweg and average bed elevation plots of the entire study reach for the base condition models can be found in Appendix D.

Table 2-10. RMSE values (feet) for the two base condition sediment transport models versus one another and the “without bridges” condition

Models Compared	RMSE for Maximum Scour	RMSE for Maximum Aggradation	RMSE for Final Thalweg
		<i>Yang*</i>	
HEC-6T vs. HEC-RAS	0.94	1.07	1.53
HEC-6T, with bridges vs. without bridges	0.03	0.05	1.10
HEC-RAS, with bridges vs. without bridges	0.53	0.23	1.32

* Note that in HEC-RAS and SRH-1D, the Yang's sediment transport function includes Yang's 1973 equation for sands and Yang's 1984 equation for gravels. In HEC-6T, the Yang's sediment transport function includes only the 1973 equation for sands.

Table 2-11. Average differences between maximum scour for the base condition models

	<i>Yang</i>
	<i>6T/RAS*</i>
Average	0.09
Count > 0 [†]	151
Count < 0 ^{††}	88
Count = 0 ^{†††}	20
Total count	259

* Positive value indicates that HEC-6T computed deeper maximum scour than HEC-RAS

[†] This row reports the number of cross sections in the model that had a positive value as defined for the sediment transport models being compared

^{††} This row reports the number of cross sections in the model that had a negative value as defined for the sediment transport models being compared

^{†††} This row reports the number of cross sections in the model that had a the same amount of maximum scour for the sediment transport models being compared

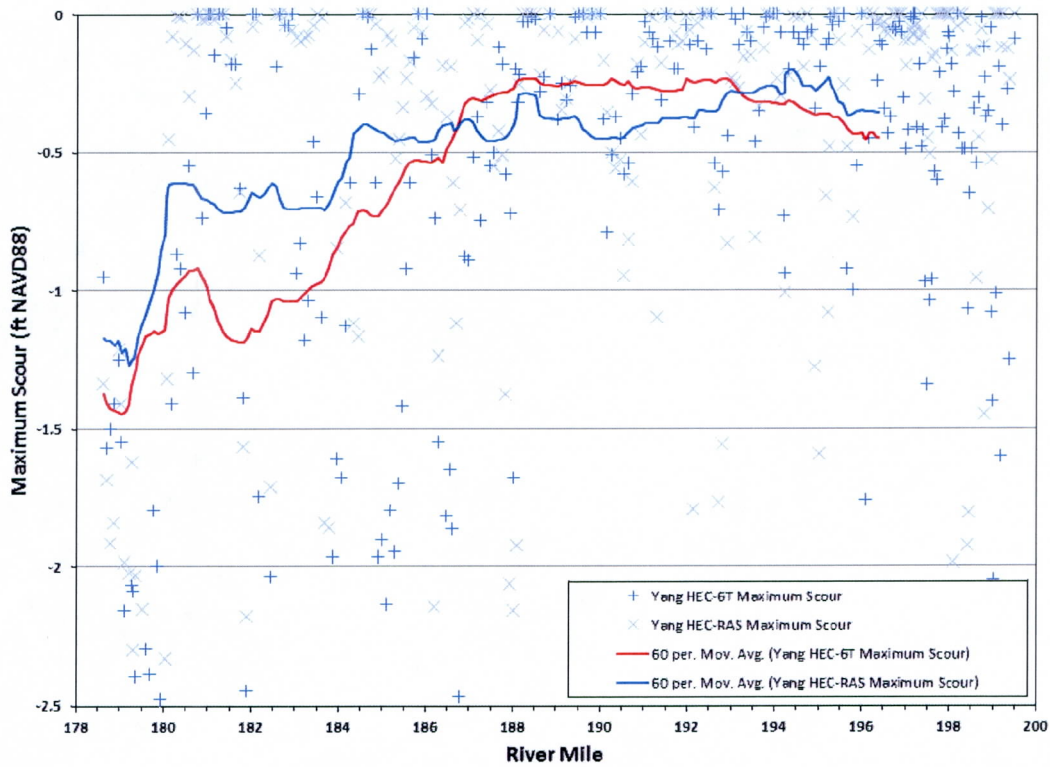


Figure 2-9. Maximum scour comparison for the base condition models with bridges

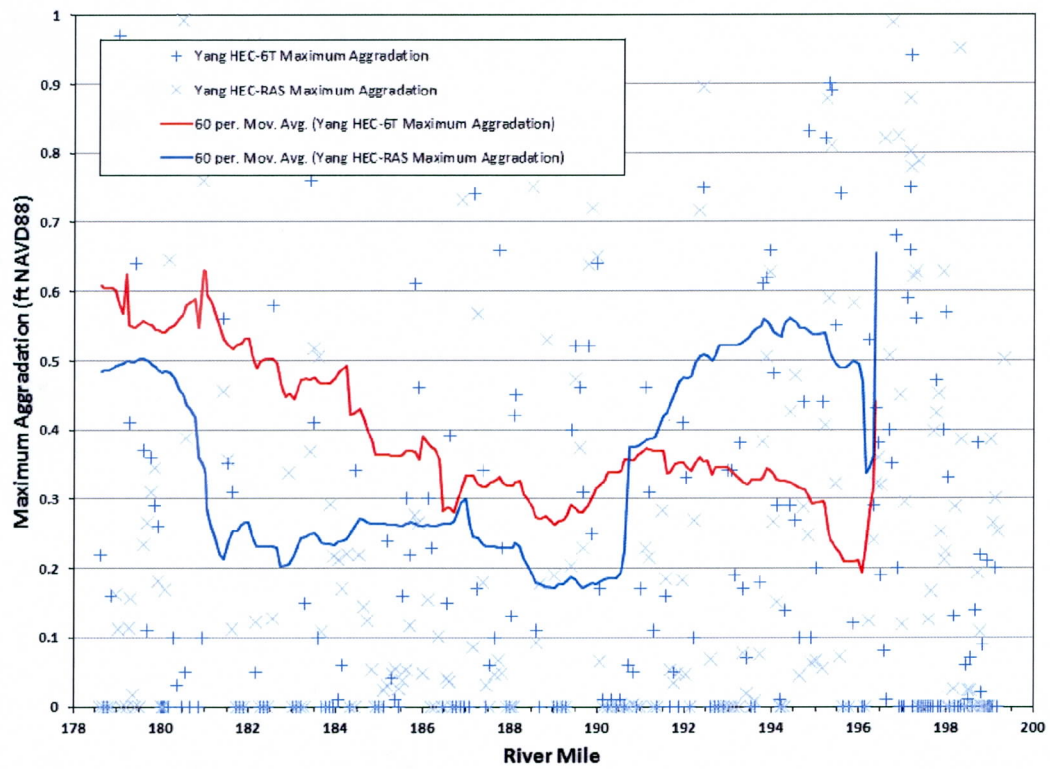


Figure 2-10. Maximum aggradation comparison for the base condition models with bridges

2.6.3 Results of the Ultimate Pit Models using HEC-RAS and HEC-6T

Following the analysis methods described in Sections 2.6.1 and 2.6.2, the ultimate pit models run for HEC-6T and HEC-RAS (were compared to one another using the RMSE calculation (see Table 2-12). Likewise, Table 2-13 shows the average difference for the maximum aggradation to compare the magnitude difference between HEC-6T and HEC-RAS.

Figure 2-11 compares the maximum scour for the different models and transport functions, and Figure 2-12 does the same for maximum aggradation; for clarity a moving average is also shown. It should be noted that Figure 2-12 shows a large aggradation for the moving average near the upstream end of the model for HEC-6T; this is due to the infilling of a pit at this location.

For the last test scenario of the Salt-Lower Gila River System, the HEC-6T model once again predicts more scour and aggradation than HEC-RAS, consistent with the results of the comparison scenarios and the base models. This can be seen in Table 2-13 in that the results from the HEC-6T model calculated a greater value for maximum scour on average than HEC-RAS. Final thalweg and average bed elevation plots of the entire study reach for the ultimate pit condition models can be found in Appendix E.

Table 2-12. RMSE values (feet) for the ultimate pit models

Models Compared	RMSE for Maximum Scour	RMSE for Maximum Aggradation	RMSE for Final Thalweg
	<i>Yang*</i>		
HEC-6T vs. HEC-RAS	1.03	12.08	5.69

* Note that in HEC-RAS and SRH-1D, the Yang's sediment transport function includes Yang's 1973 equation for sands and Yang's 1984 equation for gravels. In HEC-6T, the Yang's sediment transport function includes only the 1973 equation for sands.

Table 2-13. Average differences between maximum scour for the ultimate pit models

	<i>Yang</i>
	<i>6T/RAS*</i>
Average	0.07
Count > 0 [†]	152
Count < 0 ^{††}	87
Count = 0 ^{†††}	20
Total count	259

* Positive value indicates that HEC-6T computed deeper maximum scour than HEC-RAS

[†] This row reports the number of cross sections in the model that had a positive value as defined for the sediment transport models being compared

^{††} This row reports the number of cross sections in the model that had a negative value as defined for the sediment transport models being compared

^{†††} This row reports the number of cross sections in the model that had a the same amount of maximum scour for the sediment transport models being compared

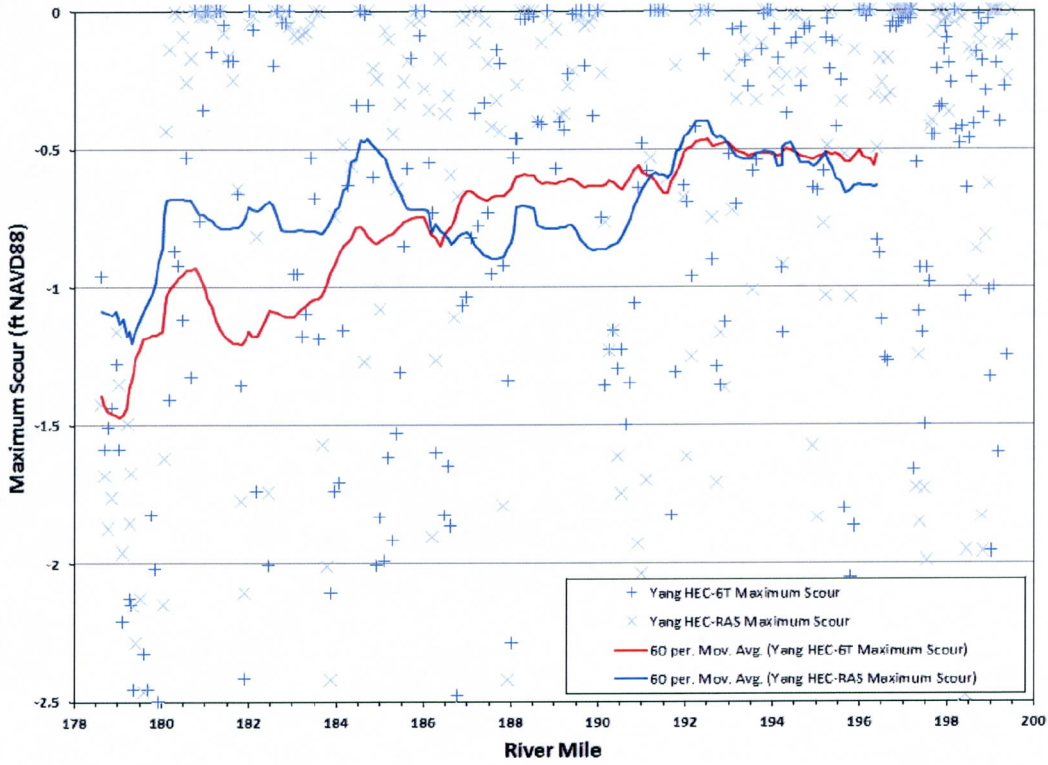


Figure 2-11. Maximum scour comparison for the ultimate pit models

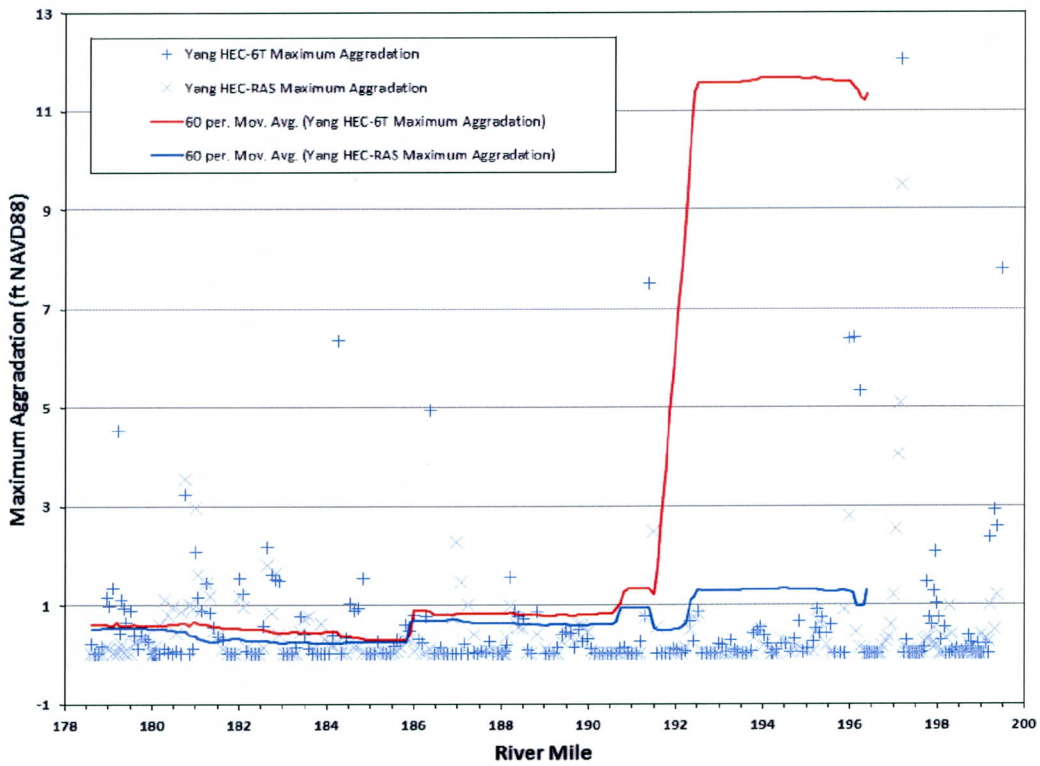


Figure 2-12. Maximum aggradation comparison for the ultimate pit models

3 Sediment Transport Modeling for the Test Cases

3.1 Introduction

This section describes a comparison between HEC-6T and HEC-RAS modeling result for a test case for a trapezoidal channel. This was done in the hopes of obtaining clear information free of the noise inherent to natural conditions, and as such to serve as a counterpoint to the field study.

However, even this simple approach required numerous factors to be considered. These factors were developed by performing the following tasks:

1. Developing the geometry data for a generalized trapezoidal channel;
2. Develop the inflow flood hydrographs to test the range of velocities used to develop the typical sediment transport functions;
3. Develop the appropriate sediment input data for the model;
4. Determine the appropriate numerical computation parameters for the sediment models.

Each of the factors determined through these tasks constituted independent variables of the study. Two dependent variables of interest were then identified: The RMSE between HEC-RAS and HEC-6T predictions for maximum scour and maximum deposition.

The next section provides the specifics on how the independent variables were established.

3.2 Independent Variables

3.2.1 Cross-Section Geometry

A 5,000-foot long trapezoidal channel with a bottom width w of 200 feet and 2H:1V side slopes was used as the generalized test case for the sediment transport functions. These parameters were not varied, but three longitudinal bed slopes S (ft/ft) were tested: 0.0005, 0.001, and 0.01. Moveable bed limits were defined to allow erosion and deposition within all portions of the trapezoidal channel.

3.2.2 Sediment Transport Functions

Three sediment transport functions (F) were used for the comparison: Toffaleti (T), Engelund-Hansen (EH), and Yang (Y). Like the functions considered in the field case study, these sediment transport functions were chosen based on their widespread use in sediment transport modeling and the preference of the District. Thus, F is a categorical variable representing the three possible values (EH, T, and Y). A full list of the transport functions available in several commonly utilized 1-dimensional sediment transport models are provided in Table B-1 of Appendix B of this report.

3.2.3 Flow Rates

Three flows Q (cfs) were considered in the study: 50 cfs, 1,000 cfs, and 2,000 cfs. These flows were chosen in an attempt to bracket the ranges of velocities used to develop the analyzed sediment transport functions. Table 3-1 below provides the hydraulic parameters used in the development of these functions. Flows required to reach a range of flow velocities between approximately 1.2 and 6.3 feet per second were computed based normal depth calculations in a trapezoidal channel with a channel bottom width, side slopes, and a Manning's roughness coefficient of 200 ft, 2H:1V, and 0.03, respectively. The Federal Highways Administration's *Hydraulic Toolbox* computer software (version 2.1) was used to complete these calculations (FHWA, 2011). Roughly 50 cfs and 2,000 cfs bounded this range. A third value of 1,000 cfs was chosen as a midpoint value.

Table 3-1. Hydraulic parameters from the datasets by which the transport functions were developed

Transport Function	Overall particle diameter (mm)		Median particle diameter (mm)		Sediment specific gravity		Flow Velocity (fps)	
	Min	Max	Min	Max	Min	Max	Min	Max
Engelund Hansen (flume)	N/A	N/A	0.19	0.93	N/A	N/A	0.65	6.34
Toffaleti Transport Function (field)	0.062	4	0.095	0.76	N/A	N/A	0.7	7.8
Toffaleti Transport Function (flume)	0.062	4	0.45	0.91	N/A	N/A	0.7	6.3
Yang Transport Function (field-sand)	0.15	1.7	N/A	N/A	N/A	N/A	0.8	6.4
Yang Transport Function (field-gravel)	2.5	7	N/A	N/A	N/A	N/A	1.4	5.1

Table 3-1. Hydraulic parameters from the datasets by which the transport functions were developed (cont'd)

Transport Function	Flow Depth (ft)		Slope (ft/ft) x 10 ⁻³		Top Width (ft)		Water Temp. (°F)	
	Min	Max	Min	Max	Min	Max	Min	Max
Engelund Hansen (flume)	0.19	1.33	0.055	19.0	N/A	N/A	45	93
Toffaleti Transport Function (field)	0.07	56.7	0.002	1.1	63	3,640	32	93
Toffaleti Transport Function (flume)	0.07	1.1	0.14	19.0	0.8	8	40	93
Yang Transport Function (field-sand)	0.04	50	0.043	28.0	0.44	1,750	32	94
Yang Transport Function (field-gravel)	0.08	0.72	1.2	29.0	0.44	1,750	32	94

3.2.4 Downstream Boundary Conditions

For each flow rate and each bed slope in all of the test runs, a downstream boundary condition was calculated using a normal depth assumption. The Federal Highways Administration's *Hydraulic Toolbox* computer software (version 2.1) was used to complete these calculations (FHWA, 2011). The downstream boundary condition in each model was set to be a known water surface elevation throughout the duration of the model runs.

3.2.5 Bed Gradations

The generalized artificially sorted sand gradation from Vanoni (1975) was used as a basis for the bed sediment gradations used in the test cases. This gradation is shown in Figure 3-1 below. A total of five different bed gradations (g_{bed}) were considered for the test cases based on this artificially sorted sand: 0.5g, 1g, 2g, 4g, and 8g. Since these gradations are on the fine end of the sand gradation spectrum, the base condition (i.e., 1g) was considered to be double the gradation from Vanoni (1975). In other words, the gradation shown in Figure 3-1 was

considered to be the 0.5g gradation condition, and the 1g, 2g, 4g, and 8g are increasing multiples of 2 of this gradation.

All five of these gradations are shown in Table 3-2 below as well. It should be noted in this table that, although some cohesive sediments (i.e., d_{50} less than 62.5 micrometers) are shown in the Vanoni chart for artificially sorted sands (Figure 3-1), these cohesive sediments were not included in the test cases; only coarse grained sediments were included in this analysis.

For the statistical analysis, the gradations were represented as a variable G_{bed} with values equal to the gradation coefficients (0.5, 1, 2, 4, and 8).

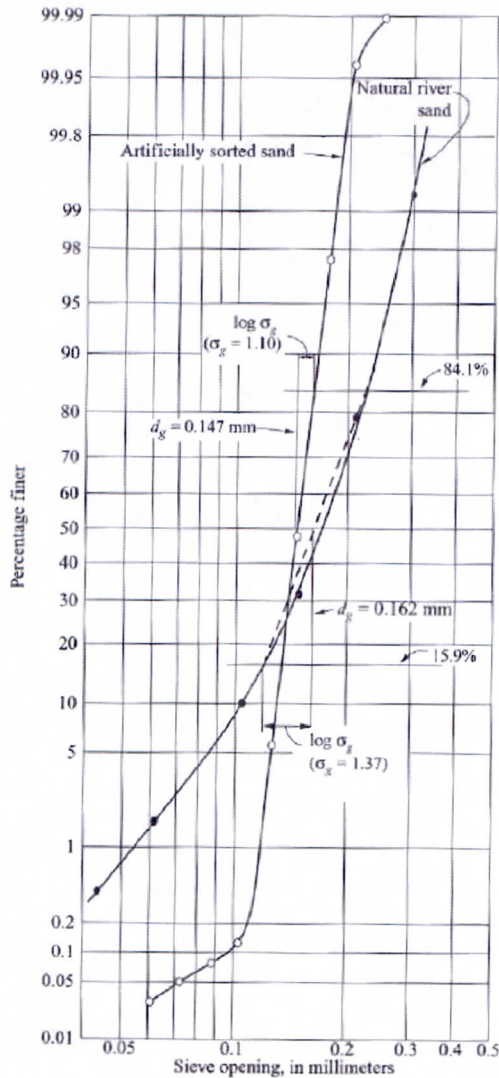


Figure 3-1. Generalized gradations for artificially sorted sand and river sand (Vanoni, 1975)

Table 3-2. Bed sediment gradations based on the artificially sorted sand gradation from Vanoni (1975)

Grain Size (mm)	Classification	Percent Finer					
		Vanoni artificially sorted sand	0.5g	1g	2g	4g	8g
< 0.0625	Silt and clays	0.04	0	0	0	0	0
0.0625 – 0.125	Very fine sand	5	5	0.04	0	0	0
0.125 – 0.25	Fine sand	99.9	99.9	5	0.04	0	0
0.25 – 0.5	Medium sand	100	100	99.9	5	0.04	0
0.5 – 1	Coarse sand	100	100	100	99.9	5	0.04
1 – 2	Very coarse sand	100	100	100	100	99.9	5
2 – 4	Very fine gravel	100	100	100	100	100	99.9
4 – 8	Fine gravel	100	100	100	100	100	100

3.2.6 Sediment Inflow

One problem encountered for the test case scenarios was determining an equilibrium inflowing sediment load (Q_s) for the various bed slopes, flow velocities, etc. To determine these, HEC-RAS was used to calculate the equilibrium sediment inflow based channel slope, depth, discharge, and bed gradation. This value was then used as a starting point for the sediment transport model. This idea was followed to test the three sediment transport functions on three slopes with three different discharges.

Thus, a total of 27 test cases were set up to determine the sediment inflow based on 3 slopes, 3 functions, 1 gradation, and an upstream sediment boundary condition set to equilibrium. The bed slope and discharges were chosen based on the range of velocity and energy slope that are recommended for the three functions. Once all the runs were completed, the mass capacity in tons/day was recorded. To calculate the final sediment inflow, the average mass capacity for the 3 functions was used. The final values are shown in Table 3-3 below.

Like the bed gradations, the sediment inflows were entered in their non-dimensional form for the statistical analysis by introducing a variable Q_{sed} with values 0.5, 1.0, and 1.5.

3.3 Final Design

The final experimental design for the test case analysis is shown in Table 3-4 below, with the non-dimensional equivalents used for the statistical analysis shown in parentheses.

Table 3-3. Inflowing sediment load rating curve and gradations for the test cases*

Sediment Transport Function	Flow Rate (cfs)	Bed Slope (ft/ft)	Eq. Sediment Inflow (tons/day)	Ave. Eq. Sediment Inflow (tons/day)	Final Adopted Sediment Inflow Values for All Test Cases (tons/day)		
					0.5Qs	1.0Qs	1.5Qs
Yang	2000	0.001	4,325	4,238.7	2,100	4,200	6,300
Engelund-Hansen	2000	0.001	7,233				
Toffaleti	2000	0.001	1,158				
Yang	1000	0.001	1,433	1,364.7	700	1,400	2,100
Engelund-Hansen	1000	0.001	2,253				
Toffaleti	1000	0.001	408				
Yang	50	0.001	4.35	6.3	3.0	6.0	9.0
Engelund-Hansen	50	0.001	14.3				
Toffaleti	50	0.001	0.212				
Yang	2000	0.0005	1,258	1,320.7	650	1,300	1,950
Engelund-Hansen	2000	0.0005	2,289				
Toffaleti	2000	0.0005	415				
Yang	1000	0.0005	394	419.3	210	420	630
Engelund-Hansen	1000	0.0005	714				
Toffaleti	1000	0.0005	150				
Yang	50	0.0005	0.35	1.63	1.0	2.0	3.0
Engelund-Hansen	50	0.0005	4.5				
Toffaleti	50	0.0005	0.05				
Yang	2000	0.01	156,229	170,574.7	85,000	170,000	255,000
Engelund-Hansen	2000	0.01	330,196				
Toffaleti	2000	0.01	25,299				
Yang	1000	0.01	59,993	61,798.3	31,000	62,000	93,000
Engelund-Hansen	1000	0.01	102,661				
Toffaleti	1000	0.01	22,741				
Yang	50	0.01	656	667.3	350	700	1,050
Engelund-Hansen	50	0.01	637				
Toffaleti	50	0.01	709				

*Note that these inflowing sediment load rating curves were developed using the "equilibrium sediment load" boundary condition option in HEC-RAS. This option automatically calculates an equilibrium sediment load for the associated transport function. Differences in equilibrium load computation algorithms between HEC-RAS and the other sediment transport models were not considered.

Table 3-4. Final comparison study design

Parameter	Dependent Variable	Values				
Bed Slope	S	0.0005	0.001	0.01	-	-
Sediment Transport Function	F	EH	T	Y	-	-
Flow	q (cfs)	50 cfs	1000 cfs	2000 cfs	-	-
Bed Gradation	g_{bed} (G_{bed})	0.5g (0.5)	1g (1.0)	2g (2.0)	4g (4.0)	8g (8.0)
Sediment Inflow	q_{sed} (ton/day) (Q_{sed})	0.5Qs (0.5)	1.0Qs (1.0)	1.5Qs (1.5)	-	-

3.4 Results

A total of 405 runs were made to account for every permutation of the independent factors. The entire table of results may be found in Table F-1 of Appendix F. All 405 runs were completed in HEC-6T and HEC-RAS.

The differences between the output features of HEC-6T and HEC-RAS caused some difficulties. For example, in HEC-RAS, the maximum deposition allowed at any cross section in a run is 20.0 feet. In HEC-6T, this restriction is not implemented. For the test runs with $S = 0.01$ ft/ft, the maximum deposition exceeded twenty feet at 68 cross sections for all the runs of this scenario (135 iterations were completed with each slope value of 0.0005, 0.001, and 0.01 for a total of 405 iterations). With 11 cross sections in the model and 135 iterations, there were 1,485 final data points for maximum deposition at a cross section; therefore, 68 data points exceeding twenty feet of deposition represent 4.5% of the total sample population. Due to the small number of cross sections that exceeded the 20' maximum imposed by HEC-RAS, and due to the fact that many of these values were obviously not physically possible (i.e., the single greatest maximum deposition for any cross section was 24,004 feet at cross section 4500 for the EH run at $S = 0.01$, 1Qs, 0.5g, and 2,000 cfs; additionally, half of these 68 cross sections showed greater than 50 feet of deposition), all of the maximum deposition data points for the HEC-6T runs that were greater than 20' were replaced with 20' of deposition for the final statistical analysis. This provided for a more reasonable estimation of Root Mean Square Error.

For the present applications, wherein deposits of less than 10 feet are expected, all model runs that produced depositions of 20 feet or more were considered highly unrealistic and erroneous, caused by model instabilities or other errors. Additionally, numerical instabilities can cause fatal errors in the calculations causing the model to crash. Unlike the HEC-RAS results, fatal errors were not encountered in HEC-6T (i.e., the model never ceased the sediment transport computations before the prescribed end of the simulation period). However, highly unrealistic results still occurred. For instance, 34 cross sections showed deposition of greater than 50 feet, 24 cross sections show deposition of greater than 100 feet, and 8 cross sections show deposition greater than 1,000 feet. All of these unrealistic results occurred in test case runs with the bed slope equal to 0.01 ft/ft.

The developers of HEC-RAS have built in some additional error analysis tools for fatal errors and unrealistic results in the sediment module of HEC-RAS. For example, as mentioned previously, deposition at a cross section is limited to 20 feet. Additionally, if a single time step has too great of a change in bed sediment volume (erosion or deposition) at any given cross section, the computations will cease at that point in the simulation and a fatal error stating "Unrealistic vertical adjustment at [River Name, Reach Name, Cross Section Number]" will appear in the computation window. Four of the test case runs encountered fatal errors with this message including the following: EH-8G-2000-0.01-1Qs (run ended on time step 1,026 of 1,489), EH-4G-1000-0.01-1.5Qs (run ended on time step 591 of 1,489), EH-4G-2000-0.01-1.5Qs (run ended on time step 843 of 1,489), and EH-8G-2000-0.01-1.5Qs (run ended on time step 36 of 1,489).

Finally, HEC-6T had some issues with calculating maximum and minimum channel thalweg elevations of 1.0. In the maximum/minimum tables produced by HEC-6T for the end of the run maximum deposition (maximum elevation at a cross section) for all of the test cases, there were 31 cell values showing “***” instead of values for the maximum deposition. Of these 31 values, 19 occurred at cross section 2000 for the bed slope of 0.0005 ft/ft cases (where the initial channel thalweg was equal to 1.0 foot), and 12 occurred at cross section 1000 for the bed slope of 0.001 ft/ft cases (where the initial channel thalweg was equal to 1.0 foot).

In the maximum/minimum tables produced by HEC-6T for the end of the run maximum scour (minimum elevation at a cross section) for all of the test cases, there were 33 cell values showing “***” instead of values for the maximum scour. Of these 31 values, 25 occurred at cross section 2000 for the bed slope of 0.0005 ft/ft cases (where the initial channel thalweg was equal to 1.0 foot), and 5 occurred at cross section 1000 for the bed slope of 0.001 ft/ft cases (where the initial channel thalweg was equal to 1.0 foot). The remaining three occurred sporadically throughout test case runs for bed slope of 0.01 ft/ft cases (2 at cross section 2000 and 1 at cross section 0), the inherently most stable of the test cases due to the high slopes and high velocities.

Finally, many of the 50-cfs simulations did not produce any significant scour or deposition. For these runs, and any other runs where no scour or deposition occurred, the data were rejected for further consideration and missing data delimiters were used. A total of 31 of the deposition runs and 103 of the scour runs were eliminated for this reason. The 103 runs that were eliminated from the analysis due to little or no scour occurring in these runs are shown in Table F-2 of Appendix F. The 31 runs that were eliminated from the analysis due to little or no deposition occurring in these runs are shown in Table F-3 of Appendix F.

3.4.1 Data Transformation

A Box-Cox analysis of the two RMSE terms (scour and deposition) indicated that an accurate statistical analysis would require a logarithmic transformation. This is fairly common for data generated from complex processes, and hence is not a surprising result for the current effort.

3.4.2 Descriptive Statistics

A number of descriptive statistics are shown in Table 3-5 for the both the raw and transformed RMSE results.

In general, the deposition RMSE is quite a bit higher than the scour RMSE, with means of 1.81 feet and 0.79 feet, respectively. Moreover, the scatter of the deposition RMSE is also higher than the scour RMSE, reflected by both a greater range of values (19.91 feet versus 6.79 feet respectively), as well as a greater standard deviation (4.21 feet versus 1.41 feet, respectively). Transforming those data result in better agreement between the deposition and scour statistics (columns 3 and 4).

Table 3-5. Test case descriptive statistics

Variable	Deposition RMSE	Scour RMSE	log ₁₀ Deposition RMSE	log ₁₀ Scour RMSE
N	405	405	405	405
Eliminated Runs	31	103	31	103
Effective N	374	302	374	302
Minimum	7.24E-06 ft	4.68E-05 ft	-4.33	-5.14
Mean	1.813	0.79 ft	-1.19	-1.20
Median	0.069 ft	0.041 ft	-1.16	-1.40
Maximum	19.91 ft	6.79 ft	1.30	0.83
Mean Standard Error	0.22 ft	0.081 ft	0.068	0.067
Standard Deviation	4.21 ft	1.41 ft	1.31	1.21
Variance	17.74 ft ²	1.98 ft ²	1.73	1.46

3.4.3 MANOVA Analysis Results

The inherent danger to any study with multiple dependent and independent variables is the tendency for one or more of the variables to appear significant when in reality they are not. That is, as the number of variables increase, so does the probability that an apparent, but not real, relationship between at least one of the independent and dependent variables will be indicated.

The way to avoid this problem is to initially analyze the data globally. If significant variables are then identified, more focused tests can then be used to further analyze their effects. For multiple independent variables and one dependent variable, an Analysis of Variance (ANOVA) test is used. When there are multiple independent and dependent variables, as is the case here, a MANOVA test is used.

Therefore, the log₁₀ transformed RMSE values were initially analyzed using the general MANOVA analysis with six independent variables and two dependent variables (log₁₀ scour RMSE and log₁₀ deposition RMSE). Minitab (release 14.20) was used for the computations.

The results of this analysis, as shown in Table 3-6 below, found all factors to be highly significant ($P < 0.0005$), indicating that the HEC-RAS and the HEC-6T models yield significantly different scour and deposition predictions across the entire spectrum of independent variables considered here. The well-behaved residuals (Figure 3-2 and Figure 3-3) indicate that the results adequately follow a normal distribution, consistent with the MANOVA testing assumptions.

Table 3-6. MANOVA testing results for the full test case database

MANOVA for Qsed						
s = 2	m = -0.5	n = 128.5				
Criterion	Test	F	Num	DF	Denom	P
Wilks'	Statistic	18.750	4	518	518	0.000
Lawley-Hotelling	0.31054	20.030	4	516	516	0.000
Pillai's	0.23696	17.473	4	520	520	0.000
Roy's	0.31052					
MANOVA for F						
s = 2	m = -0.5	n = 128.5				
Criterion	Test	F	Num	DF	Denom	P
Wilks'	Statistic	22.562	4	518	518	0.000
Lawley-Hotelling	0.72527	24.399	4	516	516	0.000
Pillai's	0.27511	20.734	4	520	520	0.000
Roy's	0.37691					
MANOVA for Gbed						
s = 2	m = 0.5	n = 128.5				
Criterion	Test	F	Num	DF	Denom	P
Wilks'	Statistic	43.021	8	518	518	0.000
Lawley-Hotelling	0.36097	52.362	8	516	516	0.000
Pillai's	1.62361	34.387	8	520	520	0.000
Roy's	0.69198	1.52759				
MANOVA for q						
s = 2	m = -0.5	n = 128.5				
Criterion	Test	F	Num	DF	Denom	P
Wilks'	Statistic	147.609	4	518	518	0.000
Lawley-Hotelling	0.21839	230.062	4	516	516	0.000
Pillai's	3.56685	83.858	4	520	520	0.000
Roy's	0.78424	3.56346				
MANOVA for s						
s = 2	m = -0.5	n = 128.5				
Criterion	Test	F	Num	DF	Denom	P
Wilks'	Statistic	248.640	4	518	518	0.000
Lawley-Hotelling	0.11728	477.978	4	516	516	0.000
Pillai's	7.41051	105.573	4	520	520	0.000
Roy's	0.89631	7.39484				

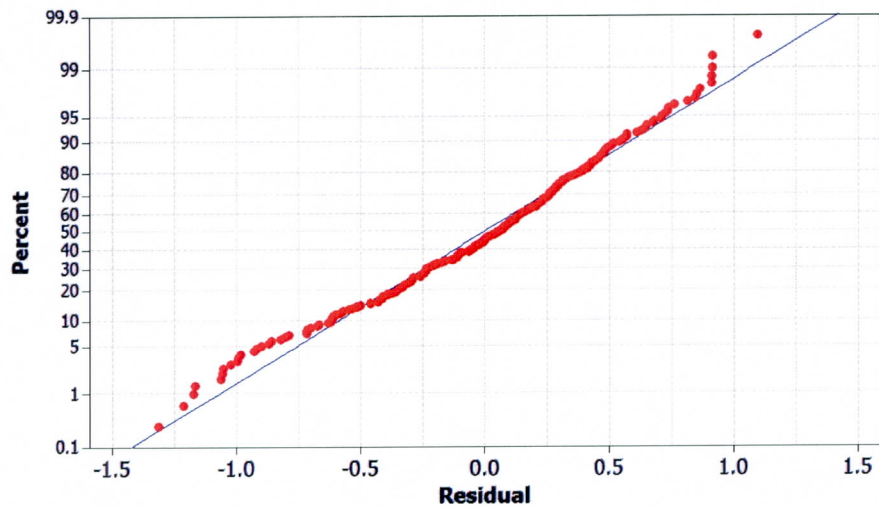


Figure 3-2. Log₁₀ transformed deposition normal fit

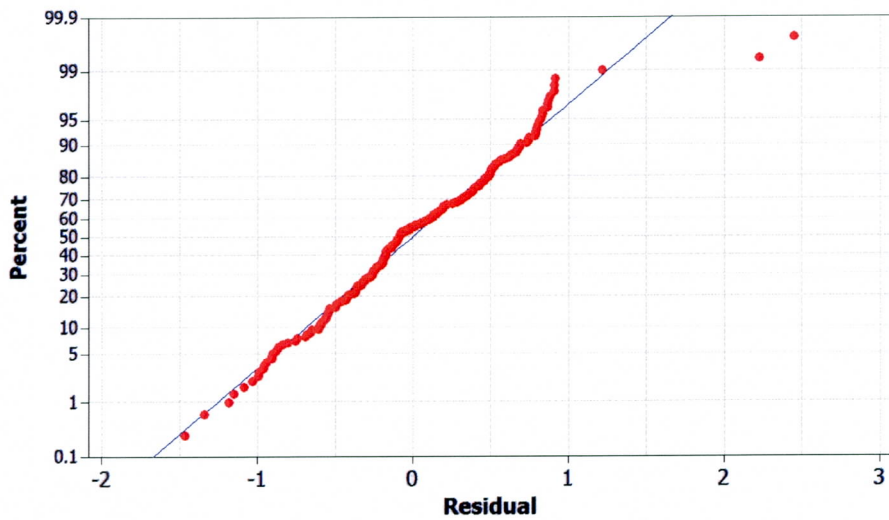


Figure 3-3. Log₁₀ transformed scour normal fit

When a global analysis indicates significant interactions between the independent variables, a more focused consideration is then justified. With the MANOVA results highly significant, the next refinement is to consider individual ANOVA tests for the log₁₀ Scour RMSE and the log₁₀ Deposition RMSE. Accordingly, these were conducted and the results reported and discussed in sections 3.5 (scour results) and 3.6 (deposition results).

3.5 Scour Effects

3.5.1 Overall

The \log_{10} Scour RMSE ANOVA test results are shown below. The analysis indicates that there are not significant differences between HEC-RAS and HEC-6T in terms of F and Q_{sed} . The other factors are highly significant however ($p < 0.0005$) indicating that the different approaches taken by the programs to account for gradation, flows, and slopes cause nontrivial differences in scour predictions.

Table 3-7. Scour ANOVA testing

Source	DF	Seq SS	Adj SS	Adj MS	F	P
Qsed	2	0.434	1.047	0.524	1.71	0.184
F	2	7.055	0.355	0.177	0.58	0.562
Gbed	4	75.781	116.696	29.174	95.04	0.000
q	2	72.383	140.198	70.099	228.35	0.000
S	2	195.425	195.425	97.713	318.31	0.000
Error	289	88.716	88.716	0.307		
Total	301	439.794				

S = 0.554054 R-Sq = 79.83% R-Sq(adj) = 78.99%

3.5.2 Main Effects

Figure 3-4 below shows the main effects for the scour analysis. Consistent with the hypothesis testing, the Q_{sed} and F factors show little effect on the overall RMSE. However, the other factors are more significant. The gradation effect is highest for low values but then decreases by more than an order of magnitude. In an opposite trend, q and S both increase RMSE by more than an order of magnitude over the tested ranges.

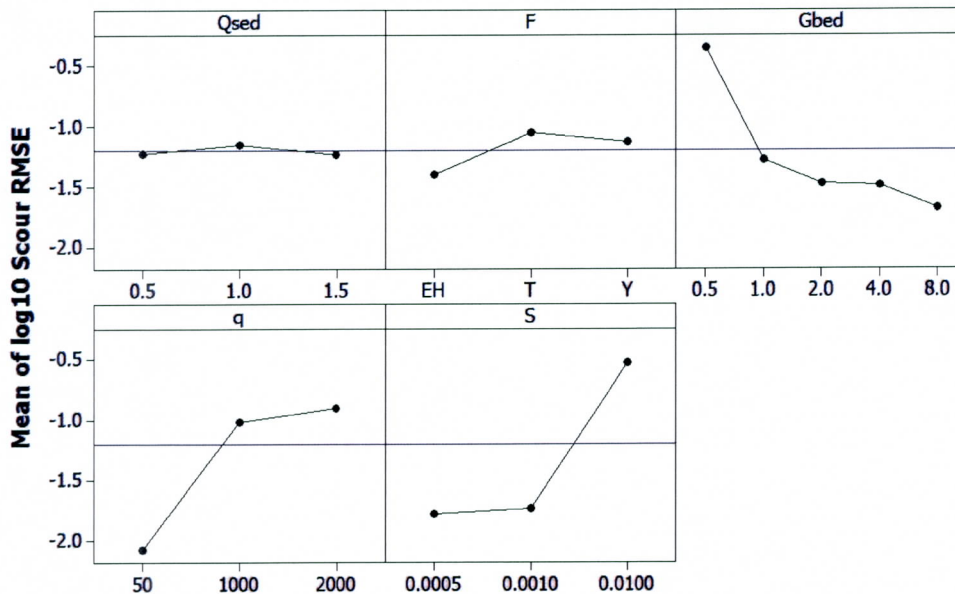


Figure 3-4. Scour main effects

3.5.3 Interaction Effects

Figure 3-5 below shows the interaction effects between the independent variables and predicted scour RMSE. Generally speaking, the interaction effects appear to be minimal, with the lines in each graph each following more or less the same path. The exceptions all involve the G_{bed} variable, specifically the lowest gradation of 0.5. These effects are:

1. The $0.5Q_s$ sediment inflow corresponds to the highest Scour RMSE for low G_{bed} values, but then corresponds to the lowest Scour RMSE for high G_{bed} values.
2. Likewise, the EH, Y, and T transport functions cross at several points for the different G_{bed} values before finally converging at about the same value for the highest G_{bed} value of 8.0.
3. Inspection of both the $q \times G_{bed}$ and $S \times G_{bed}$ interaction plots indicate that the scour RMSE for the lowest G_{bed} value of 0.5 is much higher than for the other G_{bed} values, with the difference increasing for higher values of q , but decreasing for higher values of S .

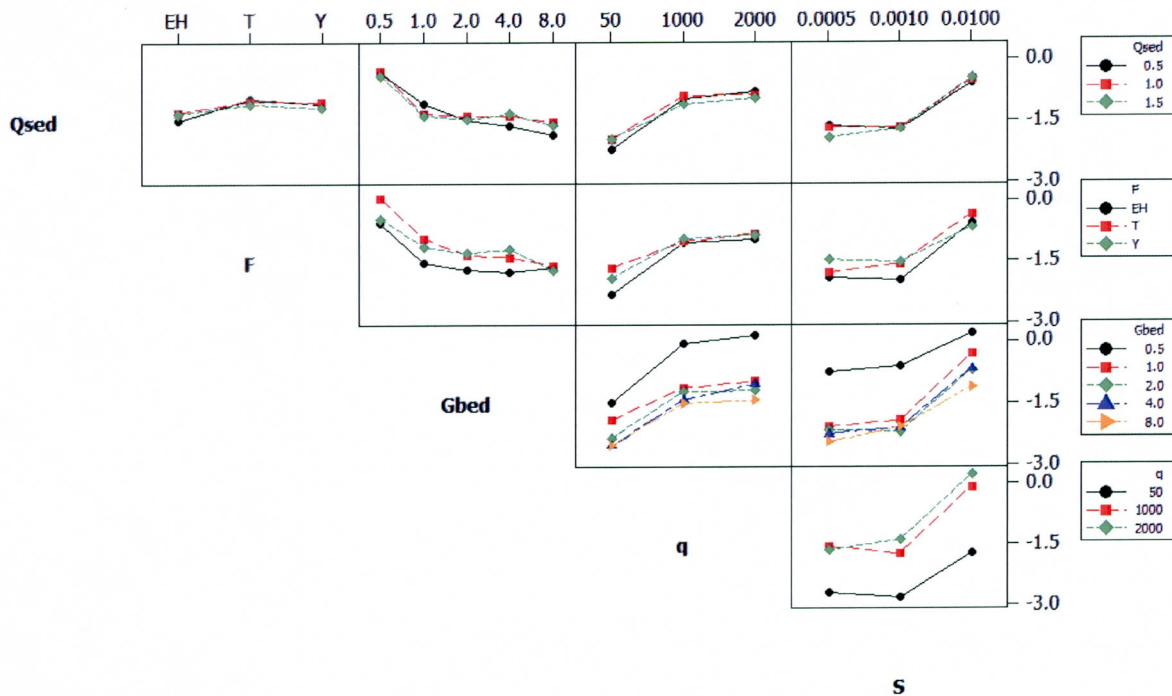


Figure 3-5. Scour interaction effects

3.6 Deposition Effects

3.6.1 Overall

The \log_{10} Deposition RMSE ANOVA test results are shown in Table 3-8 below. Unlike the scour analysis, every factor is seen to be a significant contributor to differences between the program predictions: all independent variables except gradation are significant at $p < 0.0005$; gradation is highly significant at $p < 0.005$.

Table 3-8. Deposition ANOVA testing

Source	DF	Seq SS	Adj SS	Adj MS	F	P
Qsed	2	6.916	16.037	8.019	34.98	0.000
F	2	16.605	27.862	13.931	60.77	0.000
Gbed	4	2.401	3.622	0.906	3.95	0.004
q	2	167.669	186.811	93.405	407.45	0.000
S	2	368.358	368.358	184.179	803.42	0.000
Error	361	82.757	82.757	0.229		
Total	373	644.706				

S = 0.478794 R-Sq = 87.16% R-Sq(adj) = 86.74%

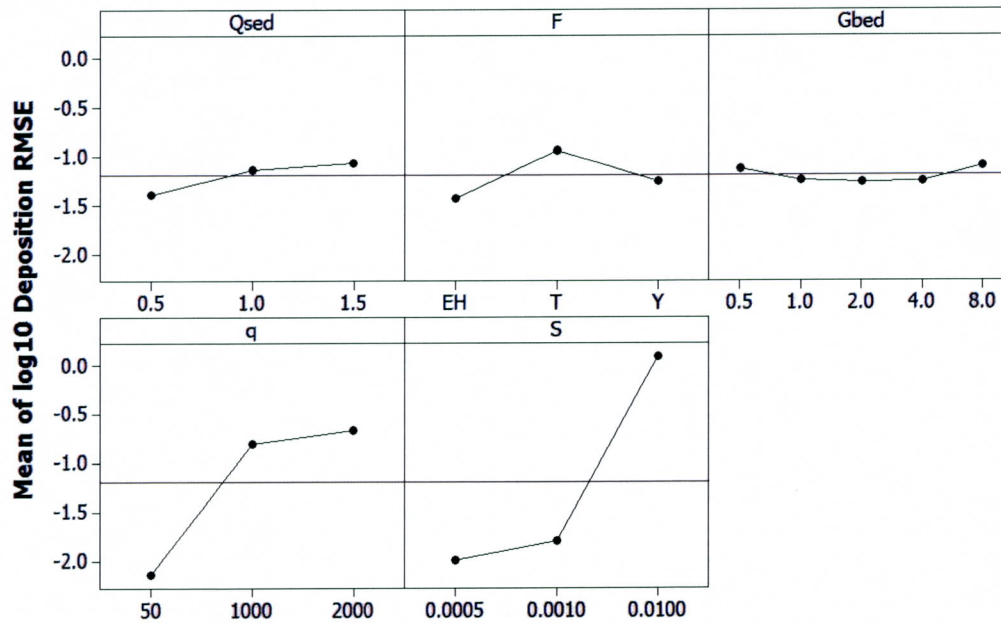


Figure 3-6. Deposition main effects

3.6.2 Main Effects

As seen in Figure 3-6, although the ANOVA analysis indicated that all of the independent variables were significant factors, from a practical standpoint only the q and S variables affect the deposition RMSE non-trivially, with the difference increasing by an order of magnitude over the range of tested flow values, and increasing by more than two orders of magnitude when the S increases from 0.05% to 1%. In particular, it should be noted that the slope effect causes more than a 1 ft RMSE error for $S = 1\%$.

3.6.3 Interaction Effects

Like the effects seen in the Scour RMSE data, it appears that the bed gradation is the most significant contributor to the interaction effects (Figure 3-7). In particular, EH data in the $F \times G_{bed}$ interaction significantly decreases with increasing values of G_{bed} changing from the highest RMSE at $G_{bed} = 0.5$ to the lowest RMSE at $G_{bed} = 8.0$. For the $G_{bed} \times q$ interaction, the $G_{bed} = 0.5$ data is seen to correspond to the highest Deposition RMSE values for $q = 50$ cfs and 2000 cfs, but corresponds to the lowest RMSE for $q = 1000$ cfs.

The transport function variable is seen to also be a part of another significant interaction with q , wherein the EH data changes from corresponding to the highest RMSE for low q values, to the lowest RMSE value at the highest q .

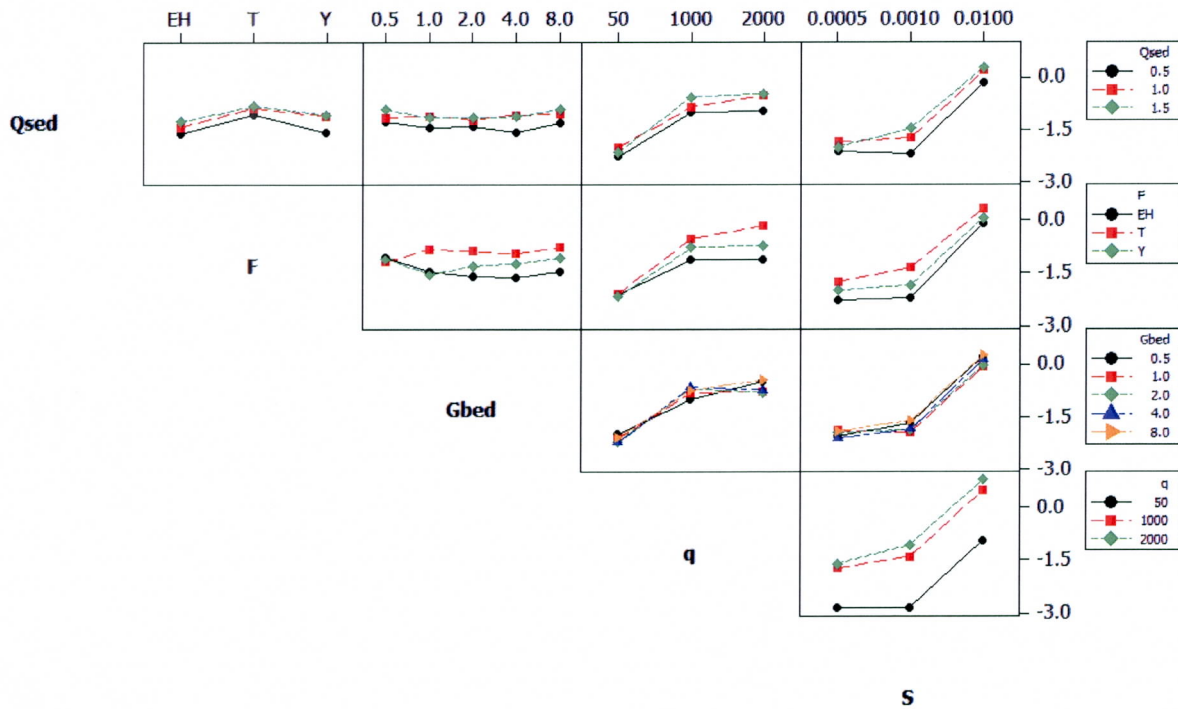


Figure 3-7. Deposition interaction effects

3.7 Comparison of Test Case Modeling Output to Brownlie's Dataset

Brownlie (1981a) compiled a large sediment transport database, as Brownlie states, "...in an attempt to provide a historically complete set of alluvial channel observations." This database is a compilation of data from 79 different datasets (55 from laboratory experiments and 24 from field tests and observations) totaling 7,027 records (5,263 laboratory data records and 1,764 field data records). Huybrechts (2008) extracted a subset of the Brownlie dataset and provided maximum and minimum values of various sediment transport parameters from this subset of data, including sediment discharge, median particle diameter, energy grade slope, and water discharge. From the Huybrechts data, the maximum and minimum values of sediment loading compared to the maximum and minimum values of median particle diameter, energy grade slope, and water discharge are shown in Figure 3-8, Figure 3-9, and Figure 3-10, respectively. Lines are shown on each of these plots as estimates of the envelope boundaries of the subset of Brownlie data (Huybrechts, 2008). These "Huybrechts envelopes," as they will be referenced for the remainder of the report, were developed by developing a logarithmic regression of the Huybrechts data, and then offsetting that regression to pass through the upper or lower data outlier. In other words, the Huybrechts envelopes were developed such that all of the Brownlie data taken from Huybrechts (2008) fall within the Huybrechts envelopes.

The final sediment discharge at the end of the test case runs (representing a quasi-equilibrium state) are plotted against median particle diameter, energy grade slope, and water discharge for all of the test cases in Figure 3-11, Figure 3-12, and Figure 3-13, respectively. The Huybrechts envelopes are shown as well. It is seen that some points fall outside of the range of the envelopes. It should be noted, however, that the lower envelope corresponds to approximately 10 mg/L. This concentration is very low, and it can be argued that any values below this number are inconsequential. That is, numerical sediment transport models will calculate very small loading rates for situations in which very low shear stresses occur; however, these sediment loadings can be ignored in general.

Note however, that the high Huybrechts envelope is also exceeded regularly on all three plots. These high concentrations primarily correspond to the test case scenarios for bed slopes of 0.01. As can be seen in Figure 3-9, the maximum energy grade slope represented in the subset of Brownlie data used for these figures (Huybrechts, 2008) is approximately 0.003, well below the 0.01 of the maximum bed slope of the test cases. Thus, a fair comparison between the data and the Huybrechts envelopes requires that data associated with the 0.01 bed slope test case runs be removed from the comparison. This will ensure that a direct comparison in the test case runs and the Brownlie data is carried out. Accordingly, the results for the test cases with bed slopes of 0.0005 or 0.001 are shown in Figure 3-14, Figure 3-15, and Figure 3-16, representing sediment discharge plotted against (a) median particle diameter, (b) energy grade slope, and (c) water discharge, respectively. As can be seen from these final three plots, the data calculated for the test cases falls below the upper Huybrechts envelope. Since the results of the test case runs as shown in Figure 3-14, Figure 3-15, and Figure 3-16 fall within the upper Huybrechts envelopes, and the data below the lower Huybrechts envelopes are largely inconsequential in sediment transport modeling studies, the results of the test case runs for all of the sediment transport models and all of the sediment transport functions tested appear to be reasonable as compared to data collected from rivers and laboratory tests around the world.

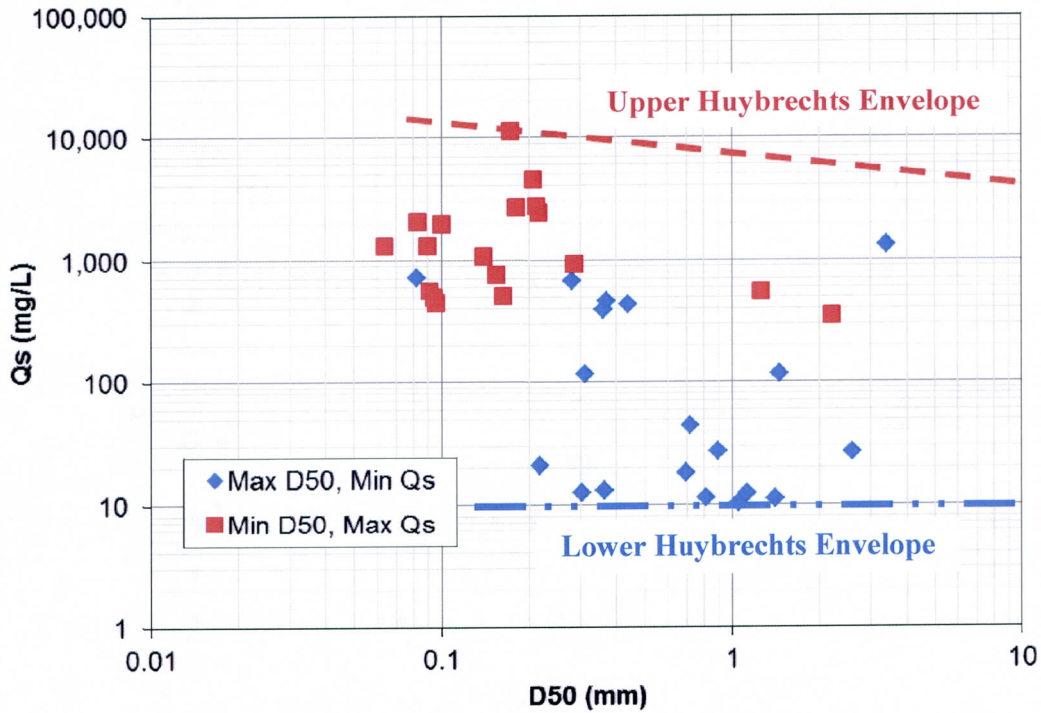


Figure 3-8. Minimum and maximum D_{50} values plotted against minimum and maximum sediment loadings from a subset of Brownlie's database

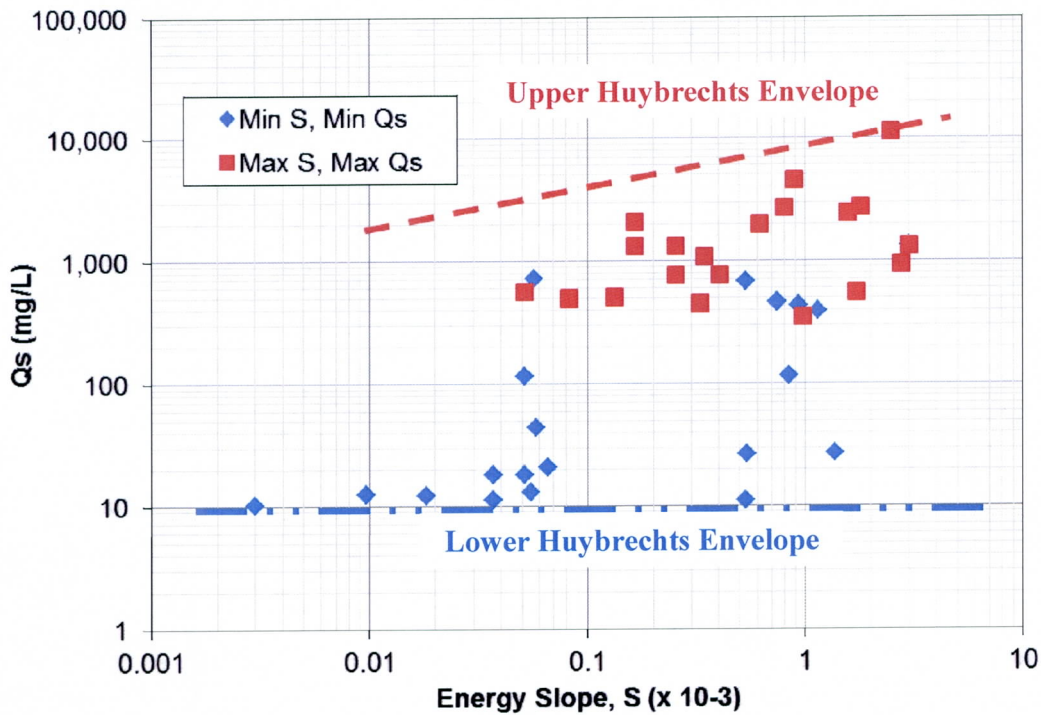


Figure 3-9. Minimum and maximum energy slope values plotted against minimum and maximum sediment loadings from a subset of Brownlie's database

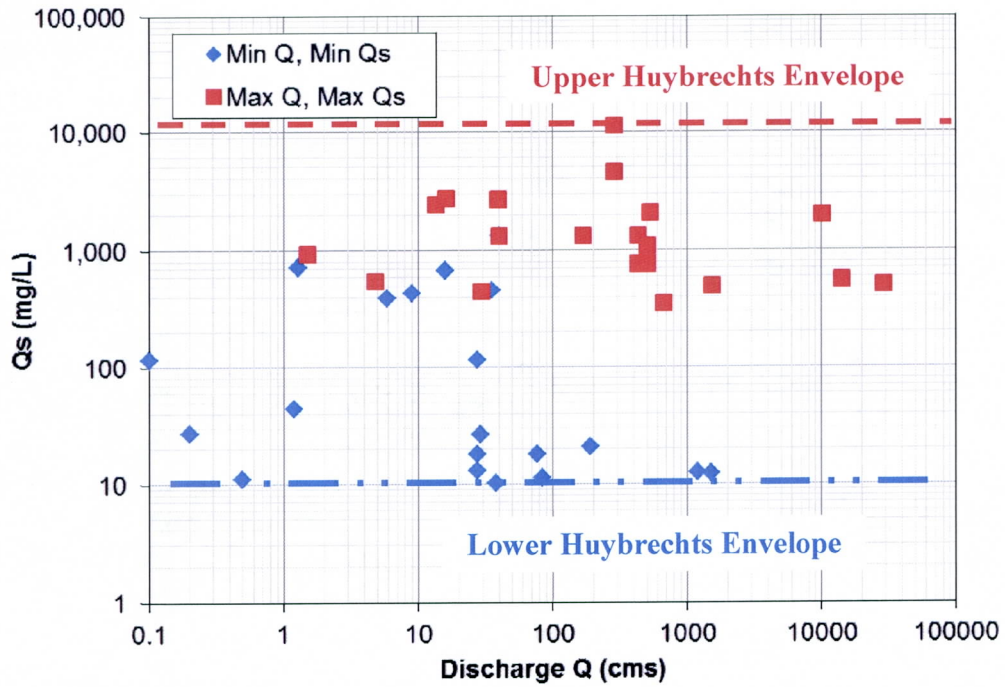


Figure 3-10 Minimum and maximum water discharge values plotted against minimum and maximum sediment loadings from a subset of Brownlie's database

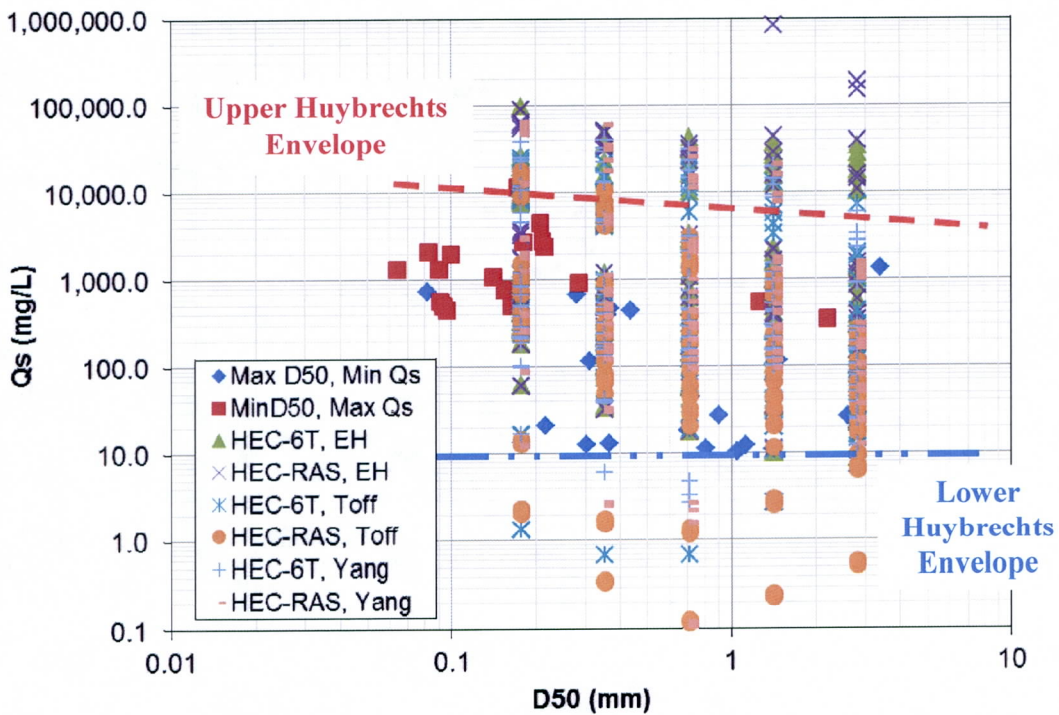


Figure 3-11 Results of all of the test case runs compared to minimum and maximum D50 values and sediment loadings from a subset of Brownlie's database

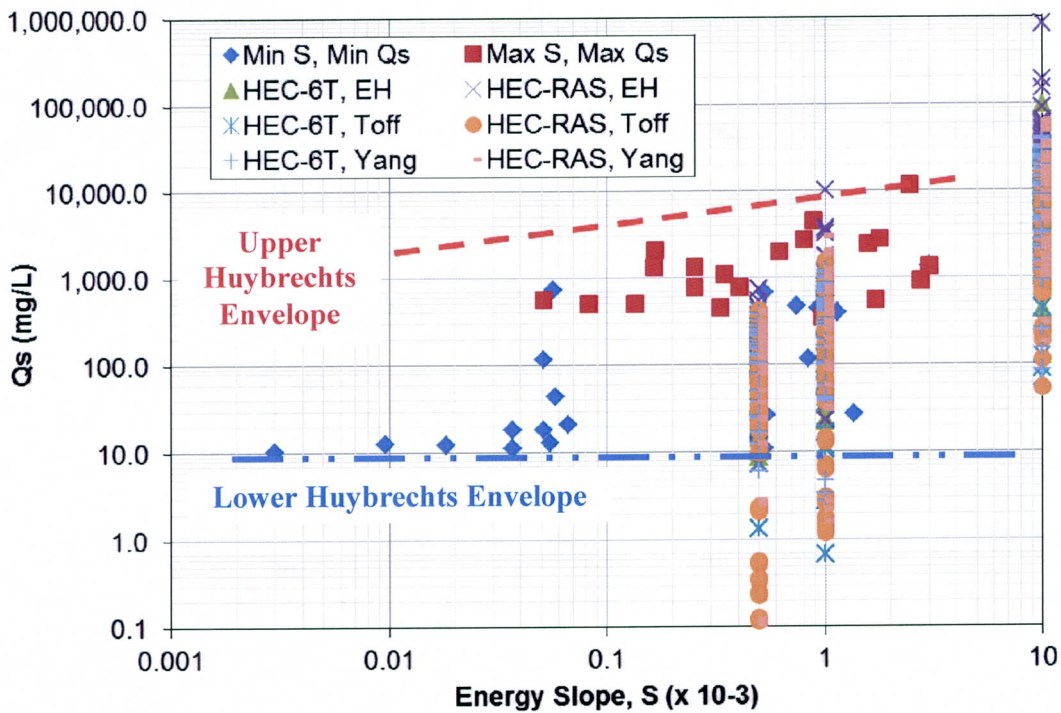


Figure 3-12 Results of all of the test case runs compared to minimum and maximum energy slope values and sediment loadings from a subset of Brownlie's database

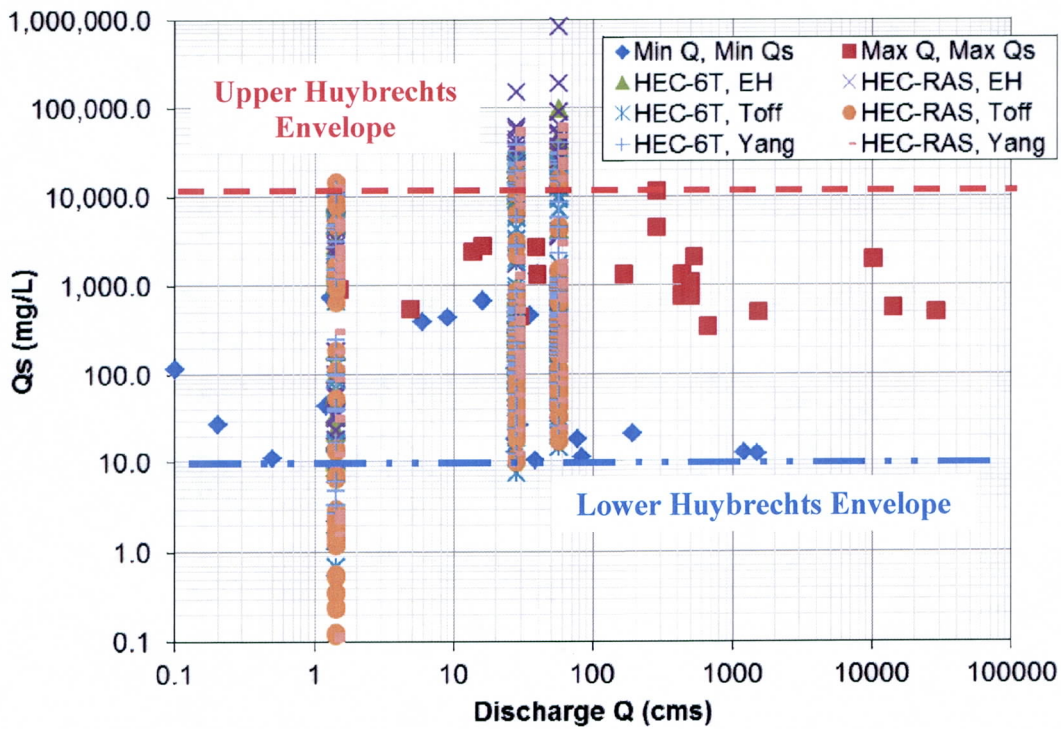


Figure 3-13 Results of all of the test case runs compared to minimum and maximum water discharge values and sediment loadings from a subset of Brownlie's database

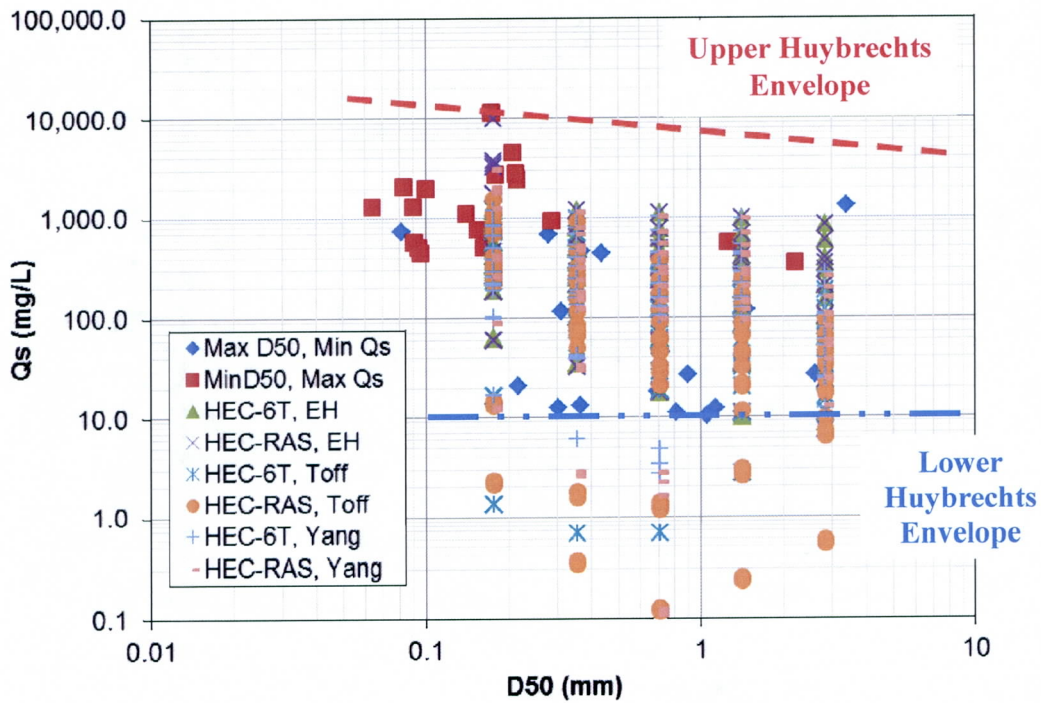


Figure 3-14 Results of the test case runs for $S = 0.0005$ and $S = 0.001$ compared to minimum and maximum D50 and sediment loadings from a subset of Brownlie's database

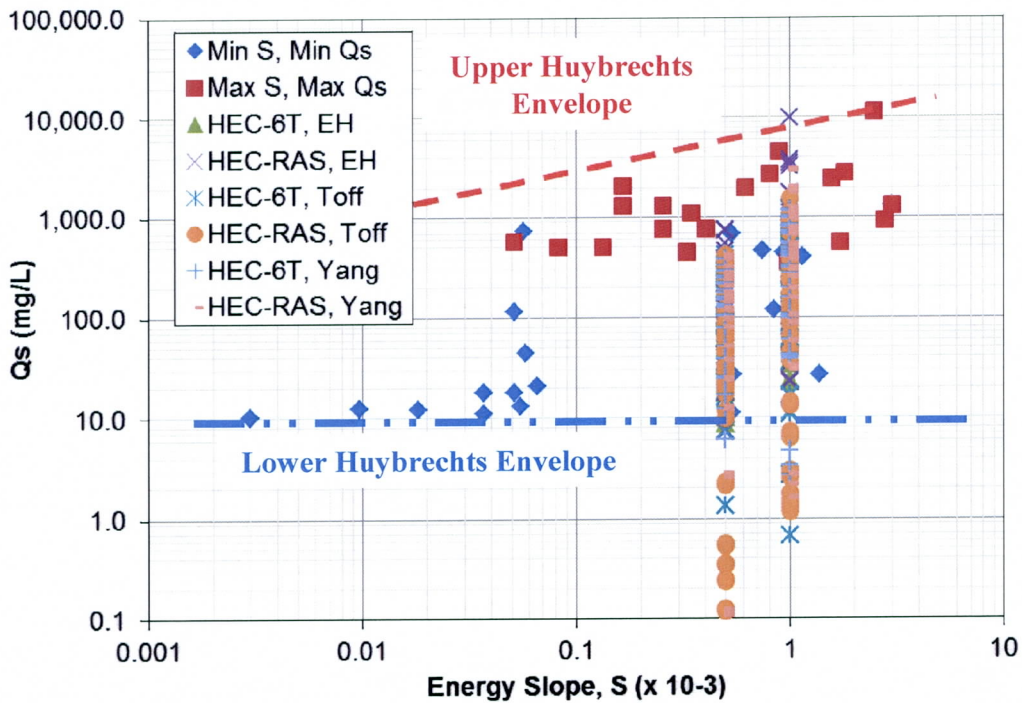


Figure 3-15 Results of the test case runs for $S = 0.0005$ and $S = 0.001$ compared to minimum and maximum energy slope values and sediment loadings from a subset of Brownlie's database

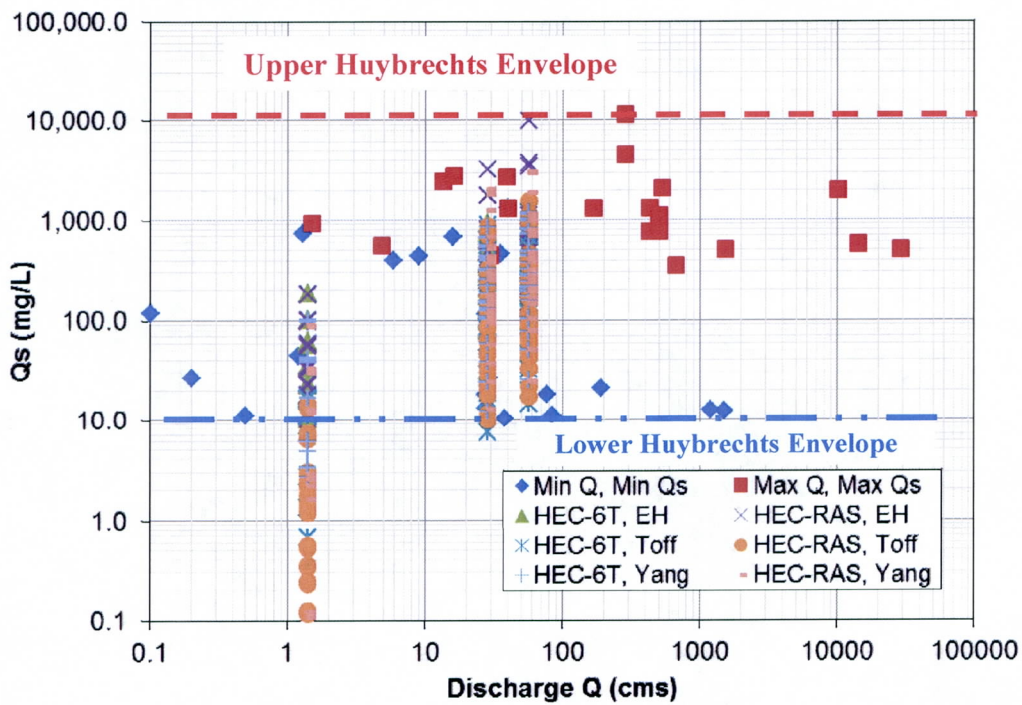


Figure 3-16 Results of the test case runs for $S = 0.0005$ and $S = 0.001$ compared to minimum and maximum water discharge values and sediment loadings from a subset of Brownlie's database

4 Conclusions and Recommendations

This section will provide a concise list of conclusions from this study, as well as recommendations regarding the application of these results and possible future directions of research based on these findings.

4.1 Conclusions

- 1) Based on a comparison of three common sediment transport models (HEC-6T, HEC-RAS Sediment Transport, and SRH-1D) for the Gila River System from the confluence of the Salt and Gila Rivers to approximately 8,000 feet west of Arizona SR 85, it was determined that HEC-6T model tends to predict the greatest maximum scour, followed by SRH-1D and finally HEC-RAS, which predicts the least scour. Additionally, HEC-RAS predicts less aggradation than either HEC-6T or SRH-1D for this modeling application to the Gila River.
- 2) For the comparison models of the Gila River System, the Engelund Hansen transport function consistently predicted the greatest maximum scour and greatest maximum aggradation. The Yang transport function predicted the second-most maximum scour and maximum aggradation, while the Toffaleti transport function predicted the least maximum scour and maximum aggradation. Additionally, the estimates of maximum scour and maximum aggradation for each sediment transport function are of a similar order of magnitude for each sediment transport model. This would lead to the conclusion that the sediment transport functions compared herein (Engelund Hansen, Yang, and Toffaleti) are coded similarly in all three sediment transport models (HEC-6T, HEC-RAS, and SRH-1D, noting that SRH-1D does not include Toffaleti).
- 3) Based on a comparison of the two base sediment transport models (HEC-6T and HEC-RAS) for the Gila River System with several bridges added to the comparison models, three conclusions were reached:
 - a. Bridges affect the HEC-RAS sediment module much more significantly than bridges coded into HEC-6T; this occurs because the momentum equation or the empirical bridge hydraulics equations utilized in the steady-state hydraulics module of HEC-RAS can be explicitly computed within the sediment module of HEC-RAS as well, while HEC-6T only utilizes the backwater computations of the energy equation through bridges. Therefore, even calibration of the fixed-bed hydraulics in HEC-6T will often not influence the sediment transport of the system as significantly as a bridge entered into the bridge geometric data editor in HEC-RAS.
 - b. The overall effects of the bridges on the final sediment routing of the Gila River system based on an RMSE comparison was less than 1.0 foot, indicating that the HEC-RAS bridge routines for the momentum equation or empirical bridge hydraulics equations account for sediment passing through bridges in HEC-RAS.

- c. HEC-6T computed greater maximum scour and maximum aggradation compared to HEC-RAS for the base conditions with bridges, which is consistent to the results of the without bridge condition.
- 4) Based on a comparison of the two ultimate pit sediment transport models representing currently developed sand and gravel pits in the Gila River study reach (HEC-6T and HEC-RAS), it was concluded that HEC-6T computed greater maximum scour and maximum aggradation compared to HEC-RAS. This finding was consistent with the model runs for the geometries without the bridges and with the bridges but without the gravel pits.
- 5) Based on the test case runs completed for a trapezoidal channel and detailed statistical analyses of these results, it was concluded that sediment transport function and inflowing sediment load have little overall effect on the RMSE between the HEC-6T and HEC-RAS maximum scour calculations, whereas the other parameters (sediment gradation, water discharge, and bed slope) all have significant effects. For depositional systems, however, gradation has little overall effect on the RMSE between the HEC-6T and HEC-RAS maximum aggradation calculations, while the other parameters (inflowing sediment load, sediment transport function, water discharge, and bed slope) affect the RMSE significantly. Interaction effects are minimal for all parameters except gradation for both maximum scour and maximum aggradation.
- 6) A comparison of the quasi-equilibrium outflowing sediment loading from the trapezoidal channels of the system with a subset of data from the Brownlie dataset (Huybrechts, 2008) shows good agreement with the numerical sediment transport calculations of HEC-RAS and HEC-6T.

4.2 Recommendations on the Application of the Study Results

- 1) The maximum aggradation and degradation for each sediment transport function tested (Yang, Toffaleti, and Engelund Hansen) are of a similar order of magnitude for each sediment transport model tested (HEC-6T, HEC-RAS, and SRH-1D). This finding suggests that each of these models is generally applicable to the Gila River System. WEST recommends that consultants working with the District on sediment transport studies along the Gila River can use any or all of these sediment transport models if deemed appropriate for the particular application. Based on the general agreement of the various sediment transport functions for the sediment transport models as applied to the trapezoidal channel test cases developed herein for both aggradational and degradational alluvial systems, WEST also recommends that HEC-6T, HEC-RAS, and SRH-1D be investigated for other watercourses in Maricopa County as each of these models would likely be applicable to the range of hydraulic and sediment conditions represented in the county's rivers.
- 2) For the application of this modeling study to the Gila River system, the Engelund Hansen transport function consistently predicted the greatest maximum scour and greatest maximum aggradation; the Yang transport function predicted the second-most maximum

scour and maximum aggradation; and the Toffaleti transport function predicted the least maximum scour and maximum aggradation consistently across the various models. This is consistent with other studies that have indicated that the Engelund Hansen function would predict a higher sediment transport capacity than the Yang equation in a system with sands (Williams, 1995). Also, applying the Williams methodology for selecting a transport function for a particular system indicated that the Engelund Hansen equation is most applicable to this system, primarily due to the coarse sediment size of the bed sediment (Williams, 1995). However, no single sediment transport function can be used for every sediment transport modeling application; each individual physical system will require analysis and engineering judgment to determine the appropriate sediment transport function for each individual model.

- 3) HEC-RAS appears to show good agreement with HEC-6T predictions of headcut and tailcut erosion processes associated with sand and gravel mining pits. Currently, the District specifies that HEC-6 or HEC-6T must be used for erosion analysis in the sand and gravel mining permitting process. It appears that HEC-RAS could be utilized for this process as well for sand and gravel mining permits in the Lower Gila River, considering the good agreement shown between these two tools in the study herein. Additionally, the extensive graphical output features of HEC-RAS compared to HEC-6T may prove to be useful to the District in the review process for sand and gravel mining permits along the Lower Gila River.
- 4) The test case runs in this report provided some interesting results regarding interactions between various sediment transport modeling input parameters. The physical parameters driving the hydraulic calculations of the systems that were varied for these test runs (i.e., water discharge and bed slope) significantly affected the results for all of the sediment transport models. The model inputs directly related to sediment affected the results differently for aggradational and degradational systems, however. For rivers that are generally aggrading throughout the system, sediment bed gradation had less of an effect on the results from all of the sediment transport models, and the other sediment input parameters including inflowing sediment load and sediment transport function affect the results significantly. Conversely, for rivers that are generally degradational throughout the system, sediment transport function and inflowing sediment load had little overall effect on the results from all of the sediment transport models, and the sediment bed gradation affects the results significantly.

These findings intuitively make sense, and one can look to the Rouse dimensionless number as to the reasons why this is true. The initiation of sediment transport in a system depends on the ratio of sediment fall velocity compared to the uplift forces acting on sediment (i.e., shear stresses mobilizing and transporting sediment); this ratio is the definition of the Rouse number. If sediment fall velocity dominates the physical processes acting on sediment in the system compared to the uplift forces, the system generally will be more aggradational. While sediment size is important in determining fall velocity of sediment in the system, highly aggradational systems (i.e., systems in which fall velocity is the dominant physical process for all sediment sizes) will be much more dependent on the volume of sediment entering the system in regards to the maximum scour or deposition occurring in the system. One example of this type of

system would be a river with a very low energy grade slope where all sand-sized particles would settle out of the water column. In these systems, sediment transport function and inflowing sediment load would dictate the total volume of sediment entering the system that will eventually deposit to the bed.

On the contrary, if uplift forces acting on sediment dominate the physical processes in the system compared to fall velocity, then the bed sediment gradation will be very important in determining how much material can be eroded from the bed. In highly degradational systems, the volume of sediment in the water column (as defined upstream by the inflowing sediment load) and the sediment transport function may not be as important because the sediment transport capacity of the reach as calculated by any transport function would be greater than the volume of sediment that could be eroded from the bed to fulfill this transport capacity. Then the limiting factor of the calculations becomes the physics of uplift forces versus particle size in the bed.

As a recommendation from this finding, the District could direct that sensitivity analyses in degradational systems focus more on the effects of varying bed sediment gradations, while sensitivity analyses in aggradational systems focus more on the effects of varying inflowing sediment load and sediment transport function. In systems near equilibrium or displaying aggradational and degradational sub-reaches within the entire study reach, sensitivity analyses should focus on all of these parameters.

- 5) Both HEC-6T and HEC-RAS began having instability issues for the test case runs with a bed slope of 0.01 feet/feet. Additionally, most of the runs with instabilities were associated with larger grain sizes (4G and 8G test cases). These high values tend to extend outside the physically tested ranges of the sediment transport functions. For example, the Yang equation was developed using experimental data that has a narrower range of hydraulic parameters than the range tested for the 0.01 slope trapezoidal test cases (e.g., flow rate, flow velocity, and flow depth). This extrapolation of the applicability of the function appears to cause instabilities. Therefore, special care should be given when developing sediment transport models for high slopes and large grain sizes.
- 6) Based on the results of this study, it was shown that various one-dimensional sediment transport models estimate similar results for sediment transport capacity and volumetric sediment routing in both idealized test cases and real-world applications for the same sediment transport function. Additionally, the results of the application of the models to the Gila River in this study agree well with the results of other numerical sediment transport studies of the Gila River. However, the current District standards require that HEC-6, HEC-6T, and Fluvial-12 be utilized as the sediment transport modeling tool for numerical sediment modeling studies in Maricopa County. Based on this standard and the limited historical use of other sediment transport models for regulatory purposes in Maricopa County, the District recommends consultants continue to use HEC-6, HEC-6T, and Fluvial-12 for numerical sediment transport modeling studies. However, other models such as HEC-RAS and SRH-1D may be used with prior approval from the District.

4.3 Recommendations for Future Research Based on the Study

- 1) WEST recommends extending this analysis to include additional sediment transport functions currently available in the various models. The methodology developed herein would be useful for application to other functions included in these models. Other functions that could be tested based on the current implementation of sediment transport functions in the models include the Ackers and White function (1973), Copeland's extension (1989) of the Laursen function (1958), and the Meyer-Peter Müller function (1948). It should be noted that Meyer-Peter Müller is a bedload transport function only, and comparison between this function and other bed-material load functions would not be consistent with their intended applications.
- 2) Additionally, WEST recommends incorporating additional sediment transport models into this analysis. FLUVIAL-12, MIKE-11, and others could be incorporated into the analysis to extend the comparisons beyond HEC-6T, HEC-RAS, and SRH-1D. The methodology developed herein would be useful for application to other functions included in the models compared herein as well as functions available in additional sediment transport models.
- 3) Finally, WEST recommends extending this analysis to test the various sediment transport models and functions on other primary watercourses in Maricopa County and the entire arid southwest region. Determining the applicability of these sediment models to analyze other watercourses would provide the District with additional tools to predict sediment processes occurring in other river systems within their jurisdiction, including long-term sediment balance, impacts of sand and gravel mines for permitting purposes, impacts of capital improvement projects on sediment processes, and others.

5 References

- Ackers, P., and White, W.R. (1973). "Sediment transport: new approach and analysis," *Journal of Hydraulic Division, ASCE*, Vol. 99(11), 2041-2060.
- Brown, C. B. (1950) "Sediment transport," In: *Engineering Hydraulics*, (H. Rouse, ed.), Wiley, New York.
- Brownlie, W.R. (1981a). "Compilation of Alluvial Channel Data: Laboratory and Field," Report KH-R-43B, W.M. Keck Laboratory of Hydraulics and Water Resources, Division of Engineering and Applied Science, California Institute of Technology, Pasadena, CA.
- Brownlie, W.R. (1981b). "Prediction of flow depth and sediment discharge in open channels," Report KH-R-43A, W.M. Keck Laboratory of Hydraulics and Water Resources, Division of Engineering and Applied Science, California Institute of Technology, Pasadena, CA.
- Colby, B. R. (1964). "Practical computations of bed-material discharge," *Proceedings, ASCE*, Vol. 90, No. HY2.
- Copeland, Ronald R., and Thomas, W.A. (1989). *Corte Madera Creek Sedimentation Study, Technical Report HL 89-6*, USACE, Waterways Experiment Station, Vicksburg, MS, April.
- Copeland, Ronald R. (1990). *Waimea Sedimentation Study, Kauai, Hawaii, Numerical Model Investigation, Technical Report HL 90-3*, USACE, Waterways Experiment Station, Vicksburg, MS, May 1990.
- David Evans and Associates, Inc., 2009. *Gillespie ADMP Mapping, Phase II-Addendum, Survey Report*. Completed for Sanborn Map Company. Contract Number FCD 2007C045. Provided by the FCDMC.
- Einstein, H.A. (1950). *The bed-load function for sediment transportation in open channel flows*. U.S. Department of Agriculture, Soil Conservation Service, Technical Bulletin No. 1026.
- Engelund, F., and Hansen, E. (1967). A monograph on sediment transport in alluvial streams, Teknisk Forlag, Technical Press, Copenhagen, Denmark.
- FCDMC, 2010a. *Draft Drainage Design Manual for Maricopa County – Hydraulics*. June 2010.
- FCDMC, 2010b. *Draft Drainage Policies and Standards for Maricopa County*. July 2010.
- Federal Highways Administration. (2011). *Hydraulic Toolbox, User's Manual, Version 2.1*, FHWA Central Federal Lands, Lakewood, CO.

- Gaeuman, D., E. D. Andrews, A. Krause, and W. Smith (2009). "Predicting fractional bed load transport rates: Application of the Wilcock-Crowe equations to a regulated gravel bed river," *Water Resour. Res.*, 45, W06409, doi:10.1029/2008WR007320.
- Graf, W. H. (1970). *Hydraulics of Sediment Transport*, McGraw-Hill Book Co.
- HR Wallingford (1990). *Sediment transport, the Ackers and White theory revised*. Report SR237, HR Wallingford, England.
- Huybrechts, N. (2008). "Fully coupled 1D model of mobile-bed alluvial hydraulics: application to silt transport in the Lower Yellow River," PhD Dissertation, Universite libre de Bruxelles, Brussels, Belgium.
- Kimley-Horn and Associates, Inc. (KHA). 2001. *Sediment Trend Analysis Final Report: Agua Fria Watercourse Master Plan*. Provided by the FCDMC.
- Laursen, E. M. (1958). "The total sediment load of streams," *Journal of the Hydraulics Division*, ASCE, Vol. 84, No. HY1, p. 1530-1 to 1530-36, February 1958.
- Madden, E. B. (1963). "Channel Design for Modified Sediment Regime Conditions on the Arkansas River," Paper No. 39, Proceedings of the Federal Interagency Sedimentation Conference, Miscellaneous Publication No. 970, Agricultural Research Service, U.S. Government Printing Office, pp. 335-352.
- Madden, E.B. (1993). *Modified Laursen Method for Estimating Bed-Material Sediment Load*, U.S. Army Corps of Engineers, U.S. Army Engineer Waterways Experiment Station, Contract report HL-93-3.
- Meyer-Peter, E., and Müller, R. (1948). "Formulas for bed-load transport," *International Association of Hydraulic Research*, 2nd Meeting, Stockholm.
- Mobile Boundary Hydraulics, PLLC. (2006). *Sedimentation in Stream Networks (HEC-6T)*, Engineering Description corresponding to Version 05.13.22.08t, Clinton, Mississippi.
- Parker, G., Klingeman, P. C., and McLean, D. G. (1982). "Bed Load and Size Distribution in Paved Gravel-Bed Streams," *Journal of the Hydraulics Division*, ASCE, 108(HY4), 544-571.
- Parker, G. (1990). "Surface based bedload transport relationship for gravel rivers," *Journal of Hydraulic Research*, Vol. 28(4), 417-436.
- Proffitt, G.T., and Sutherland, A.J. (1983). "Transport of Non-Uniform Sediments," *Journal of Hydraulic Research*, 21(1), 33-43.
- River Research and Design, Inc. (R2D), 2006. *Cotton Lane Bridge/King Ranch Floodplain Redelineation: Gila River, Goodyear, Arizona*. Completed for S.D. Construction, L.L.C. Provided by the FCDMC.

- Schoklitsch, A. (1930). *Handbuch des Wasserbaues*, Springer, Vienna (2nd ed.), English Translation (1937) by S. Shulits.
- Singer, M.B., and T. Dunne. (2004). "Modeling Decadal Bed-Material Sediment Flux Based on Stochastic Hydrology", *Water Resources Research*, 40, W03302, doi: 10.1029/2003WR002723.
- Stantec, 2009. *Technical Memorandum: Gila River Sediment Program Phase I, Bed Material Sampling Plan*. Provided by the FCDMC.
- Stantec, 2003. *El Rio Watercourse Master Plan and Area Drainage Master Plan*. Contract Number FCD 2001C024. Provided by the FCDMC.
- Strickler, A. (1923). "Beitrage zur Frage der Geschwindigkeitsformel und der Rauheitszahlen fur Strome, Kanale und geschlossene Leitungen" ("Some Contributions to the Problem of the Velocity Formula and Roughness Factors for Rivers, Canals, and Closed Conduits"), *Mitteilungen des eidgenossischen Amtes fur Wasserwirtschaft, Bern, Switzerland*, No. 16.
- Toffaleti, F. B. (1968). "A Procedure for Computation of Total River Sand Discharge and Detailed Distribution, Bed to Surface," *Committee on Channel Stabilization, U.S. Army Corps of Engineers*, November 1968.
- Vanoni, V. (ed.). (1975). *Sedimentation Engineering, ASCE Manual 54*, ASCE, New York.
- WEST Consultants, Inc., 2004. *PED Hydraulic Design of Tres Rios North Levee, Maricopa County: Pre-Final Project Analysis*. Completed for the Los Angeles District of the U.S. Army Corps of Engineers. Provided by the FCDMC.
- Wilcock, P.R. (2001). "Toward a Practical Method for Estimating Sediment-Transport Rates in Gravel Bed Rivers," *Earth Surface Processes and Landforms*, 26:1395-1408.
- Wilcock, P.R., and Crowe J.C. (2003). "Surface-Based Transport Model for Mixed-Size Sediment," *Journal of Hydraulic Engineering, ASCE*, 129(2):120-128.
- Williams, D.T. (1995). "Selection and Predictability of Sand Transport Relations Based upon a Numerical Index," *PhD Dissertation, Colorado State University, Fort Collins, Colorado*.
- Wong, M. and G. Parker (2006). "Reanalysis and Correction of Bed Load Relation of Meyer-Peter and Muller Using Their Own Database," *J. Hydraulic Engineering, ASCE*, Vol. 132(11). p.1159-1168.
- Wu, W., S.S.Y. Wang, and Y. Jia (2000). "Nonuniform sediment transport in alluvial rivers," *Journal of Hydraulic Research*, Vol. 38(6):427-434.
- Yang, C.T. (1973). "Incipient motion and sediment transport," *Journal of Hydraulic Division, ASCE*, Vol. 99(10), 1679-1704.

Yang, C.T. (1979). "Unit stream power equations for total load," Journal of Hydrology, Vol. 40, 123-128.

Yang, C.T. (1984). "Unit stream power equation for gravel," Journal of Hydraulic Division, ASCE, Vol. 110(12)1783-1797.

Yang, C.T., Molinas, A., and Wu, B. (1996). "Sediment transport in the Yellow River," Journal of Hydraulic Engineering, ASCE, Vol. 122(5), 237-244.

US Army Corps of Engineers. (2010). HEC-RAS River Analysis System, Hydraulic Reference Manual, Version 4.1.0, Hydrologic Engineering Center, Davis, CA.

US Army Corps of Engineers. (1993). HEC-6 Scour and Deposition in Rivers and Reservoirs, User's Manual, Hydrologic Engineering Center, Davis, CA.

US Bureau of Reclamation. (2010). Sedimentation and River Hydraulics in One Dimension (SRH-1D), User's Manual, Version 2.6, Technical report SRH-2010-25, Technical Service Center, Sedimentation and River Hydraulics Group, Denver, CO.

**Appendix A: Final Bed Sediment Samples
from GSRP utilized in the Sediment
Transport Modeling, and the WEST
Technical Memorandum to the District
Summarizing Data Collection**

Table A-1 Summary of sediment samples in the Salt-Gila River System used for numerical sediment transport model development

Cross Section	Location	Sample Name	Depth	Type	Sample to Use	Reason
179.5	Main channel	El Rio 1 El Rio 2	0 0	B B	Average El Rio 1 and 2	Both good samples
179.91	Left side of channel	TP-1-1.5 TP-1-4 TP-1-8.5	1.5 4 8.5	C C C	TP-1-4	Discard 1-1.5 (too coarse) and 1-8.5 (too deep)
180.75	Main channel	TP-2E-1	1	C	None	Too coarse
180.94	Main channel	TP-2B-1 TP-2B-3 TP-2B-8.5	1 3 8.5	B B B	Average TP-2B-1 and TP-2C-1	Use the two surface gradations
	Main channel	TP-2C-1 TP-2C-7.5	1 7.5	B C		
	Main channel	TP-2D-1	3	C		
182.55	Vegetated ROB	El Rio 6	0	A	None	Discard Type A
182.64	Right side of channel	El Rio 7	0	B	El Rio 7	Good sample
183.49	Vegetated ROB	TP-2C1-2 TP-2C1-10	2 10	A B	TP-2C1-10	Discard Type A
184.24	Vegetated LOB	TP-3-6	6	C	Terracon 1 (1)	Discard Terracon 1 (too coarse). Use sample next closest to surface
	Vegetated LOB	Terracon 1 (0)	0	C		
		Terracon 1 (1) Terracon 1 (bank)	1 0	B B		
185.1	Side channel (left)	Terracon 2 (0) Terracon 2 (1.75) Terracon 2 (bank)	0 1.75 0	B A A	Terracon 2 (0)	Use surface gradation
185.46	Main channel	TP-4-1 TP-4-7	4 7	B B	TP-4-1	Use surface gradation
186.1	Main channel	Terracon 3 (0) Terracon 3 (0.33) Terracon 3 (0.75) Terracon 3 (bank)	0 0.33 0.75 0	C B C C	Terracon 3 (0)	Use surface gradation
186.27	Main channel	El Rio 8	0	B	El Rio 8	Good sample
186.36	Main channel	TP-5C-2 TP-5C-10	2 10	C C	TP-5C-2	Use surface gradation
186.46	Vegetated LOB	TP-5D-1 TP-5D-10	1 10	A A	None	Discard all Type A samples

Table A-1 Summary of sediment samples in the Salt-Gila River System used for numerical sediment transport model development (cont'd)

Cross Section	Location	Sample Name	Depth	Type	Sample to Use	Reason
186.55	Vegetated ROB	TP-5A-2	2	A	Average TP-5B-4, TP-5B-7, and TP-5B-9	Discard all Type A samples
		TP-5A-8	8	A		
	Vegetated ROB	TP-5B-1	1	A		
		TP-5B-4	4	B		
		TP-5B-7	7	B		
TP-5B-9	9	B				
187.06	Main channel	Terracon 4 (0)	0	C	Terracon 4 (0)	Use surface gradation
		Terracon 4 (1)	1	C		
		Terracon 4 (bank)	0	C		
188.59	Main channel	El Rio 9	1	C	El Rio 9	Good sample
189.02	Vegetated ROB	TP-6A-1	1	A	Average TP-6B-3.5, TP-6C-2, and TP-6D-3	Use an average of the three samples closest to surface
		TP-6A-8	8	A		
	Main channel	TP-6B-3.5	3.5	C		
	Main channel	TP-6C-2	2	C		
	Main channel	TP-6D-3	3	B		
		TP-6D-9	9	B		
189.39	Right side of channel	El Rio 10	1.5	C	El Rio 10	Good sample
190.53	Main channel	WPT 169	0	C	WPT 169	Good sample
191.57	Main channel	TP-7F-1	1	B	WPT 163	Discard both TP-7F samples (mostly sand)
		TP-7F-10	10	B		
	Main channel	WPT 163	0	C		
191.67	Main channel	TP-7B-1	1	B	None	Discard 7B-1 (mostly sand) and 7B-10 (too deep)
		TP-7B-10	10	C		
191.76	Right side of channel	TP-7A-1	1	B	TP-7D-2	Discard 7A-1, 7E-2 (mostly sand) and 7A-11, 7E-6 (too deep)
		TP-7A-11	11	C		
	Main channel	TP-7D-2	2	C		
	Main channel	TP-7E-2	2	B		
TP-7E-6		6	C			
191.86	Main channel	TP-7C-3	3	C	TP-7C-3	Good sample
192.42	LOB	BA1L	5 to 10	C	BA6R	Use BA6R (in main channel and closest to surface)
	Main channel	BA5L	10 to 15	C		
		BA6R	0 to 5	C		
		BA7L	5 to 10	C		
		BA8R	10 to 15	C		
		BA15R	0 to 5	C		
ROB	BA2L	0 to 5	C			
192.79	Main channel	WPT 161	0	C	WPT 161	Good sample

Table A-1 Summary of sediment samples in the Salt-Gila River System used for numerical sediment transport model development (cont'd)

Cross Section	Location	Sample Name	Depth	Type	Sample to Use	Reason
193.53	Main channel	El Rio 11	0	C	El Rio 11	Good sample
194.02	Main channel	TP-8-1	1	C	TP-8-1	Use surface gradation
		TP-8-8	8	C		
194.20	Main channel	WPT 170	0	C	WPT 170	Good sample
195.22	Main channel	El Rio 3	0	B	CI&T 1	Discard El Rio 3 and 4 (mostly sands)
	Main channel	El Rio 4	2	B		
	Main channel	CI&T 1	0	C		
195.34	Main channel	SS01-01	0	B	SS02-02	Discard SS01-01 (mostly sand)
	Main channel	SS02-02	0	C		
195.45	LOB (by road)	El Rio 12	0	B	None	Discard sample (mostly sand)
195.55	Main channel	TP-9A-1	1	C	Average TP-9A-1 and CI&T 2	Good samples at surface
	Main channel	CI&T 2	0	C		
195.65	ROB	TP-9B-1	1	B	None	Discard sample (mostly sand)
195.86	Main channel	CI&T 3	0	C	CI&T 3	Good sample
196.08	LOB (left of gravel pit)	TP-9D-1	1	B	None	Discard samples (not in active channel)
		TP-9D-5.5	5.5	B		
		TP-9D-8	8	C		
196.23	LOB	TP-9C-1	1	B	Average SS13-02 and SS14-02	Discard 9C-1 (mostly sand)
	Unknown	SS13-02	0	C		
		SS14-02	0	C		
196.32	LOB	CI&T 4	0	C	Average CI&T 4 and SS15-02	Good samples at surface
	Unknown	SS15-02	0	C		
196.81	Island left of channel	CI&T 5	0	C	CI&T 5	Good sample
197.28	Unknown	SS17-02	0	C	Average SS17-02 and SS18-02	Good samples at surface
	Unknown	SS18-02	0	C		
197.33	Left side of channel	TP-10A-1	1	C	Average TP-10A-1 and CI&T 6	Discard 10A-8 (too deep)
		TP-10A-8	8	C		
	Left side of channel	CI&T 6	0	C		
197.53	Left side of channel	TP-10B-1	1	C	TP-10B-1	Use surface gradation
		TP-10B-8	8	C		
197.64	Left side of channel	CI&T 7	0	C	CI&T 7	Good sample
197.92	Left side of channel	CI&T 8	0	C	CI&T 8	Good sample
198.33	Main channel	TP-11-1	1	C	Average TP-11-1, SS02-03, and SS02-05	Good samples at surface
	Unknown	SS02-03	0	C		
	Unknown	SS02-05	0	C		



GILA RIVER BED MATERIAL

Date: April 29, 2011
To: Brian Wahlin, WEST Consultants
From: Christine Warren, P.E., WEST Consultants
RE: **Bed Material Input for Gila River HEC-6t Model**

This memorandum summarizes the methods WEST Consultants (WEST) used to determine the bed material input for the Gila River HEC-6t model. Sediment samples provided are summarized below as well as the process to determine bed material gradations for HEC-6t input.

The Gila River Sediment Program (GRSP) developed by Stantec Consulting (Stantec, 2009) compiled sediment data on the Gila River from State Route 85 crossing upstream 20 miles to the Salt River confluence. A total of 110 samples from seven sources were included in the GRSP and compiled into a geodatabase as listed below:

- Gila River Sediment Program, Stantec Consulting (59 samples)
- El Rio Watercourse Master Plan, Stantec Consulting (12 samples)
- Burlingame, Construction Inspection & Testing (8 samples)
- Gila River at Airport Road Crossing, Terracon (13 samples)
- Cotton Lane Bridge CLOMR, River Research and Design (4 samples)
- Cotton Lane Bridge Geotechnical and Foundation Report, Richer-Atkinson-McBee & Associates (7 samples)
- Tres Rios North Levee, Los Angeles Corps of Engineers (LACOE) (7 samples)

In addition to the sediment samples provided in the GRSP, the LACOE collected 15 more sediment samples for the Tres Rios North Levee project. These samples were also analyzed for use in the Gila River HEC -6t model.

In the GRSP, Stantec classified each sample based on its size gradation characteristics where Type A defines predominantly silt and clay material, Type B defines predominantly sand material, and Type C defines predominantly gravel and cobble material. Samples classified as Type A represent the wash load and the active bed material and therefore; the Type A samples were discarded from use in the HEC-6t input. Stantec's conclusions stated that (1) Type C is the dominant bed material for the Gila River from the confluence with the Salt River downstream to the Tuthill Bridge, and (2) Type B material occurs more frequently downstream of Tuthill Bridge. Based on these conclusions, sediment samples with gradations classified as Type B (predominantly sand) were discarded for bed material input upstream of Tuthill Bridge and sediment samples with very coarse gradations (Type C) were looked at closely downstream of Tuthill Bridge.

The geodatabase provided a spatial reference of the sediment samples and WEST associated each sample to the nearest cross section from the HEC-6t model. Some cross sections had more than one corresponding sediment sample that fit the proper material classification. When this occurred, those gradations were averaged.

The majority of sediment samples were taken at the surface (depth = 0 feet); however, some samples were taken in an excavated trench at depths up to 10 feet. For the purpose of determining the bed material input for the HEC-6t model, surface samples were prioritized over samples at greater depths because the surface samples represent the bed material that will initially be eroded. In some cases, the surface sample did not appear to provide a good representation of the bed material and a deeper sample was chosen.

Table 1 summarizes the corresponding cross section of each sediment sample along with the location of the sample relative to the main channel, the depth and material type of each sample, and the conclusion of which sample to use for bed material input for the HEC-6t model.

Table 1. Summary of Sediment Sample for Gila River.

Cross Section	Location	Sample Name	Depth	Type	Sample(s) to Use
179.5	Main channel	El Rio 1	0	B	El Rio 1
179.91	Left side of channel	TP-1-1.5	1.5	C	TP-1-4
		TP-1-4	4	C	
		TP-1-8.5	8.5	C	
182.55	Vegetated ROB	El Rio 6	0	A	None – Type A not bed material
182.64	Right side of channel	El Rio 7	0	B	El Rio 7
183.49	Vegetated ROB	TP-2C1-2	2	A	TP-2C1-10
		TP-2C1-10	10	B	
184.24	Vegetated LOB	TP-3-6	6	C	Terracon 1 (1)
	Vegetated LOB	Terracon 1 (0)	0	C	
		Terracon 1 (1)	1	B	
		Terracon 1 (bank)	0	B	
185.1	Side channel (left)	Terracon 2 (0)	0	B	Terracon 2 (0)
		Terracon 2 (1.75)	1.75	A	
		Terracon 2 (bank)	0	A	
185.46	Main channel	TP-4-1	4	B	TP-4-1
		TP-4-7	7	B	
186.1	Main channel	Terracon 3 (0)	0	C	Terracon 3 (0)
		Terracon 3 (0.33)	0.33	B	
		Terracon 3 (0.75)	0.75	C	
		Terracon 3 (bank)	0	C	
186.27	Main channel	El Rio 8	0	B	El Rio 8
186.36	Main channel	TP-5C-2	2	C	TP-5C-2
		TP-5C-10	10	C	
186.46	Vegetated LOB	TP-5D-1	1	A	None – Type A not bed material
		TP-5D-10	10	A	
186.55	Vegetated ROB	TP-5A-2	2	A	AVG of TP-5B-4, TP-5B-7, and TP-5B-9
		TP-5A-8	8	A	
	Vegetated ROB	TP-5B-1	1	A	
		TP-5B-4	4	B	
		TP-5B-7	7	B	
		TP-5B-9	9	B	

187.06	Main channel	Terracon 4 (0)	0	C	Terracon 4 (0)
		Terracon 4 (1)	1	C	
		Terracon 4 (bank)	0	C	
188.59	Main channel	El Rio 9	1	C	El Rio 9
189.02	Vegetated ROB	TP-6A-1	1	A	AVG TP-6B-3.5, TP-6C-2, and TP-6D-3
		TP-6A-8	8	A	
	Main channel	TP-6B-3.5	3.5	C	
	Main channel	TP-6C-2	2	C	
Main channel	TP-6D-3	3	B		
	TP-6D-9	9	B		
189.39	Right side of channel	El Rio 10	1.5	C	El Rio 10
191.76	Main channel	TP-7D-2	2	C	TP-7D-2
	Main channel	TP-7E-2	2	B	
		TP-7E-6	6	C	
191.86	Main channel	TP-7C-3	3	C	TP-7C-3
192.42	LOB	BA1L	5 to 10	C	BA6R
		BA5L	10 to 15	C	
	Main channel	BA6R	0 to 5	C	
		BA7L	5 to 10	C	
		BA8R	10 to 15	C	
		BA15R	0 to 5	C	
	ROB	BA2L	0 to 5	C	
193.53	Main channel	El Rio 11	0	C	El Rio 11
194.02	Main channel	TP-8-1	1	C	TP-8-1
		TP-8-8	8	C	
195.22	Main channel	El Rio 3	0	B	CI&T 1
	Main channel	El Rio 4	2	B	
	Main channel	CI&T 1	0	C	
195.34	Main channel	SS01-01	0	B	SS02-02
	Main channel	SS02-02	0	C	
195.45	LOB (by road)	El Rio 12	0	B	None – Type B not applicable
195.55	Main channel	TP-9A-1	1	C	AVG of TP-9A-1 and CI&T 2
	Main channel	CI&T 2	0	C	
195.65	ROB	TP-9B-1	1	B	None – Type B not applicable
195.86	Main channel	CI&T 3	0	C	CI&T 3
196.08	LOB (left of gravel pit)	TP-9D-1	1	B	None – samples not in active channel
		TP-9D-5.5	5.5	B	
		TP-9D-8	8	C	
196.23	LOB	TP-9C-1	1	B	AVG of SS13-02 and SS14-02
	Unknown	SS13-02	0	C	
		SS14-02	0	C	
196.32	LOB	CI&T 4	0	C	AVG of CI&T 4 and SS15-02
	Unknown	SS15-02	0	C	
196.81	Island left of channel	CI&T 5	0	C	CI&T 5

197.28	Unknown	SS17-02	0	C	AVG of SS17-02 and SS18-02
	Unknown	SS18-02	0	C	
197.33	Left side of channel	TP-10A-1	1	C	AVG of TP-10A-1 and CI&T 6
		TP-10A-8	8	C	
197.53	Left side of channel	TP-10B-1	1	C	TP-10B-1
		TP-10B-8	8	C	
197.64	Left side of channel	CI&T 7	0	C	CI&T 7
197.92	Left side of channel	CI&T 8	0	C	CI&T 8
198.33	Main channel	TP-11-1	1	C	AVG of TP-11-1, SS02-03, and SS02-05
	Unknown	SS02-03	0	C	
	Unknown	SS02-05	0	C	
201.48	Unknown	SS02-08	0	C	SS02-08
202.4	Unknown	SS21-02	0	C	SS21-02
203.38	Unknown	SS22-02	0	C	AVG of SS22-02 and SS23-02
	Unknown	SS23-02	0	C	

**Appendix B: Sediment transport functions
available in common 1-dimensional sediment
transport models**

Table B-1 Sediment transport functions available in common 1-dimensional sediment transport models

Model	Available Functions	Notes*
HEC-RAS	Ackers and White (1973)	BML
	Copeland's (1989) modification of Laursen's (1958) relationship	BML
	Engelund and Hansen (1967)	BML (primarily sand)
	Meyer-Peter and Müller (1948)	BL
	Toffaletti (1968)	BML (primarily sand)
	Wilcock (2001)	BL
	Yang's stream power (1973 for sand, 1984 for gravel)	BML
HEC-6	Ackers and White (1973)	BML
	Colby (1964)	BML (primarily sand)
	Copeland's (1990) modification of Laursen's (1958) relationship (Copeland and Thomas 1989)	BML
	DuBoy (Vanoni 1975, originally from Brown 1950)	BL
	Madden's (1963) modification of Laursen's (1958) relationship	BML
	Madden's (1985, unpublished) modification of Laursen's (1958) relationship	BML
	Meyer-Peter and Müller (1948)	BL
	Toffaletti (1968)	BML (primarily sand)
	Toffaletti (1968) and Meyer-Peter and Müller (1948) combination	BML
	Toffaletti (1968) and Schoklitsch (1930) combination	BML
	Yang's stream power for sands (1973)	BML (primarily sand)
User-specified function		
HEC-6T	Ackers and White (1973)	BML
	Brownlie (with transport normalized to a D_{50} value) (1981b)	BML (primarily sand)
	Brownlie (with transport calculated for each grain size) (1981b)	BML (primarily sand)
	Colby (1964)	BML (primarily sand)
	Copeland's (1990) modification of Laursen's relationship (Copeland and Thomas 1989)	BML
	DuBoy (Vanoni 1975, originally from Brown 1950)	BL
	Einstein (1950)	BML
	Engelund and Hansen (1967)	BML (primarily sand)
	Madden's (1963) modification of Laursen's (1958) relationship	BML
	Madden's (1985, unpublished) modification of Laursen's (1958) relationship	BML
	Meyer-Peter and Müller (1948)	BL
	Parker (1990)	BL
	Profitt and Sutherland (1983)	BML

*BL = bedload transport equation, BML = total bed-material load transport equation

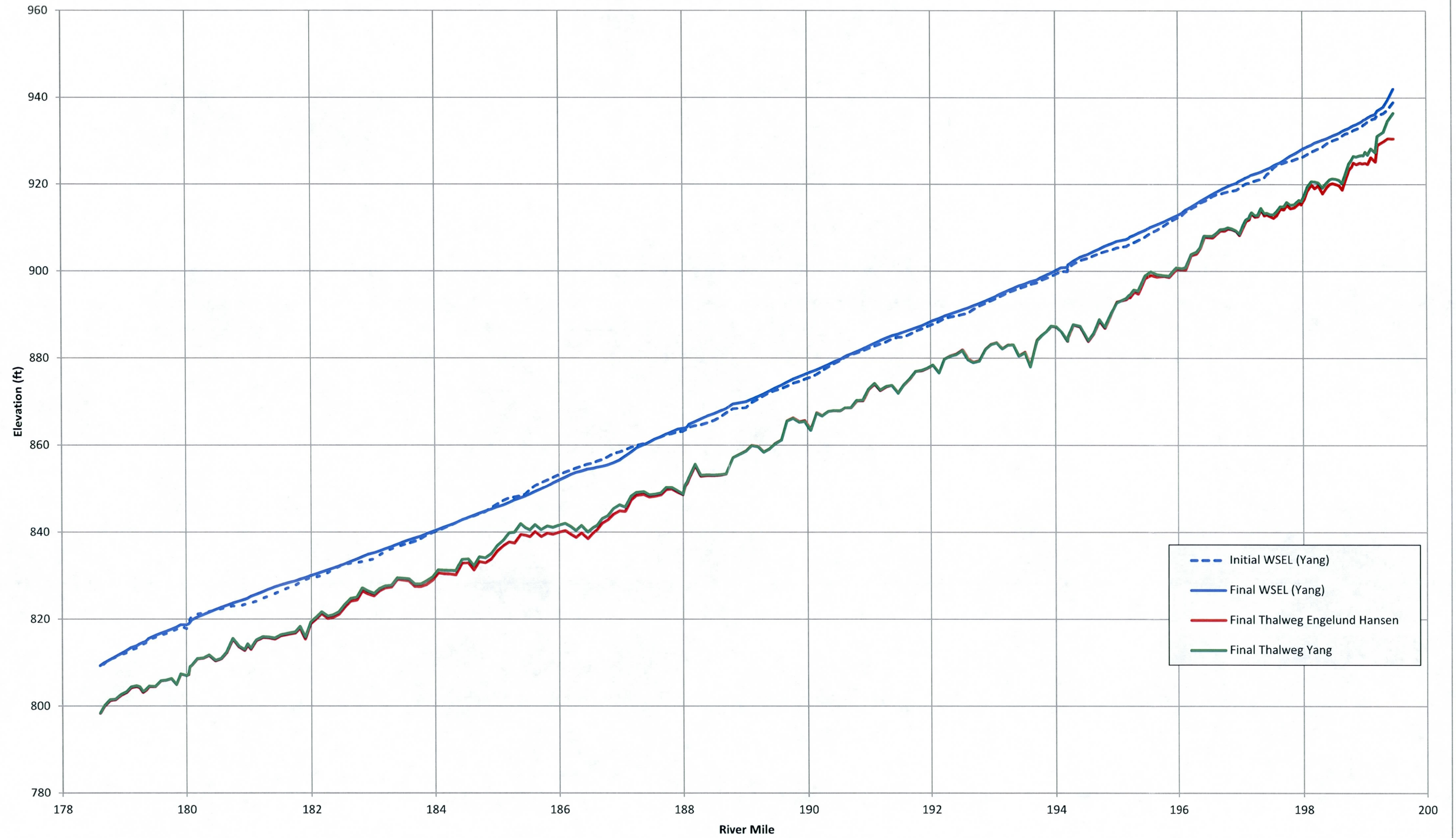
Table B-1 Sediment transport functions available in common 1-dimensional sediment transport models (cont'd)

Model	Available Functions	Notes*
HEC-6T (cont'd)	Toffaletti (1968)	BML (primarily sand)
	Toffaletti (1968) and Meyer-Peter and Müller (1948) combination	BML
	Toffaletti (1968) and Schoklitsch (1930) combination	BML
	Yang's stream power for sands (1973)	BML (primarily sand)
	Yang et al. stream power (1996 for sand w/ high wash load concentration)	BML (primarily sand)
	Wilcock (2001)	BL
	User-specified function	
FLUVIAL-12	Ackers and White (1973)	BML
	Engelund and Hansen (1967)	BML (primarily sand)
	Graf (1970)	BML
	Meyer-Peter Muller (1948)	BL
	Parker gravel (1982)	BL
	Singer-Dunne (2004)	BML
	Yang's stream power (1973 for sand, 1984 for gravel)	BML
SRH-1D	Ackers and White (1973)	BML
	Ackers and White (HR Wallingford, 1990)	BML
	Brownlie (1981b)	BML (primarily sand)
	Engelund and Hansen (1967)	BML (primarily sand)
	Engelund and Hansen for sand (1967); Gaeuman et al. (2009), Parker (1990), or Wilcock and Crowe (2003) for gravel	BML
	Gaeuman et al. (2009) modification to Wilcock and Crowe (2003)	BL
	Laursen (1958)	BML (primarily sand)
	Madden's (1993) Modification of Laursen's (1958) relationship	BML
	Meyer-Peter and Müller (1948) with the Wong and Parker (2006) correction	BL
	Parker (1990)	BL
	Yang's stream power (1973 for sand, 1984 for gravel)	BML
	Yang's stream power (1979 for high-concentration sand, 1984 for gravel)	BML
	Yang et al. stream power (1996 for sand w/ high wash load concentration)	BML (primarily sand)
	Wilcock and Crowe (2003)	BL
Wu et al. (2000)	BML	

*BL = bedload transport equation, BML = total bed-material load transport equation

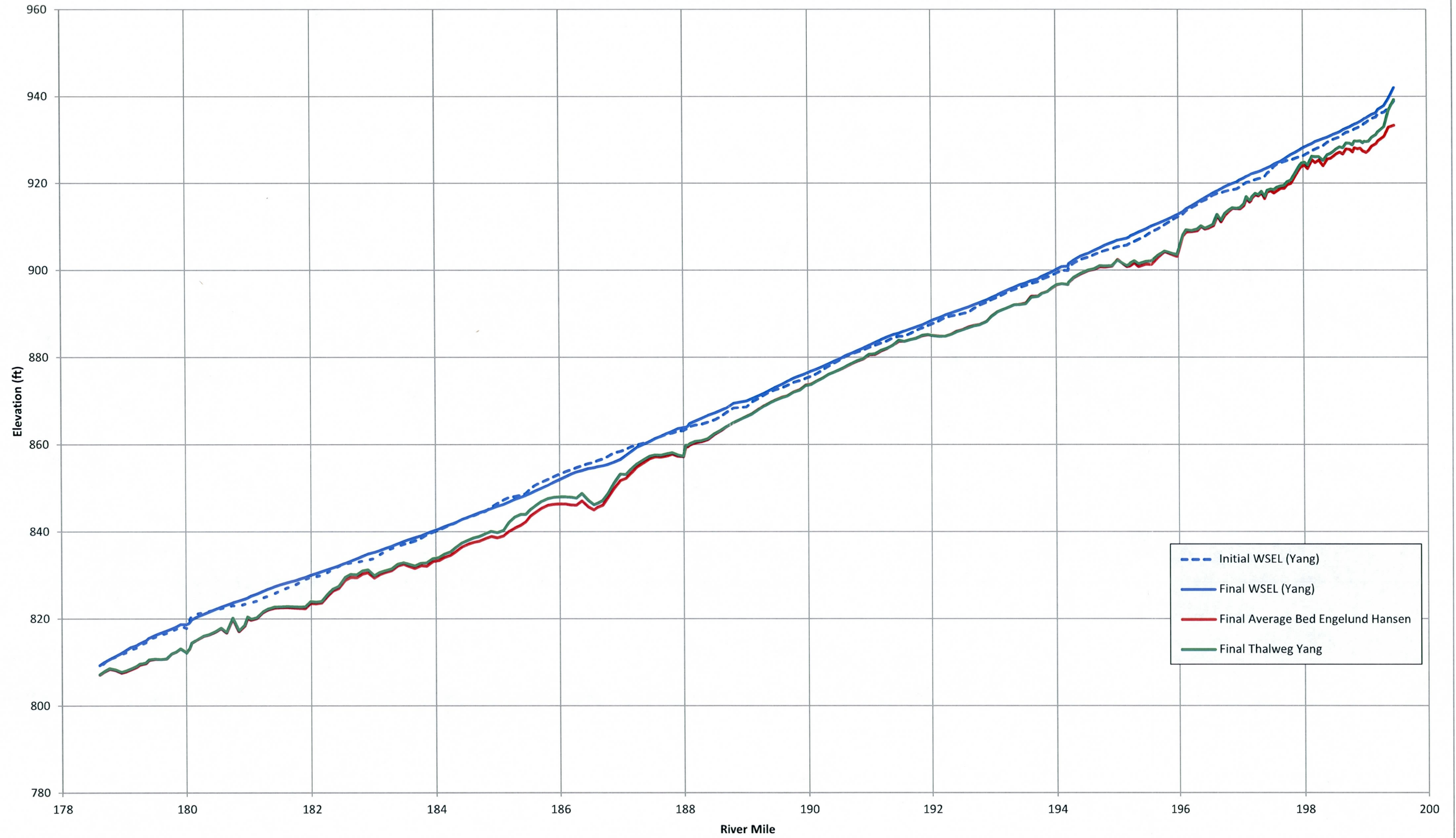
**Appendix C: Profile Output for the Model
Comparison Runs in HEC-RAS, HEC-6T,
and SRH-1D**

SRH-1D Thalweg Comparison*



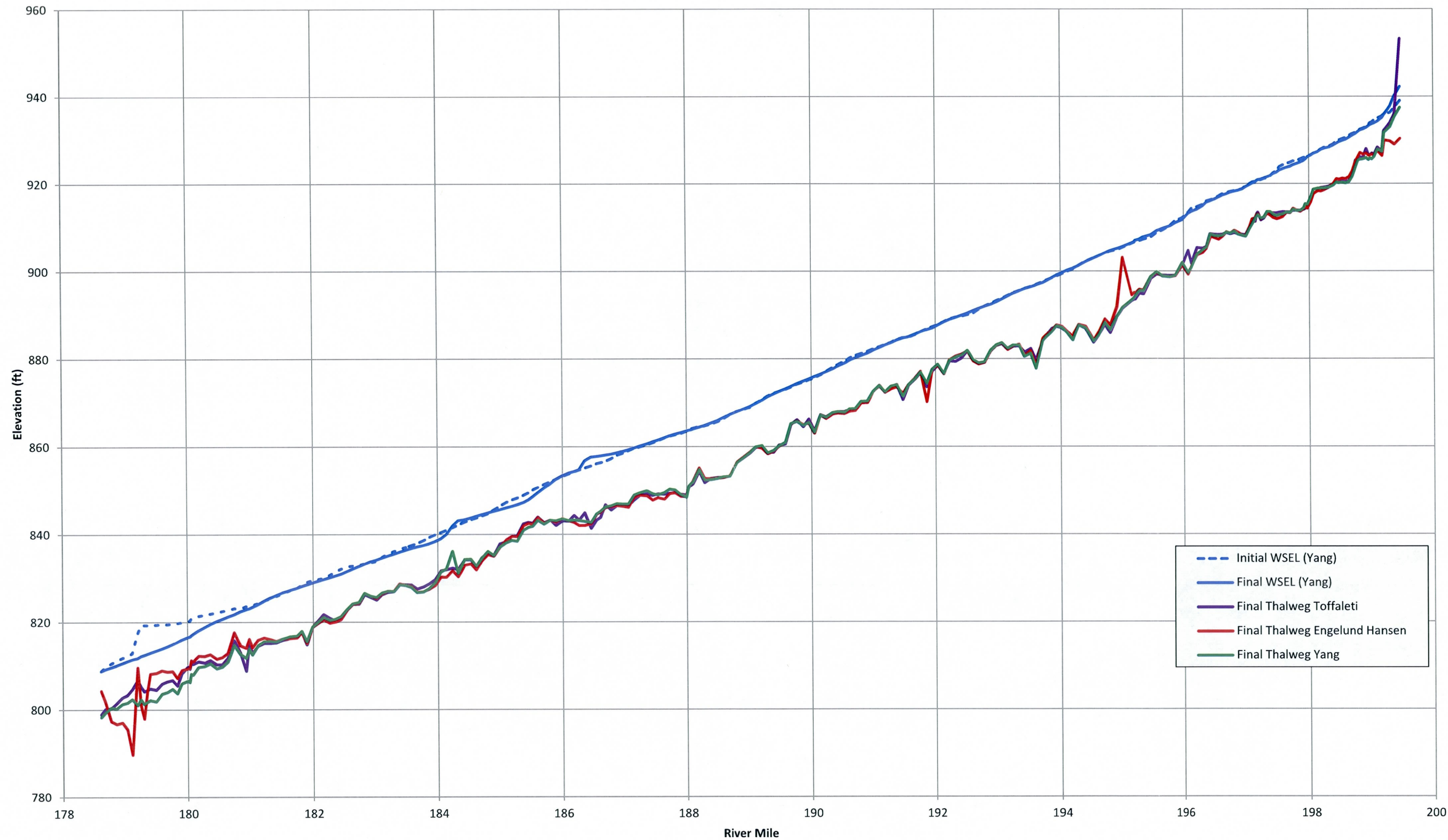
* It should be noted that the water surface elevations shown in the plot above were taken from the SRH-1D results at the initial and final time steps in the model run.

SRH-1D Average Bed Comparison*



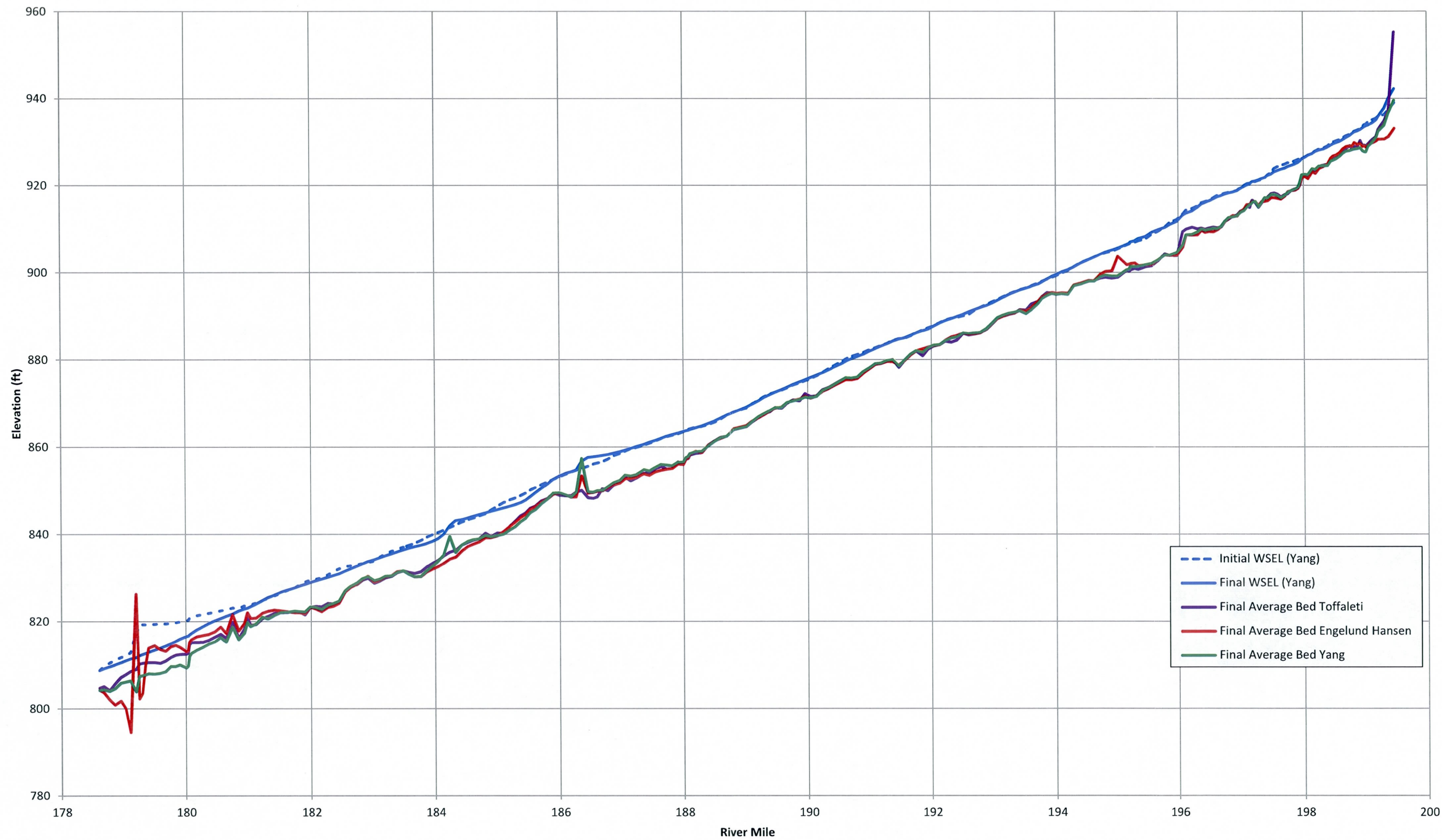
* It should be noted that the water surface elevations shown in the plot above were taken from the SRH-1D results at the initial and final time steps in the model run.

HEC-6T Thalweg Comparison*



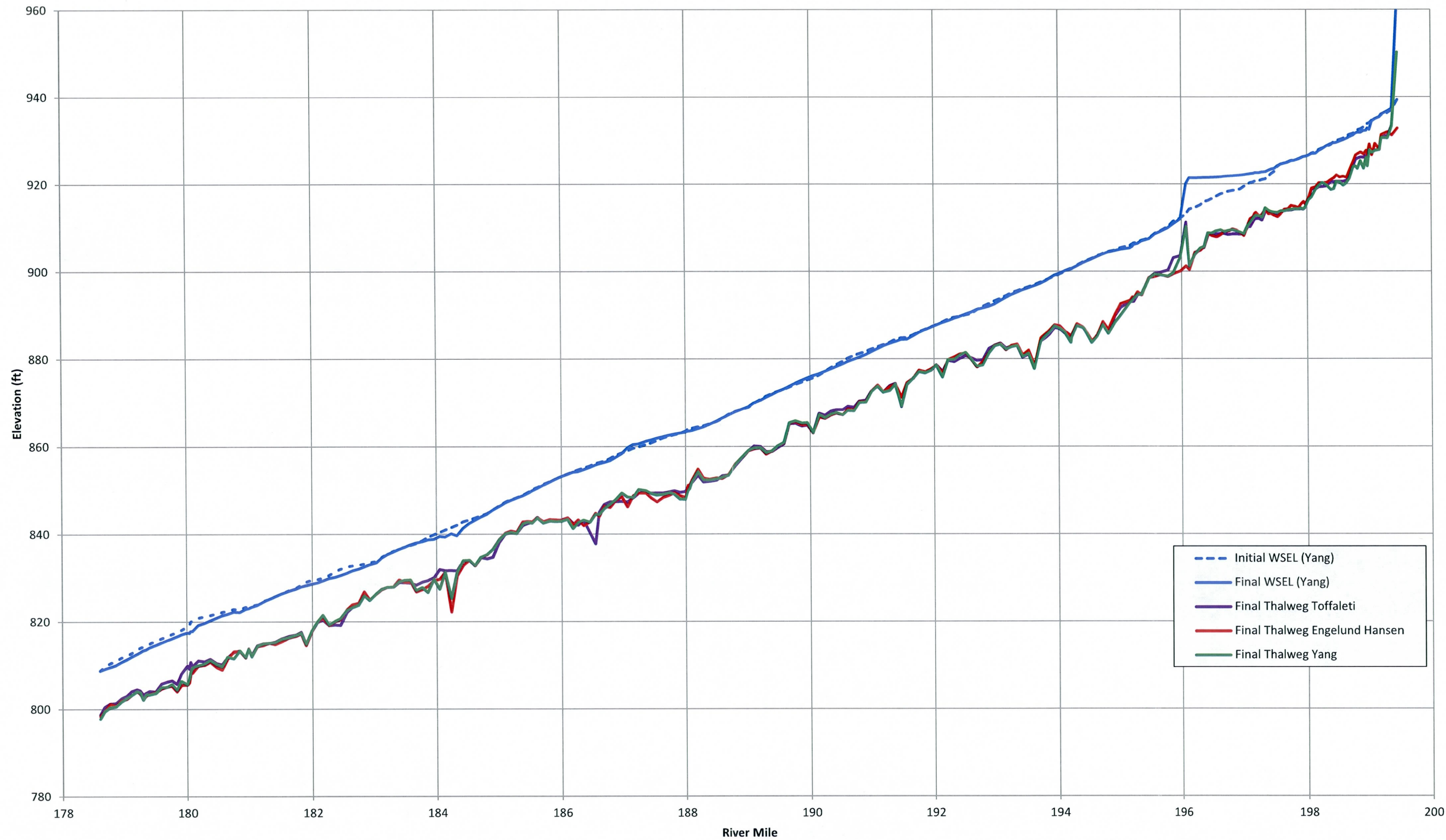
* It should be noted that the water surface elevations shown in the plot above were taken from the HEC-6T results at the initial and final time steps in the model run.

HEC-6T Average Bed Comparison*



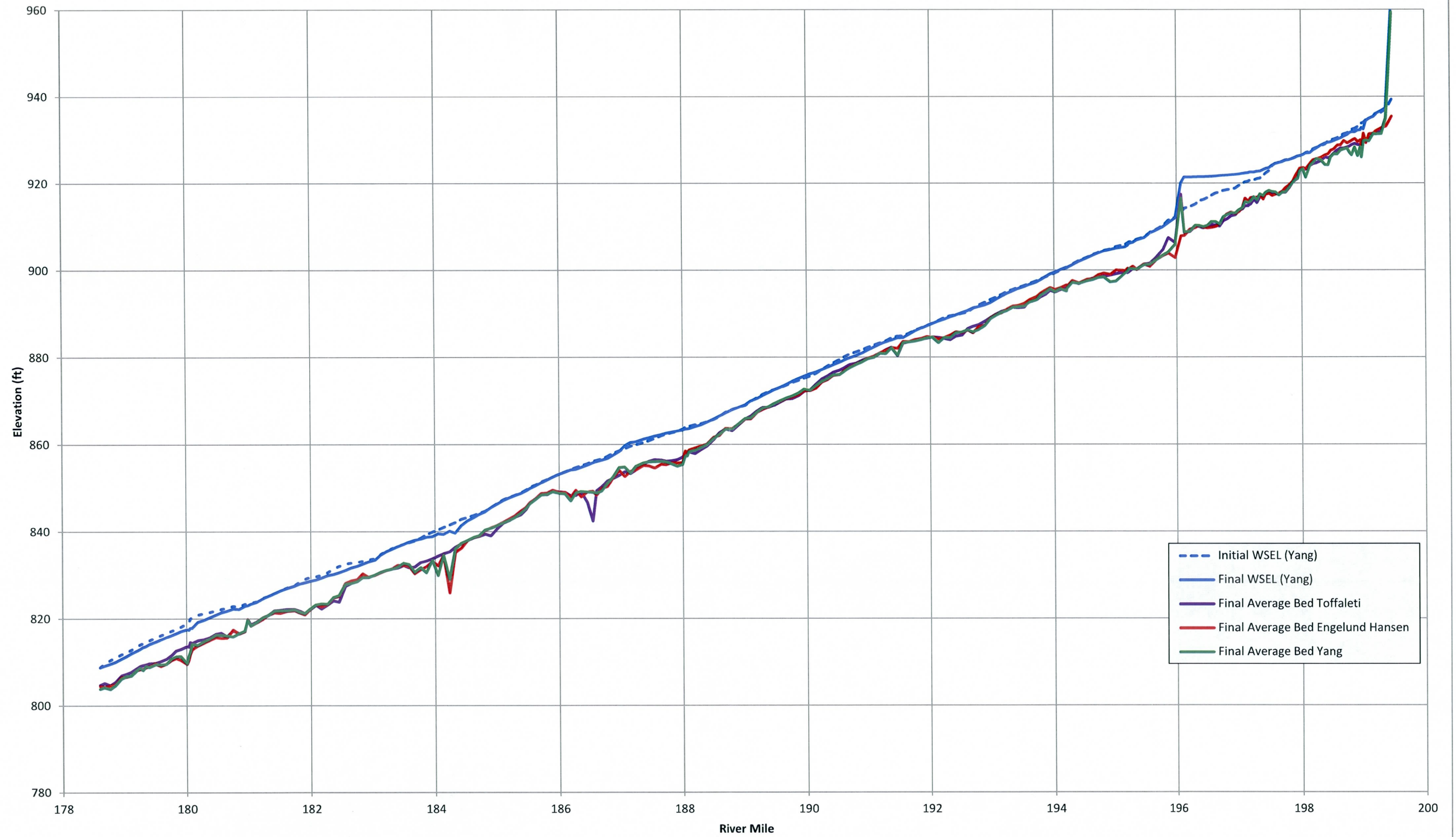
* It should be noted that the water surface elevations shown in the plot above were taken from the HEC-6T results at the initial and final time steps in the model run.

HEC-RAS Thalweg Comparison*



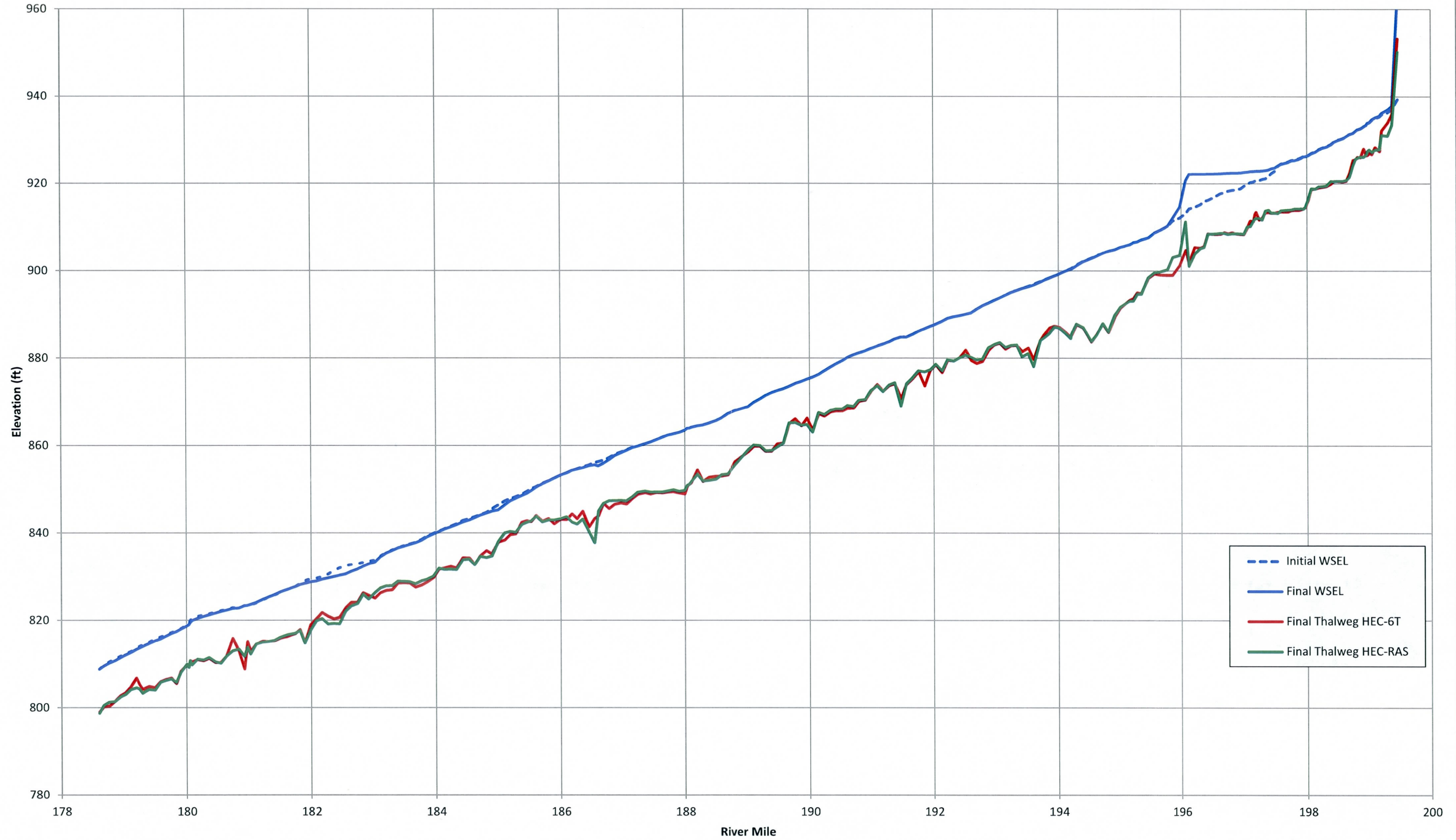
* It should be noted that the water surface elevations shown in the plot above were taken from the HEC-RAS results at the initial and final time steps in the model run.

HEC-RAS Average Bed Comparison*



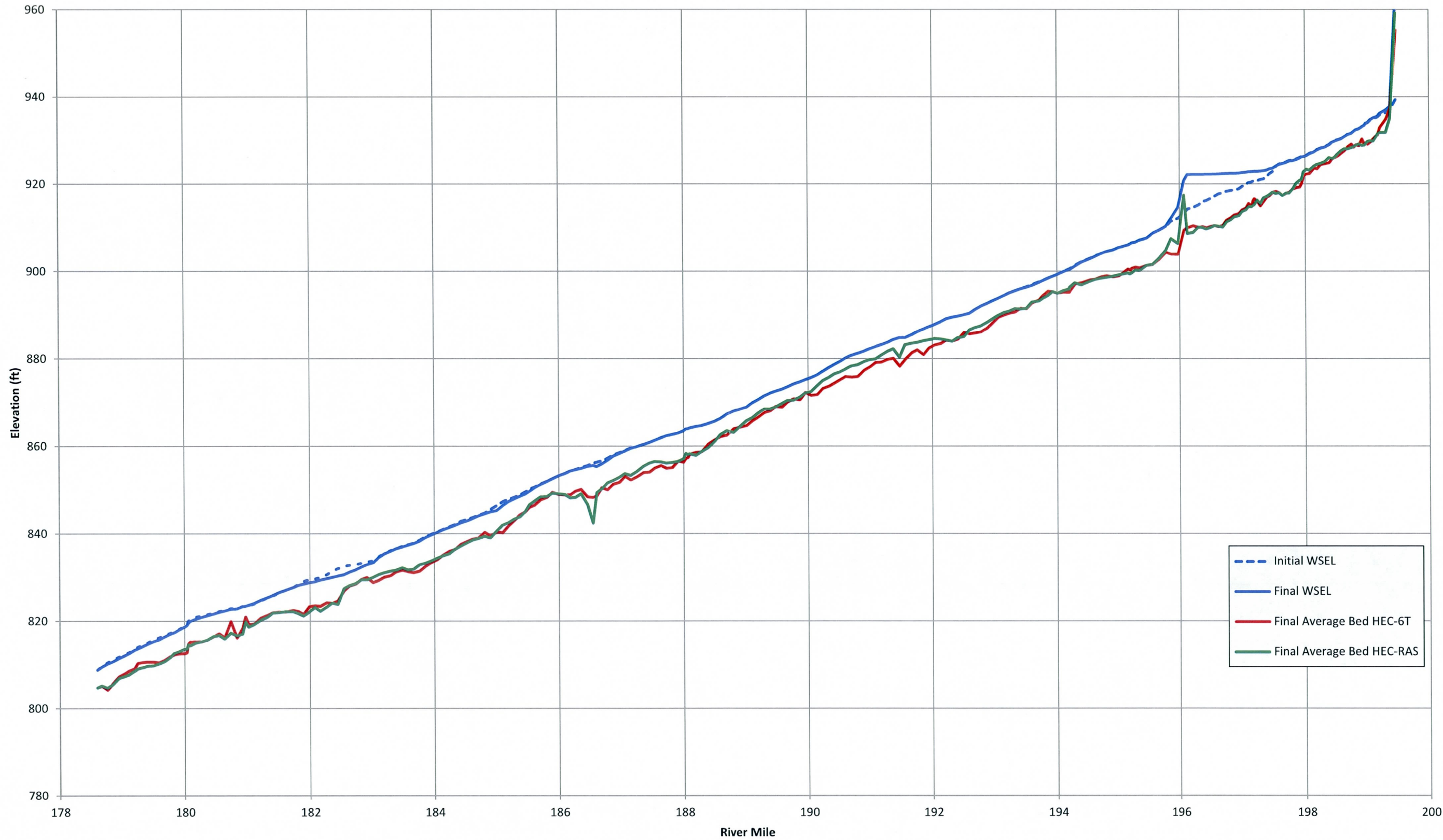
* It should be noted that the water surface elevations shown in the plot above were taken from the HEC-RAS results at the initial and final time steps in the model run.

Toffaleti Thalweg Comparison*



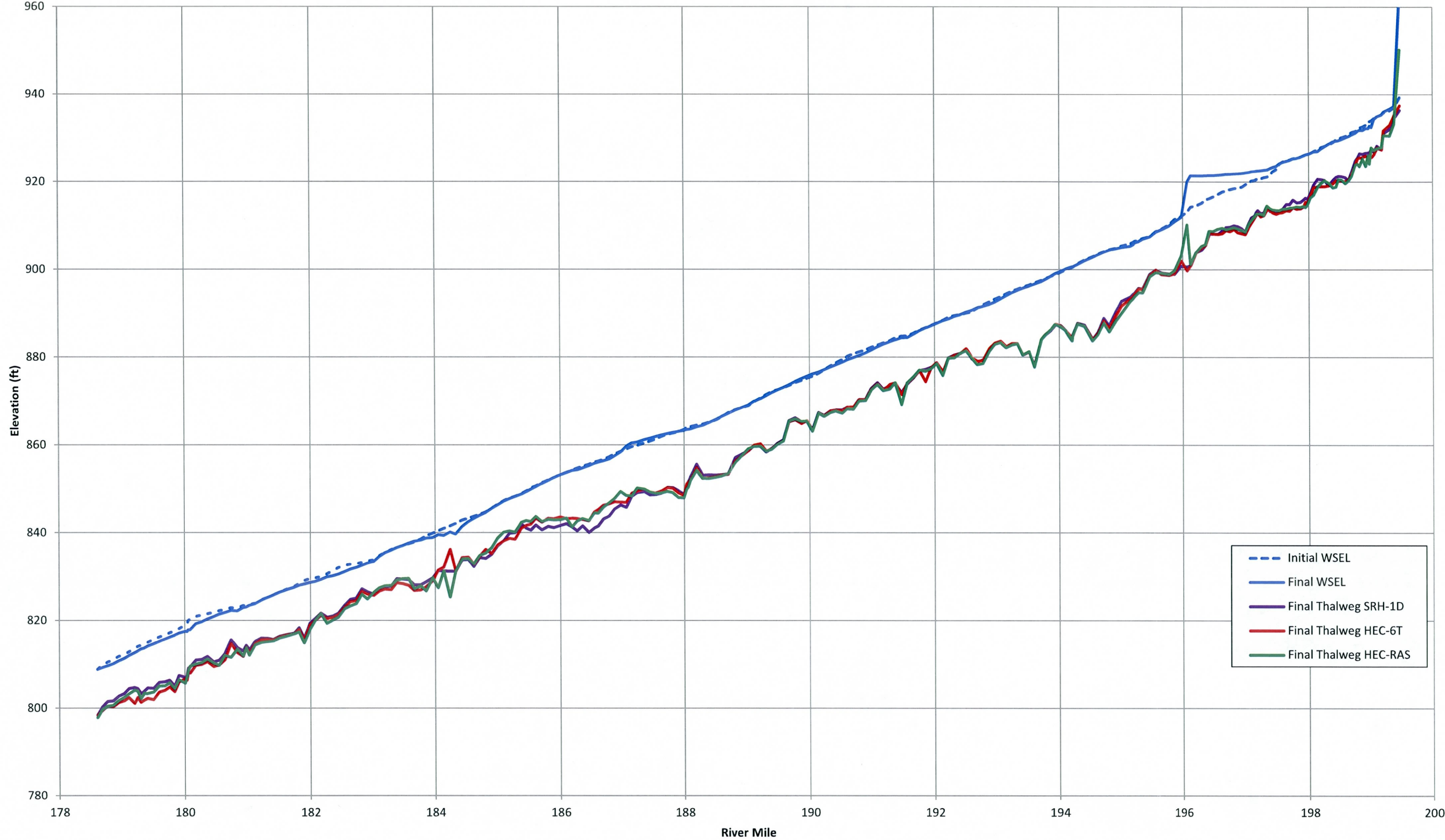
* It should be noted that the water surface elevations shown in the plot above were taken from the HEC-RAS results at the initial and final time steps in the model run.

Toffaleti Average Bed Comparison*



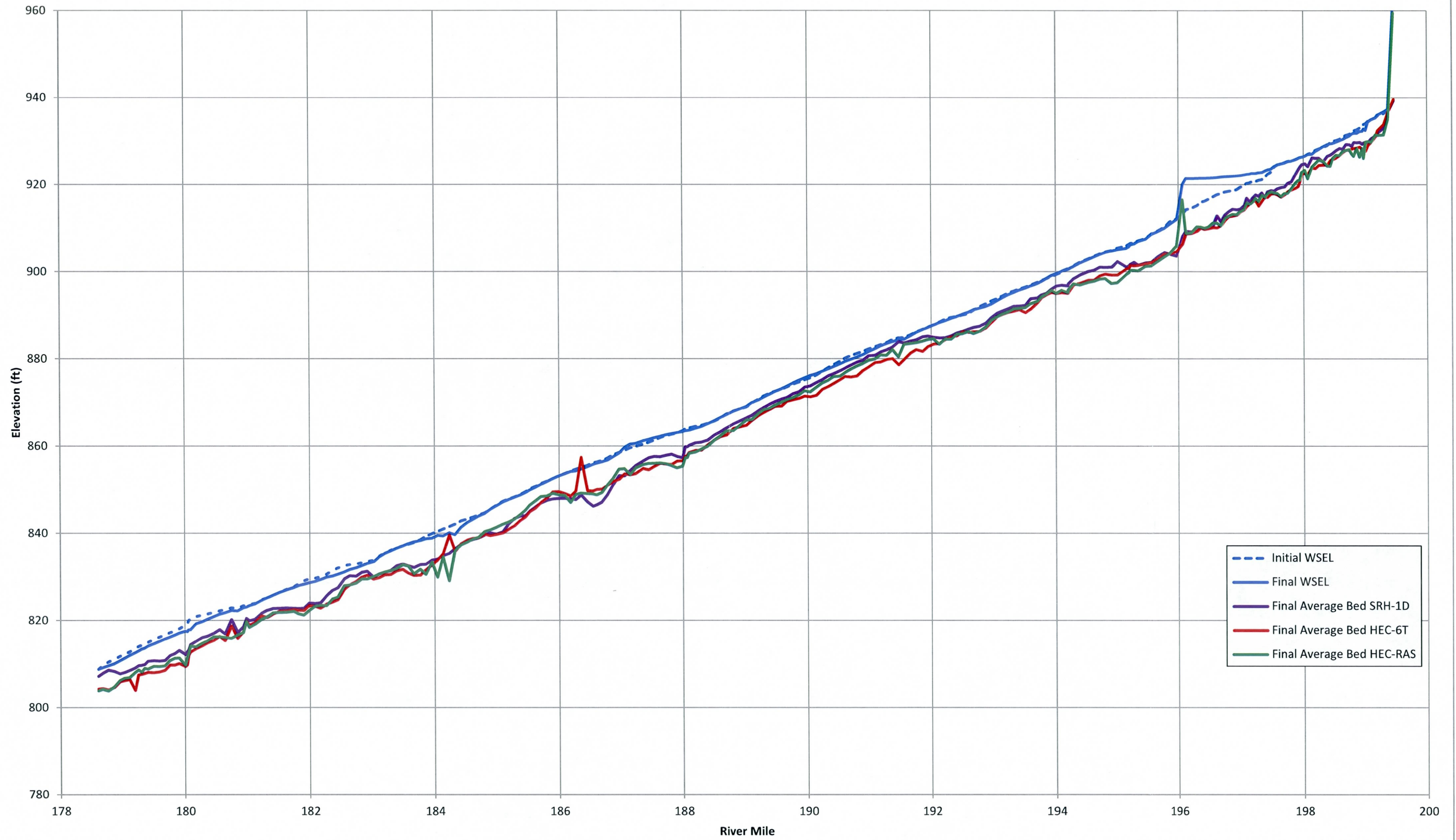
* It should be noted that the water surface elevations shown in the plot above were taken from the HEC-RAS results at the initial and final time steps in the model run.

Yang Thalweg Comparison*



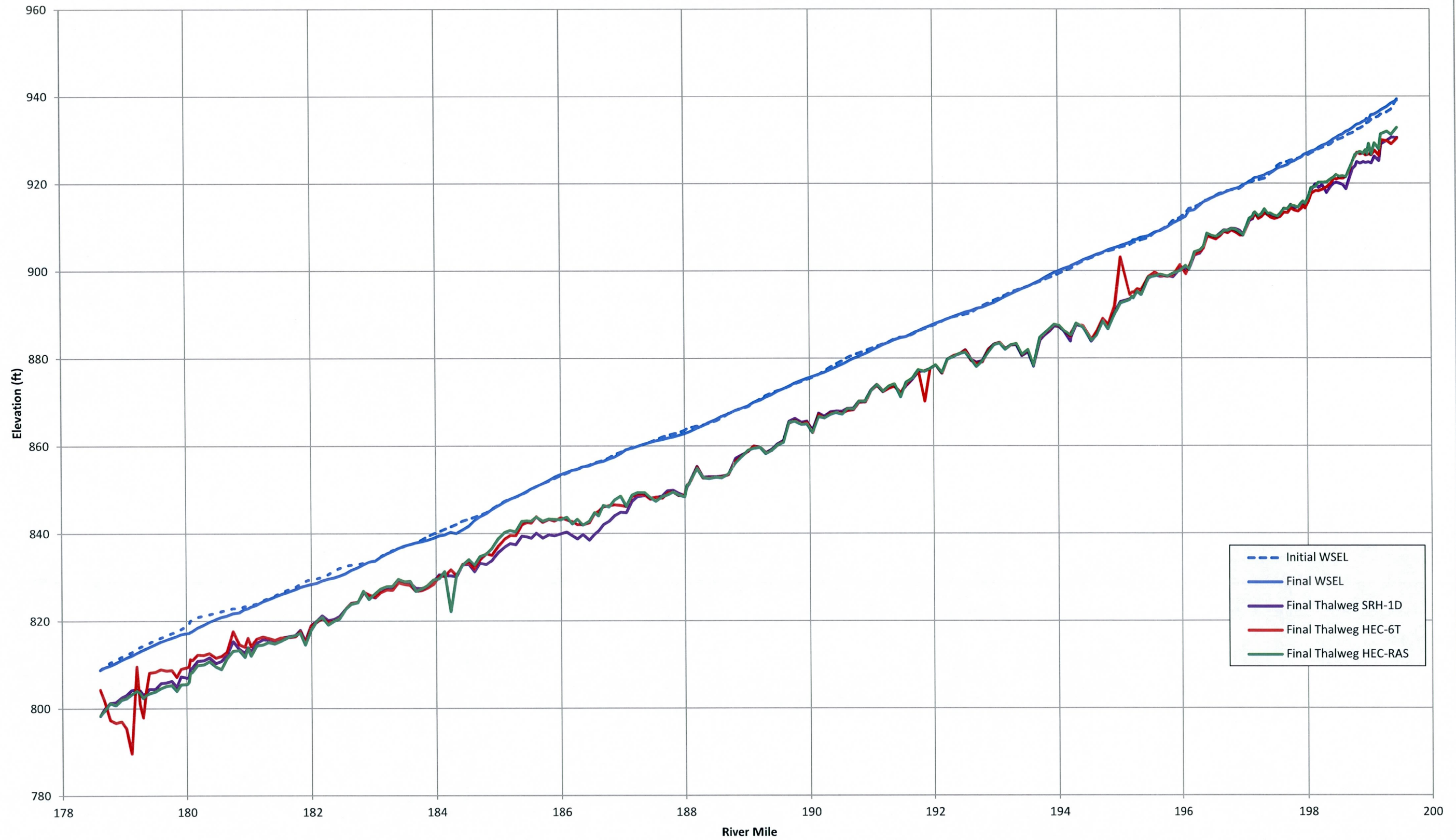
* It should be noted that the water surface elevations shown in the plot above were taken from the HEC-RAS results at the initial and final time steps in the model run.

Yang Average Bed Comparison*



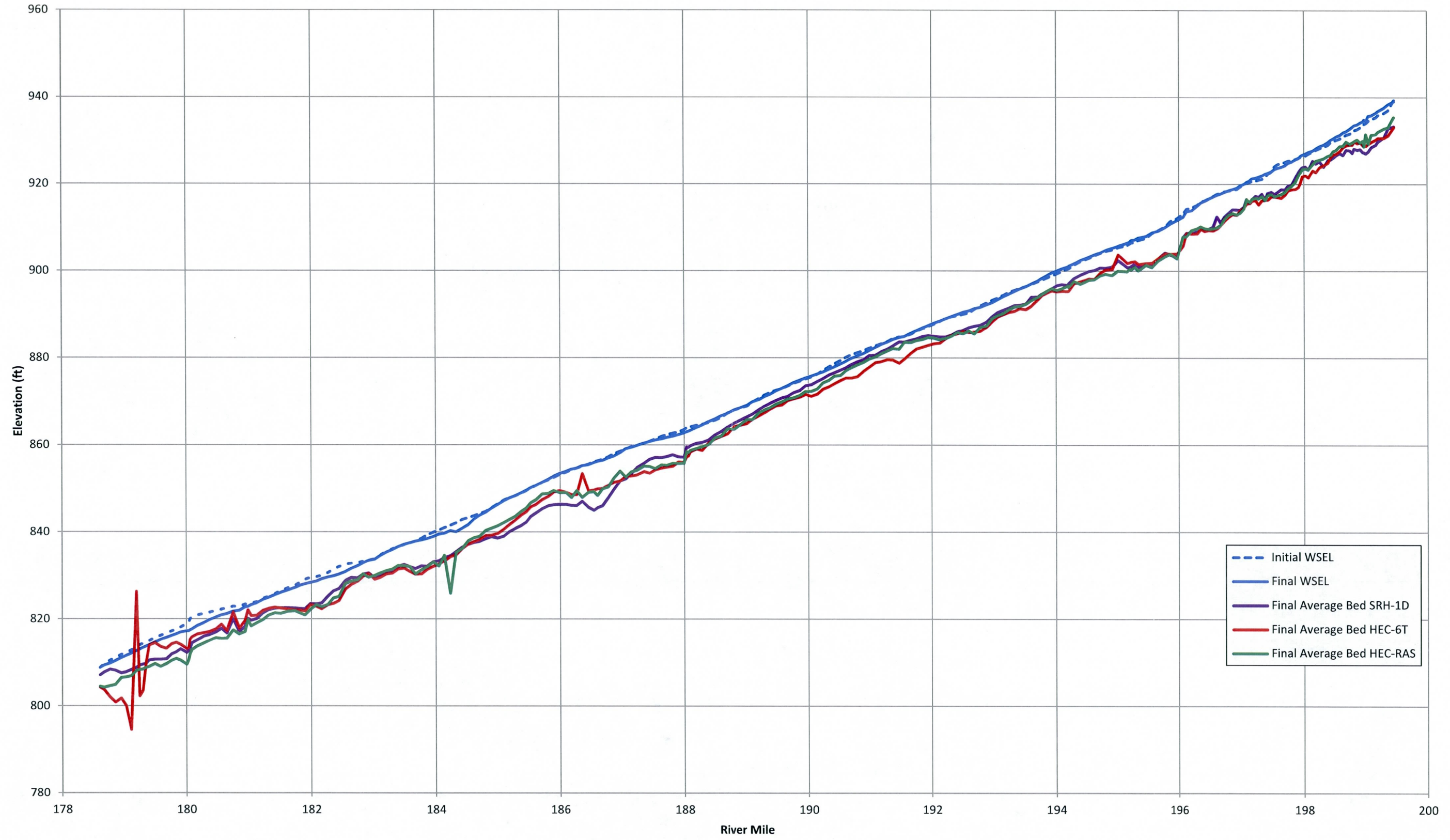
* It should be noted that the water surface elevations shown in the plot above were taken from the HEC-RAS results at the initial and final time steps in the model run.

Engelund Hansen Thalweg Comparison*



* It should be noted that the water surface elevations shown in the plot above were taken from the HEC-RAS results at the initial and final time steps in the model run.

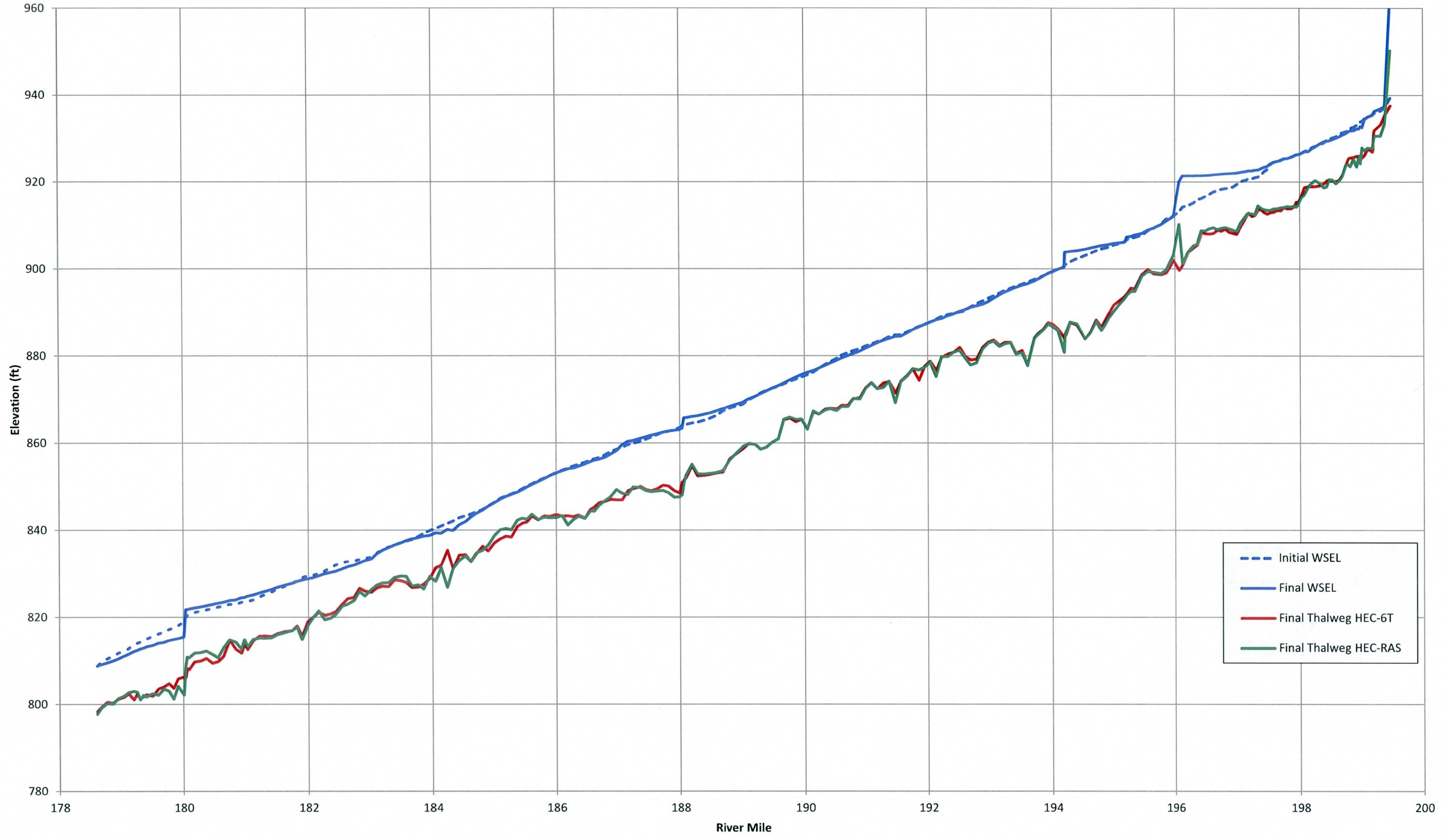
Engelund Hansen Average Bed Comparison*



* It should be noted that the water surface elevations shown in the plot above were taken from the HEC-RAS results at the initial and final time steps in the model run.

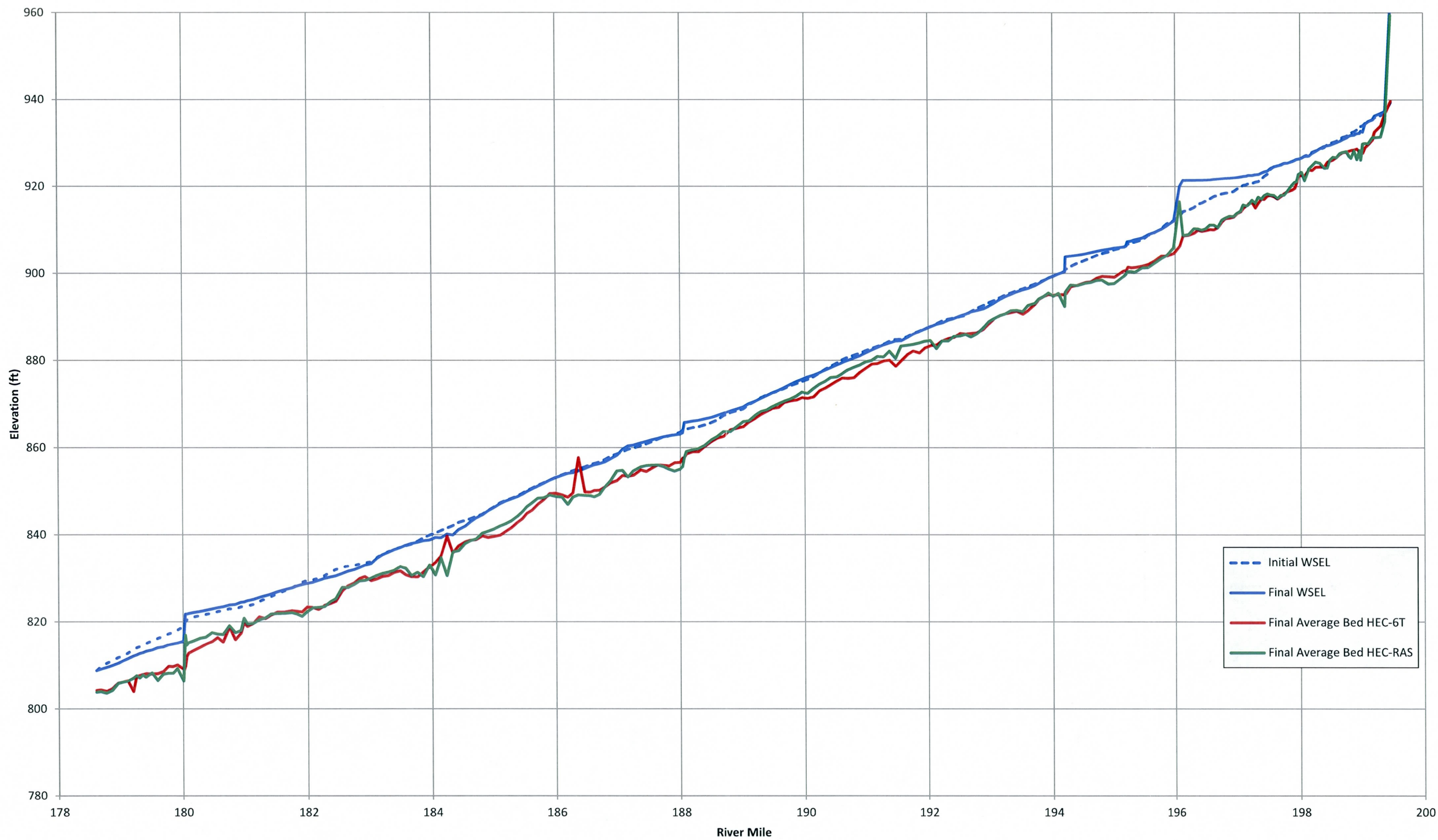
**Appendix D: Profile Output
for the Base Condition Model Runs in
HEC-RAS and HEC-6T**

Yang Thalweg Comparison*



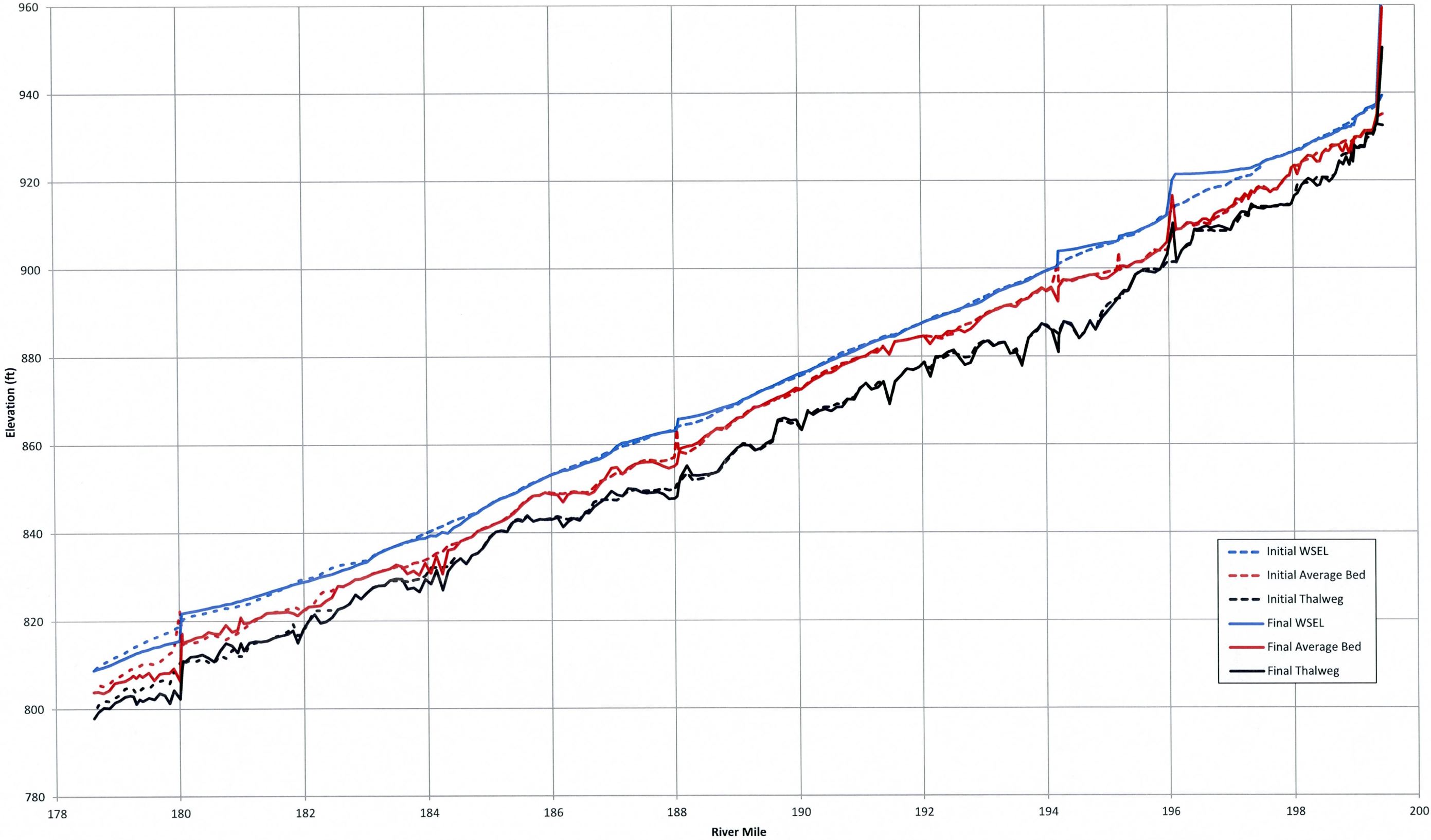
* It should be noted that the water surface elevations shown in the plot above were taken from the HEC-RAS results at the initial and final time steps in the model run.

Yang Average Bed Comparison*



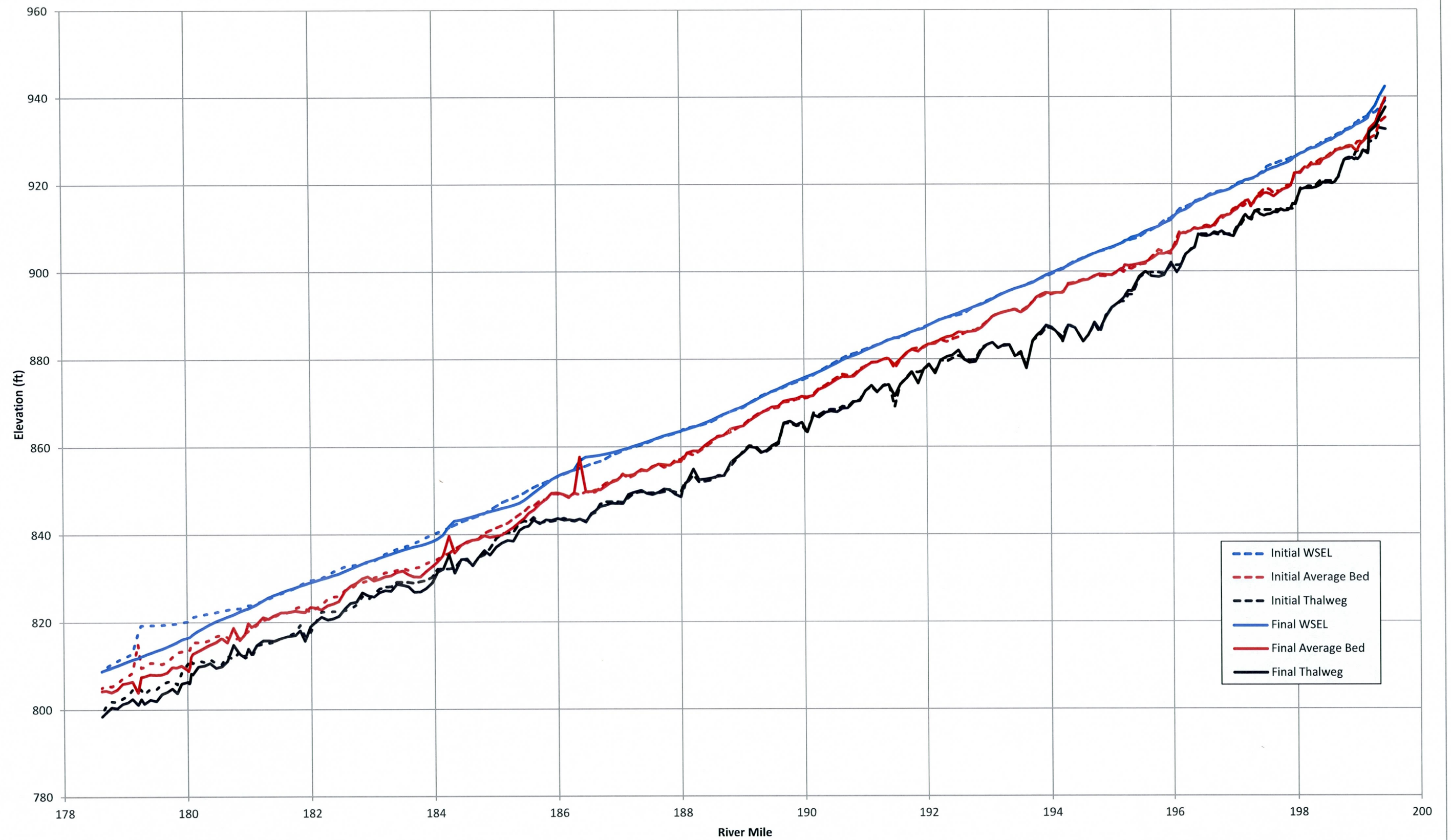
* It should be noted that the water surface elevations shown in the plot above were taken from the HEC-RAS results at the initial and final time steps in the model run.

HEC-RAS (Yang)*



* It should be noted that the water surface elevations shown in the plot above were taken from the HEC-RAS results at the initial and final time steps in the model run.

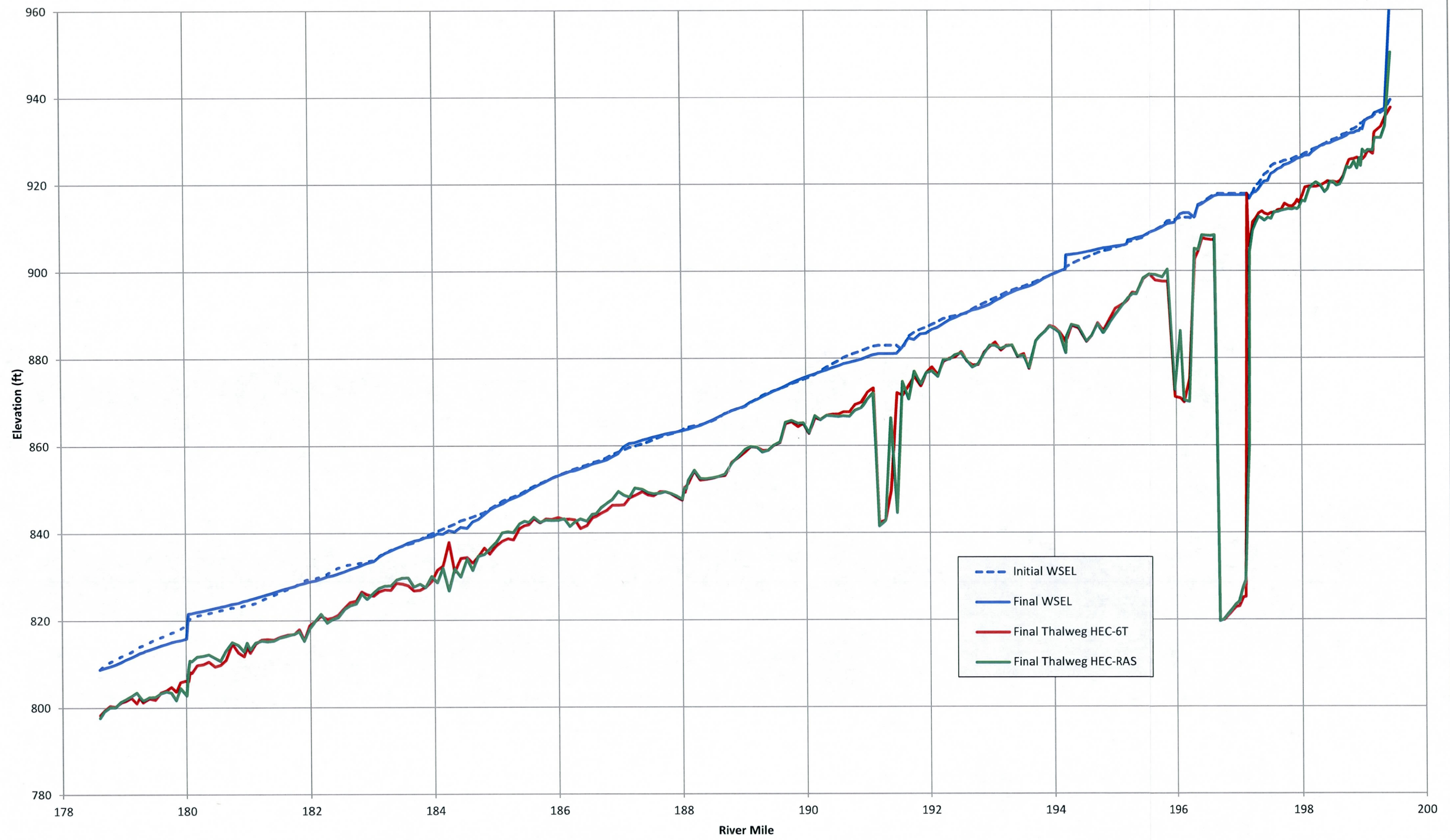
HEC-6T (Yang)*



* It should be noted that the water surface elevations shown in the plot above were taken from the HEC-6T results at the initial and final time steps in the model run.

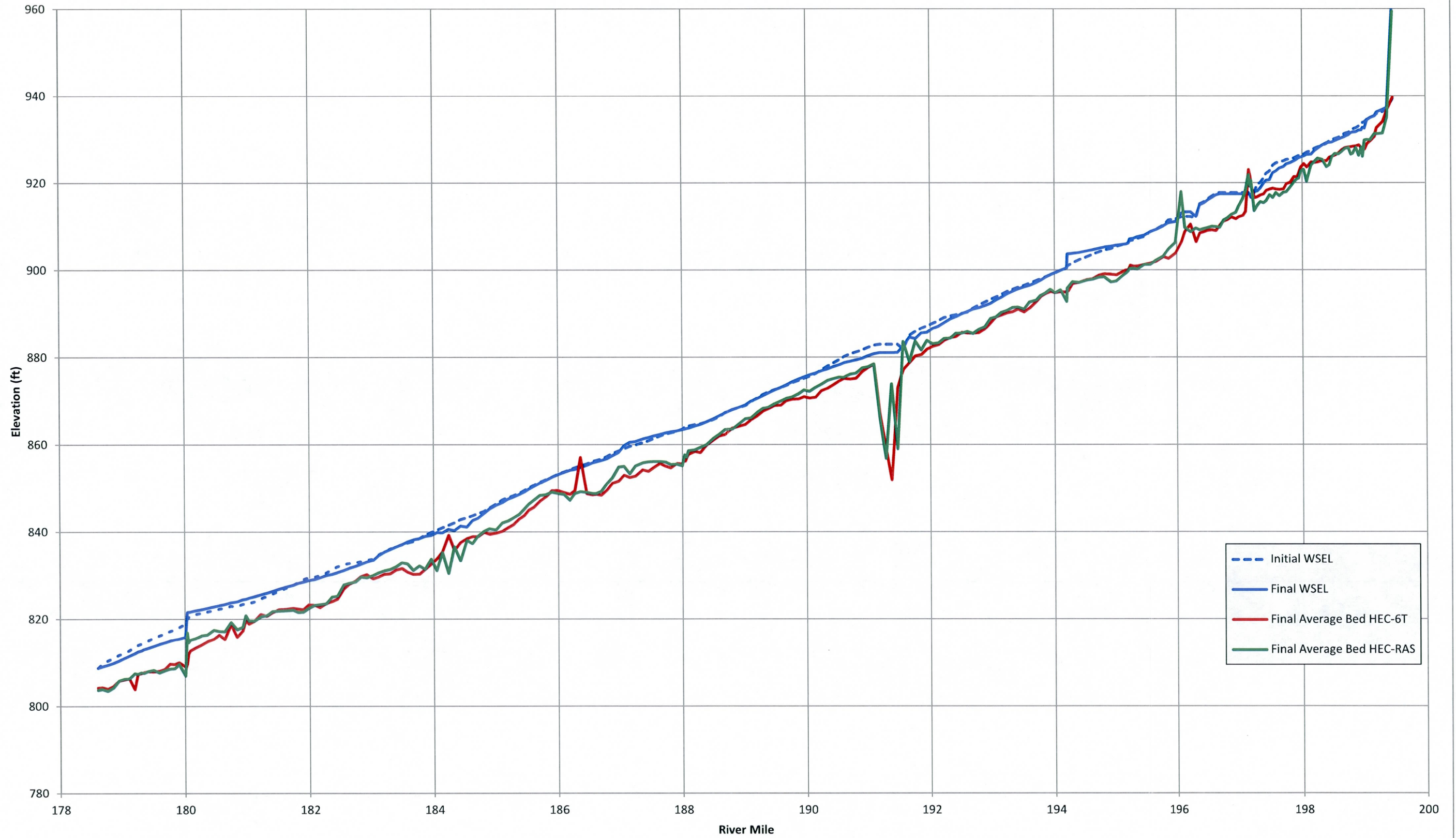
**Appendix E: Profile Output
for the Ultimate Pit Model Runs in
HEC-RAS and HEC-6T**

Yang Thalweg Comparison*



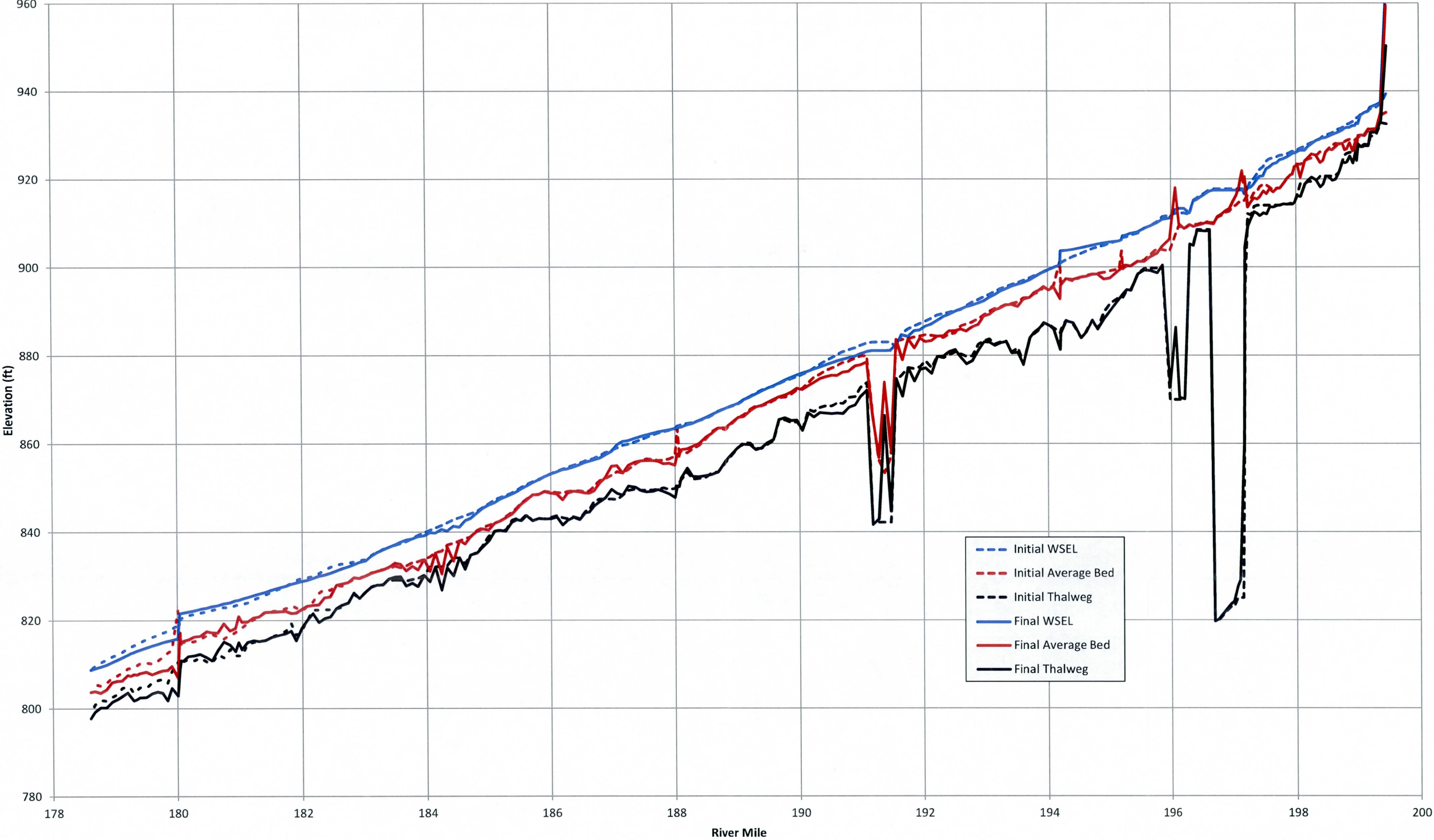
* It should be noted that the water surface elevations shown in the plot above were taken from the HEC-RAS results at the initial and final time steps in the model run.

Yang Average Bed Comparison*



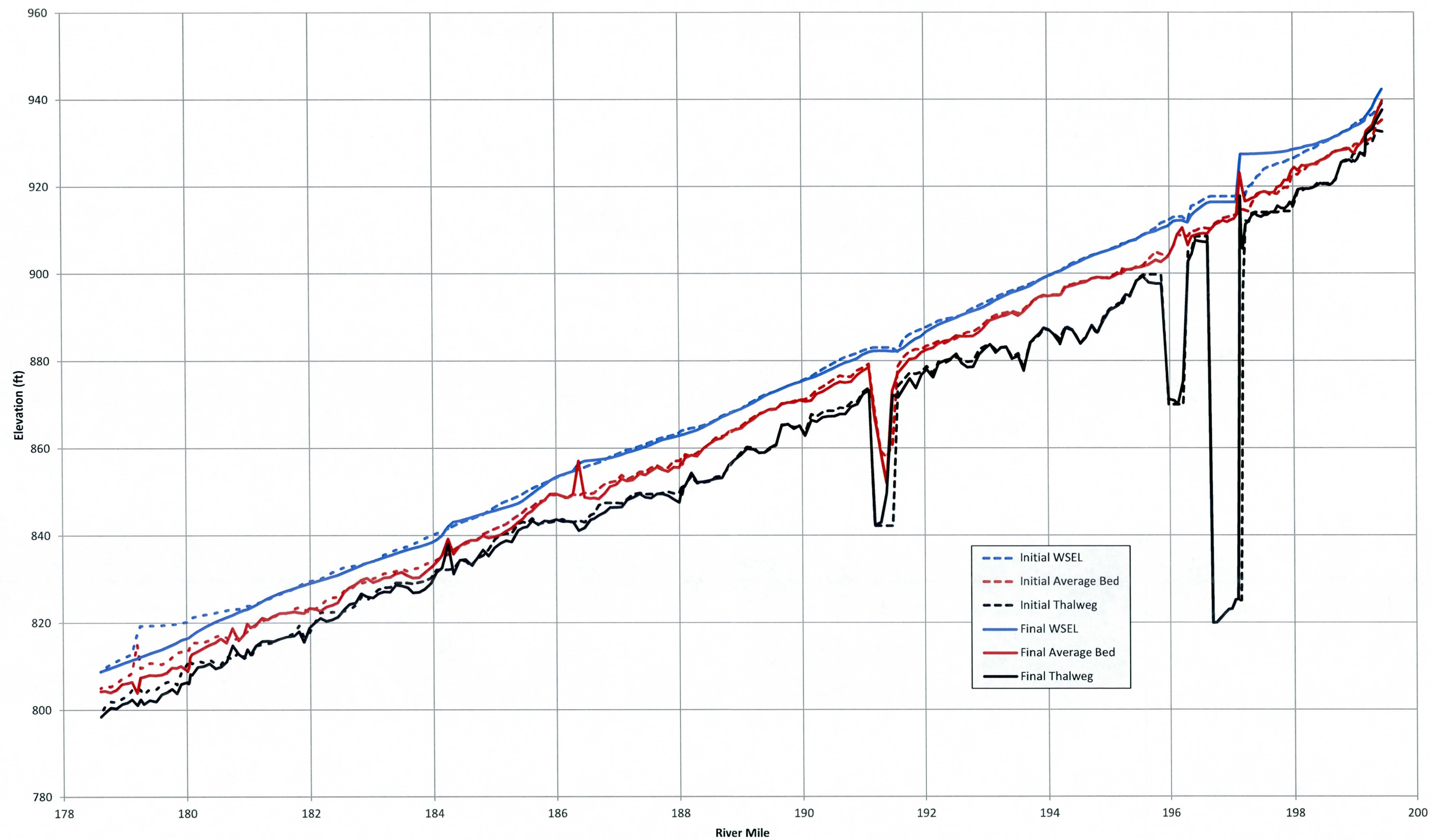
* It should be noted that the water surface elevations shown in the plot above were taken from the HEC-RAS results at the initial and final time steps in the model run.

HEC-RAS (Yang)*



* It should be noted that the water surface elevations shown in the plot above were taken from the HEC-RAS results at the initial and final time steps in the model run.

HEC-6T (Yang)*



* It should be noted that the water surface elevations shown in the plot above were taken from the HEC-6T results at the initial and final time steps in the model run.

Appendix F: Case Study Data

Table F-1 RMSE values for all of the case study runs transport models

Q_{sed}	F	G_{bed}	q	S	Scour RMSE	Deposition RMSE	\log_{10} Scour RMSE	\log_{10} Deposition RMSE
0.50	EH	0.50	1000	0.0005	0.54	0.00	-0.27	-2.37
0.50	EH	0.50	2000	0.0005	1.33	0.01	0.12	-1.90
0.50	EH	0.50	50	0.0005	0.00	*	-2.50	*
0.50	EH	1.00	1000	0.0005	0.01	*	-2.07	*
0.50	EH	1.00	2000	0.0005	0.02	0.00	-1.69	-2.52
0.50	EH	1.00	50	0.0005	0.00	*	-2.81	*
0.50	EH	2.00	1000	0.0005	0.01	*	-2.23	*
0.50	EH	2.00	2000	0.0005	0.01	0.00	-1.99	-2.51
0.50	EH	2.00	50	0.0005	0.00	*	-2.82	*
0.50	EH	4.00	1000	0.0005	0.00	*	-2.38	*
0.50	EH	4.00	2000	0.0005	0.01	0.00	-2.16	-3.30
0.50	EH	4.00	50	0.0005	0.00	*	-2.82	*
0.50	EH	8.00	1000	0.0005	*	0.00	*	-2.52
0.50	EH	8.00	2000	0.0005	*	0.01	*	-2.13
0.50	EH	8.00	50	0.0005	0.00	*	-2.52	*
0.50	T	0.50	1000	0.0005	0.47	0.00	-0.32	-2.52
0.50	T	0.50	2000	0.0005	1.09	0.01	0.04	-2.21
0.50	T	0.50	50	0.0005	*	0.00	*	-2.52
0.50	T	1.00	1000	0.0005	*	0.05	*	-1.27
0.50	T	1.00	2000	0.0005	*	0.13	*	-0.90
0.50	T	1.00	50	0.0005	*	0.00	*	-2.52
0.50	T	2.00	1000	0.0005	*	0.03	*	-1.59
0.50	T	2.00	2000	0.0005	*	0.14	*	-0.85
0.50	T	2.00	50	0.0005	*	0.00	*	-2.52
0.50	T	4.00	1000	0.0005	0.00	0.01	-2.67	-1.86
0.50	T	4.00	2000	0.0005	0.01	0.07	-2.10	-1.18
0.50	T	4.00	50	0.0005	*	0.00	*	-2.52
0.50	T	8.00	1000	0.0005	*	0.04	*	-1.40
0.50	T	8.00	2000	0.0005	0.00	0.12	-2.52	-0.93
0.50	T	8.00	50	0.0005	*	0.00	*	-2.52
0.50	Y	0.50	1000	0.0005	0.39	0.01	-0.41	-2.08
0.50	Y	0.50	2000	0.0005	0.78	0.03	-0.11	-1.60
0.50	Y	0.50	50	0.0005	0.00	*	-2.82	*
0.50	Y	1.00	1000	0.0005	0.03	*	-1.46	*
0.50	Y	1.00	2000	0.0005	0.07	0.00	-1.14	-2.51
0.50	Y	1.00	50	0.0005	*	*	*	*
0.50	Y	2.00	1000	0.0005	0.04	*	-1.45	*

Q_{sed}	F	G_{bed}	q	S	Scour RMSE	Deposition RMSE	\log_{10} Scour RMSE	\log_{10} Deposition RMSE
0.50	Y	2.00	2000	0.0005	0.08	0.00	-1.10	-3.26
0.50	Y	2.00	50	0.0005	*	0.00	*	-2.52
0.50	Y	4.00	1000	0.0005	0.03	*	-1.47	*
0.50	Y	4.00	2000	0.0005	0.08	0.00	-1.11	-3.27
0.50	Y	4.00	50	0.0005	*	0.00	*	-2.52
0.50	Y	8.00	1000	0.0005	*	0.01	*	-1.86
0.50	Y	8.00	2000	0.0005	*	0.04	*	-1.43
0.50	Y	8.00	50	0.0005	*	0.00	*	-2.52
0.50	EH	0.50	1000	0.001	1.35	0.01	0.13	-2.03
0.50	EH	0.50	2000	0.001	3.04	0.18	0.48	-0.75
0.50	EH	0.50	50	0.001	0.00	0.00	-2.65	-2.51
0.50	EH	1.00	1000	0.001	0.02	0.00	-1.82	-2.52
0.50	EH	1.00	2000	0.001	0.03	0.01	-1.47	-1.92
0.50	EH	1.00	50	0.001	0.00	0.00	-2.47	-2.52
0.50	EH	2.00	1000	0.001	0.01	*	-2.11	*
0.50	EH	2.00	2000	0.001	0.02	0.01	-1.66	-2.22
0.50	EH	2.00	50	0.001	0.00	0.00	-4.26	-3.89
0.50	EH	4.00	1000	0.001	0.01	*	-2.14	*
0.50	EH	4.00	2000	0.001	0.02	*	-1.76	*
0.50	EH	4.00	50	0.001	0.00	0.00	-5.14	-4.16
0.50	EH	8.00	1000	0.001	*	0.01	*	-2.02
0.50	EH	8.00	2000	0.001	0.00	0.02	-2.68	-1.72
0.50	EH	8.00	50	0.001	*	0.00	*	-3.53
0.50	T	0.50	1000	0.001	1.09	0.01	0.04	-2.21
0.50	T	0.50	2000	0.001	1.80	0.05	0.26	-1.33
0.50	T	0.50	50	0.001	*	0.00	*	-2.66
0.50	T	1.00	1000	0.001	*	0.13	*	-0.87
0.50	T	1.00	2000	0.001	0.01	0.40	-2.16	-0.40
0.50	T	1.00	50	0.001	*	0.00	*	-2.68
0.50	T	2.00	1000	0.001	0.01	0.08	-2.28	-1.08
0.50	T	2.00	2000	0.001	0.01	0.22	-2.21	-0.66
0.50	T	2.00	50	0.001	*	0.00	*	-2.66
0.50	T	4.00	1000	0.001	0.00	0.03	-2.52	-1.54
0.50	T	4.00	2000	0.001	0.01	0.14	-2.16	-0.86
0.50	T	4.00	50	0.001	*	0.00	*	-2.87
0.50	T	8.00	1000	0.001	0.00	0.04	-2.52	-1.39
0.50	T	8.00	2000	0.001	0.01	0.30	-2.21	-0.52
0.50	T	8.00	50	0.001	*	0.00	*	-2.68

Q_{sed}	F	G_{bed}	q	S	Scour RMSE	Deposition RMSE	\log_{10} Scour RMSE	\log_{10} Deposition RMSE
0.50	Y	0.50	1000	0.001	0.89	0.04	-0.05	-1.41
0.50	Y	0.50	2000	0.001	1.48	0.04	0.17	-1.37
0.50	Y	0.50	50	0.001	0.01	0.00	-2.26	-2.52
0.50	Y	1.00	1000	0.001	0.05	0.00	-1.33	-2.52
0.50	Y	1.00	2000	0.001	0.09	0.01	-1.05	-2.22
0.50	Y	1.00	50	0.001	0.00	0.00	-2.52	-4.33
0.50	Y	2.00	1000	0.001	0.06	*	-1.24	*
0.50	Y	2.00	2000	0.001	0.11	0.00	-0.96	-2.52
0.50	Y	2.00	50	0.001	*	0.00	*	-2.74
0.50	Y	4.00	1000	0.001	0.05	*	-1.30	*
0.50	Y	4.00	2000	0.001	0.13	0.00	-0.90	-2.52
0.50	Y	4.00	50	0.001	*	0.00	*	-3.94
0.50	Y	8.00	1000	0.001	0.00	0.04	-2.52	-1.43
0.50	Y	8.00	2000	0.001	0.01	0.07	-2.15	-1.13
0.50	Y	8.00	50	0.001	*	0.00	*	-4.10
0.50	EH	0.50	1000	0.01	2.60	6.03	0.42	0.78
0.50	EH	0.50	2000	0.01	1.59	13.51	0.20	1.13
0.50	EH	0.50	50	0.01	0.20	0.07	-0.70	-1.17
0.50	EH	1.00	1000	0.01	0.53	0.37	-0.28	-0.43
0.50	EH	1.00	2000	0.01	3.59	4.75	0.55	0.68
0.50	EH	1.00	50	0.01	0.16	0.05	-0.79	-1.31
0.50	EH	2.00	1000	0.01	1.33	0.23	0.12	-0.63
0.50	EH	2.00	2000	0.01	2.21	0.46	0.34	-0.34
0.50	EH	2.00	50	0.01	0.05	0.04	-1.34	-1.45
0.50	EH	4.00	1000	0.01	1.16	0.18	0.07	-0.75
0.50	EH	4.00	2000	0.01	0.51	0.21	-0.30	-0.67
0.50	EH	4.00	50	0.01	0.01	0.05	-2.22	-1.27
0.50	EH	8.00	1000	0.01	0.06	0.14	-1.25	-0.86
0.50	EH	8.00	2000	0.01	0.12	1.36	-0.92	0.13
0.50	EH	8.00	50	0.01	0.01	0.05	-2.28	-1.29
0.50	T	0.50	1000	0.01	6.78	1.50	0.83	0.18
0.50	T	0.50	2000	0.01	6.34	1.49	0.80	0.17
0.50	T	0.50	50	0.01	2.44	0.11	0.39	-0.97
0.50	T	1.00	1000	0.01	3.02	5.64	0.48	0.75
0.50	T	1.00	2000	0.01	4.99	17.56	0.70	1.24
0.50	T	1.00	50	0.01	0.23	0.04	-0.64	-1.35
0.50	T	2.00	1000	0.01	2.67	10.28	0.43	1.01
0.50	T	2.00	2000	0.01	2.03	12.48	0.31	1.10

Q_{sed}	F	G_{bed}	q	S	Scour RMSE	Deposition RMSE	\log_{10} Scour RMSE	\log_{10} Deposition RMSE
0.50	T	2.00	50	0.01	0.01	0.13	-2.13	-0.87
0.50	T	4.00	1000	0.01	2.56	8.46	0.41	0.93
0.50	T	4.00	2000	0.01	3.93	12.23	0.59	1.09
0.50	T	4.00	50	0.01	0.00	0.11	-2.52	-0.95
0.50	T	8.00	1000	0.01	0.15	8.17	-0.83	0.91
0.50	T	8.00	2000	0.01	0.77	10.32	-0.11	1.01
0.50	T	8.00	50	0.01	0.00	0.12	-3.51	-0.91
0.50	Y	0.50	1000	0.01	2.99	1.18	0.48	0.07
0.50	Y	0.50	2000	0.01	3.27	16.71	0.51	1.22
0.50	Y	0.50	50	0.01	0.23	0.08	-0.63	-1.09
0.50	Y	1.00	1000	0.01	0.53	0.18	-0.28	-0.75
0.50	Y	1.00	2000	0.01	0.90	0.26	-0.04	-0.59
0.50	Y	1.00	50	0.01	0.15	0.04	-0.81	-1.40
0.50	Y	2.00	1000	0.01	0.03	0.54	-1.52	-0.26
0.50	Y	2.00	2000	0.01	0.08	3.56	-1.12	0.55
0.50	Y	2.00	50	0.01	0.01	0.06	-2.10	-1.19
0.50	Y	4.00	1000	0.01	0.03	1.27	-1.47	0.10
0.50	Y	4.00	2000	0.01	3.46	5.86	0.54	0.77
0.50	Y	4.00	50	0.01	0.01	0.03	-2.13	-1.55
0.50	Y	8.00	1000	0.01	0.28	6.88	-0.55	0.84
0.50	Y	8.00	2000	0.01	0.21	5.38	-0.69	0.73
0.50	Y	8.00	50	0.01	0.00	0.16	-2.82	-0.80
1.00	EH	0.50	1000	0.0005	0.50	0.00	-0.30	-2.50
1.00	EH	0.50	2000	0.0005	0.75	0.03	-0.12	-1.57
1.00	EH	0.50	50	0.0005	0.00	*	-2.46	*
1.00	EH	1.00	1000	0.0005	0.01	*	-2.25	*
1.00	EH	1.00	2000	0.0005	0.02	0.00	-1.80	-2.52
1.00	EH	1.00	50	0.0005	0.00	*	-2.82	*
1.00	EH	2.00	1000	0.0005	*	0.01	*	-2.24
1.00	EH	2.00	2000	0.0005	*	0.01	*	-2.00
1.00	EH	2.00	50	0.0005	*	*	*	*
1.00	EH	4.00	1000	0.0005	*	0.01	*	-2.13
1.00	EH	4.00	2000	0.0005	*	0.01	*	-2.07
1.00	EH	4.00	50	0.0005	*	0.00	*	-2.40
1.00	EH	8.00	1000	0.0005	*	0.01	*	-1.99
1.00	EH	8.00	2000	0.0005	0.00	0.01	-2.52	-1.95
1.00	EH	8.00	50	0.0005	*	0.00	*	-2.69
1.00	T	0.50	1000	0.0005	0.40	0.00	-0.40	-2.52

Q_{sed}	F	G_{bed}	q	S	Scour RMSE	Deposition RMSE	\log_{10} Scour RMSE	\log_{10} Deposition RMSE
1.00	T	0.50	2000	0.0005	0.79	0.03	-0.10	-1.49
1.00	T	0.50	50	0.0005	*	0.00	*	-2.66
1.00	T	1.00	1000	0.0005	*	0.07	*	-1.16
1.00	T	1.00	2000	0.0005	0.00	0.16	-2.52	-0.80
1.00	T	1.00	50	0.0005	*	0.00	*	-2.37
1.00	T	2.00	1000	0.0005	*	0.06	*	-1.19
1.00	T	2.00	2000	0.0005	0.00	0.21	-2.52	-0.67
1.00	T	2.00	50	0.0005	*	0.00	*	-2.38
1.00	T	4.00	1000	0.0005	0.00	0.04	-2.82	-1.45
1.00	T	4.00	2000	0.0005	0.01	0.10	-2.30	-0.99
1.00	T	4.00	50	0.0005	*	0.00	*	-2.37
1.00	T	8.00	1000	0.0005	*	0.06	*	-1.25
1.00	T	8.00	2000	0.0005	0.00	0.13	-2.52	-0.88
1.00	T	8.00	50	0.0005	*	0.00	*	-2.86
1.00	Y	0.50	1000	0.0005	0.21	0.01	-0.67	-2.06
1.00	Y	0.50	2000	0.0005	0.45	0.03	-0.35	-1.52
1.00	Y	0.50	50	0.0005	*	0.00	*	-3.00
1.00	Y	1.00	1000	0.0005	0.01	0.03	-2.07	-1.53
1.00	Y	1.00	2000	0.0005	0.03	0.04	-1.55	-1.38
1.00	Y	1.00	50	0.0005	*	0.00	*	-2.57
1.00	Y	2.00	1000	0.0005	*	0.04	*	-1.43
1.00	Y	2.00	2000	0.0005	*	0.08	*	-1.11
1.00	Y	2.00	50	0.0005	*	0.00	*	-2.38
1.00	Y	4.00	1000	0.0005	*	0.03	*	-1.54
1.00	Y	4.00	2000	0.0005	*	0.07	*	-1.15
1.00	Y	4.00	50	0.0005	*	0.00	*	-2.39
1.00	Y	8.00	1000	0.0005	*	0.02	*	-1.72
1.00	Y	8.00	2000	0.0005	0.00	0.07	-2.52	-1.14
1.00	Y	8.00	50	0.0005	*	0.00	*	-2.39
1.00	EH	0.50	1000	0.001	0.89	0.01	-0.05	-2.22
1.00	EH	0.50	2000	0.001	1.46	0.03	0.17	-1.56
1.00	EH	0.50	50	0.001	0.00	0.00	-2.75	-2.52
1.00	EH	1.00	1000	0.001	0.01	0.00	-2.15	-2.52
1.00	EH	1.00	2000	0.001	0.03	0.01	-1.51	-2.04
1.00	EH	1.00	50	0.001	0.00	0.00	-2.69	-2.52
1.00	EH	2.00	1000	0.001	*	0.01	*	-1.98
1.00	EH	2.00	2000	0.001	0.00	0.02	-2.37	-1.67
1.00	EH	2.00	50	0.001	0.00	0.00	-2.82	-4.04

Q_{sed}	F	G_{bed}	q	S	Scour RMSE	Deposition RMSE	\log_{10} Scour RMSE	\log_{10} Deposition RMSE
1.00	EH	4.00	1000	0.001	0.00	0.02	-2.52	-1.65
1.00	EH	4.00	2000	0.001	0.01	0.02	-2.17	-1.64
1.00	EH	4.00	50	0.001	*	0.00	*	-2.81
1.00	EH	8.00	1000	0.001	0.00	0.03	-2.52	-1.56
1.00	EH	8.00	2000	0.001	0.01	0.03	-2.19	-1.51
1.00	EH	8.00	50	0.001	*	0.00	*	-2.80
1.00	T	0.50	1000	0.001	0.74	0.04	-0.13	-1.43
1.00	T	0.50	2000	0.001	1.11	0.10	0.04	-1.00
1.00	T	0.50	50	0.001	*	0.00	*	-2.43
1.00	T	1.00	1000	0.001	0.00	0.19	-2.52	-0.72
1.00	T	1.00	2000	0.001	0.01	0.86	-2.00	-0.07
1.00	T	1.00	50	0.001	*	0.00	*	-2.73
1.00	T	2.00	1000	0.001	0.00	0.12	-2.48	-0.91
1.00	T	2.00	2000	0.001	0.01	0.26	-1.98	-0.58
1.00	T	2.00	50	0.001	*	0.00	*	-2.71
1.00	T	4.00	1000	0.001	0.00	0.09	-2.52	-1.02
1.00	T	4.00	2000	0.001	0.01	0.17	-1.90	-0.78
1.00	T	4.00	50	0.001	*	0.00	*	-3.04
1.00	T	8.00	1000	0.001	0.00	0.07	-2.52	-1.15
1.00	T	8.00	2000	0.001	3.02	2.46	0.48	0.39
1.00	T	8.00	50	0.001	*	0.00	*	-2.38
1.00	Y	0.50	1000	0.001	0.69	0.06	-0.16	-1.24
1.00	Y	0.50	2000	0.001	1.08	0.15	0.03	-0.84
1.00	Y	0.50	50	0.001	0.01	0.00	-2.12	-2.52
1.00	Y	1.00	1000	0.001	0.06	0.00	-1.23	-2.64
1.00	Y	1.00	2000	0.001	0.09	*	-1.07	*
1.00	Y	1.00	50	0.001	*	0.00	*	-2.55
1.00	Y	2.00	1000	0.001	*	0.07	*	-1.14
1.00	Y	2.00	2000	0.001	0.00	0.12	-2.40	-0.92
1.00	Y	2.00	50	0.001	*	0.00	*	-2.42
1.00	Y	4.00	1000	0.001	*	0.06	*	-1.21
1.00	Y	4.00	2000	0.001	0.00	0.12	-2.37	-0.92
1.00	Y	4.00	50	0.001	*	0.00	*	-2.56
1.00	Y	8.00	1000	0.001	0.00	0.06	-2.52	-1.19
1.00	Y	8.00	2000	0.001	0.01	0.17	-2.04	-0.77
1.00	Y	8.00	50	0.001	*	0.00	*	-2.54
1.00	EH	0.50	1000	0.01	3.35	15.82	0.53	1.20
1.00	EH	0.50	2000	0.01	2.60	19.39	0.41	1.29

Q_{sed}	F	G_{bed}	q	S	Scour RMSE	Deposition RMSE	\log_{10} Scour RMSE	\log_{10} Deposition RMSE
1.00	EH	0.50	50	0.01	0.21	0.07	-0.67	-1.16
1.00	EH	1.00	1000	0.01	2.86	0.40	0.46	-0.40
1.00	EH	1.00	2000	0.01	4.02	17.81	0.60	1.25
1.00	EH	1.00	50	0.01	0.02	0.11	-1.78	-0.98
1.00	EH	2.00	1000	0.01	0.18	0.55	-0.75	-0.26
1.00	EH	2.00	2000	0.01	0.34	0.71	-0.46	-0.15
1.00	EH	2.00	50	0.01	0.01	0.06	-2.13	-1.20
1.00	EH	4.00	1000	0.01	0.12	0.89	-0.93	-0.05
1.00	EH	4.00	2000	0.01	3.01	10.52	0.48	1.02
1.00	EH	4.00	50	0.01	0.01	0.14	-2.17	-0.86
1.00	EH	8.00	1000	0.01	1.32	6.73	0.12	0.83
1.00	EH	8.00	2000	0.01	0.38	*	-0.42	*
1.00	EH	8.00	50	0.01	0.01	0.26	-2.21	-0.58
1.00	T	0.50	1000	0.01	1.49	7.19	0.17	0.86
1.00	T	0.50	2000	0.01	4.27	11.80	0.63	1.07
1.00	T	0.50	50	0.01	0.96	0.10	-0.02	-0.99
1.00	T	1.00	1000	0.01	6.65	12.96	0.82	1.11
1.00	T	1.00	2000	0.01	4.23	18.30	0.63	1.26
1.00	T	1.00	50	0.01	0.17	0.04	-0.77	-1.36
1.00	T	2.00	1000	0.01	1.39	10.51	0.14	1.02
1.00	T	2.00	2000	0.01	4.05	16.47	0.61	1.22
1.00	T	2.00	50	0.01	0.01	0.10	-2.21	-0.98
1.00	T	4.00	1000	0.01	2.51	9.65	0.40	0.98
1.00	T	4.00	2000	0.01	2.59	13.97	0.41	1.15
1.00	T	4.00	50	0.01	0.00	0.13	-2.35	-0.90
1.00	T	8.00	1000	0.01	0.19	8.80	-0.72	0.94
1.00	T	8.00	2000	0.01	1.06	11.52	0.03	1.06
1.00	T	8.00	50	0.01	0.00	0.17	-2.52	-0.77
1.00	Y	0.50	1000	0.01	4.37	2.71	0.64	0.43
1.00	Y	0.50	2000	0.01	5.21	14.84	0.72	1.17
1.00	Y	0.50	50	0.01	0.26	0.08	-0.59	-1.12
1.00	Y	1.00	1000	0.01	0.14	1.60	-0.84	0.20
1.00	Y	1.00	2000	0.01	0.17	8.12	-0.78	0.91
1.00	Y	1.00	50	0.01	0.02	0.10	-1.78	-1.00
1.00	Y	2.00	1000	0.01	1.05	3.61	0.02	0.56
1.00	Y	2.00	2000	0.01	1.58	*	0.20	*
1.00	Y	2.00	50	0.01	0.01	0.08	-2.17	-1.10
1.00	Y	4.00	1000	0.01	0.80	5.79	-0.09	0.76

Q_{sed}	F	G_{bed}	q	S	Scour RMSE	Deposition RMSE	\log_{10} Scour RMSE	\log_{10} Deposition RMSE
1.00	Y	4.00	2000	0.01	2.95	6.09	0.47	0.78
1.00	Y	4.00	50	0.01	0.01	0.24	-2.27	-0.61
1.00	Y	8.00	1000	0.01	0.28	7.64	-0.55	0.88
1.00	Y	8.00	2000	0.01	0.42	7.16	-0.37	0.85
1.00	Y	8.00	50	0.01	0.00	0.45	-2.47	-0.35
1.50	EH	0.50	1000	0.0005	0.35	0.01	-0.46	-1.93
1.50	EH	0.50	2000	0.0005	0.75	0.03	-0.13	-1.55
1.50	EH	0.50	50	0.0005	0.00	*	-2.68	*
1.50	EH	1.00	1000	0.0005	0.01	*	-2.24	*
1.50	EH	1.00	2000	0.0005	0.01	0.00	-1.95	-3.22
1.50	EH	1.00	50	0.0005	0.00	*	-2.82	*
1.50	EH	2.00	1000	0.0005	*	0.01	*	-2.08
1.50	EH	2.00	2000	0.0005	0.00	0.01	-2.52	-1.98
1.50	EH	2.00	50	0.0005	*	0.00	*	-2.63
1.50	EH	4.00	1000	0.0005	*	0.01	*	-1.93
1.50	EH	4.00	2000	0.0005	0.00	0.01	-2.52	-1.95
1.50	EH	4.00	50	0.0005	*	0.00	*	-3.55
1.50	EH	8.00	1000	0.0005	*	0.02	*	-1.82
1.50	EH	8.00	2000	0.0005	0.00	0.01	-2.52	-1.91
1.50	EH	8.00	50	0.0005	*	0.00	*	-2.75
1.50	T	0.50	1000	0.0005	0.31	0.01	-0.51	-2.05
1.50	T	0.50	2000	0.0005	0.50	0.08	-0.30	-1.08
1.50	T	0.50	50	0.0005	*	0.00	*	-2.79
1.50	T	1.00	1000	0.0005	*	0.09	*	-1.06
1.50	T	1.00	2000	0.0005	0.00	0.22	-2.52	-0.67
1.50	T	1.00	50	0.0005	*	0.00	*	-3.50
1.50	T	2.00	1000	0.0005	0.00	0.09	-2.52	-1.03
1.50	T	2.00	2000	0.0005	0.01	0.19	-2.22	-0.73
1.50	T	2.00	50	0.0005	*	0.00	*	-3.75
1.50	T	4.00	1000	0.0005	0.00	0.06	-2.47	-1.22
1.50	T	4.00	2000	0.0005	0.01	0.10	-2.18	-0.98
1.50	T	4.00	50	0.0005	*	0.00	*	-3.59
1.50	T	8.00	1000	0.0005	0.00	0.04	-2.52	-1.40
1.50	T	8.00	2000	0.0005	0.01	0.27	-2.22	-0.57
1.50	T	8.00	50	0.0005	*	0.00	*	-2.59
1.50	Y	0.50	1000	0.0005	0.09	0.02	-1.05	-1.66
1.50	Y	0.50	2000	0.0005	0.17	0.09	-0.78	-1.07
1.50	Y	0.50	50	0.0005	*	0.00	*	-2.60

Q_{sed}	F	G_{bed}	q	S	Scour RMSE	Deposition RMSE	\log_{10} Scour RMSE	\log_{10} Deposition RMSE
1.50	Y	1.00	1000	0.0005	*	0.04	*	-1.39
1.50	Y	1.00	2000	0.0005	*	0.07	*	-1.13
1.50	Y	1.00	50	0.0005	*	0.00	*	-2.97
1.50	Y	2.00	1000	0.0005	*	0.04	*	-1.39
1.50	Y	2.00	2000	0.0005	0.00	0.08	-2.52	-1.09
1.50	Y	2.00	50	0.0005	*	0.00	*	-3.75
1.50	Y	4.00	1000	0.0005	*	0.03	*	-1.46
1.50	Y	4.00	2000	0.0005	0.00	0.08	-2.52	-1.11
1.50	Y	4.00	50	0.0005	*	0.00	*	-4.01
1.50	Y	8.00	1000	0.0005	0.00	0.06	-2.52	-1.24
1.50	Y	8.00	2000	0.0005	0.01	0.09	-2.22	-1.02
1.50	Y	8.00	50	0.0005	*	0.00	*	-4.02
1.50	EH	0.50	1000	0.001	0.72	0.04	-0.14	-1.41
1.50	EH	0.50	2000	0.001	1.23	0.08	0.09	-1.11
1.50	EH	0.50	50	0.001	0.00	0.00	-2.40	-2.52
1.50	EH	1.00	1000	0.001	0.01	*	-2.16	*
1.50	EH	1.00	2000	0.001	0.02	0.00	-1.69	-2.52
1.50	EH	1.00	50	0.001	0.00	0.00	-2.47	-2.52
1.50	EH	2.00	1000	0.001	0.00	0.02	-2.52	-1.61
1.50	EH	2.00	2000	0.001	0.01	0.03	-2.18	-1.56
1.50	EH	2.00	50	0.001	*	0.00	*	-2.92
1.50	EH	4.00	1000	0.001	0.00	0.04	-2.52	-1.43
1.50	EH	4.00	2000	0.001	0.01	0.04	-2.03	-1.39
1.50	EH	4.00	50	0.001	*	0.00	*	-3.01
1.50	EH	8.00	1000	0.001	0.00	0.04	-2.52	-1.37
1.50	EH	8.00	2000	0.001	0.01	0.07	-1.91	-1.14
1.50	EH	8.00	50	0.001	*	0.00	*	-3.00
1.50	T	0.50	1000	0.001	0.41	0.19	-0.38	-0.72
1.50	T	0.50	2000	0.001	0.49	0.54	-0.31	-0.27
1.50	T	0.50	50	0.001	*	0.01	*	-2.27
1.50	T	1.00	1000	0.001	0.00	0.27	-2.52	-0.56
1.50	T	1.00	2000	0.001	0.01	0.83	-1.91	-0.08
1.50	T	1.00	50	0.001	*	0.00	*	-2.81
1.50	T	2.00	1000	0.001	0.01	0.15	-2.22	-0.82
1.50	T	2.00	2000	0.001	0.02	0.33	-1.80	-0.48
1.50	T	2.00	50	0.001	*	0.00	*	-2.79
1.50	T	4.00	1000	0.001	0.01	0.23	-2.22	-0.64
1.50	T	4.00	2000	0.001	3.02	1.74	0.48	0.24

Q_{sed}	F	G_{bed}	q	S	Scour RMSE	Deposition RMSE	\log_{10} Scour RMSE	\log_{10} Deposition RMSE
1.50	T	4.00	50	0.001	*	0.00	*	-2.48
1.50	T	8.00	1000	0.001	0.01	0.79	-2.22	-0.10
1.50	T	8.00	2000	0.001	0.02	3.22	-1.82	0.51
1.50	T	8.00	50	0.001	*	0.00	*	-2.52
1.50	Y	0.50	1000	0.001	0.35	0.08	-0.45	-1.10
1.50	Y	0.50	2000	0.001	0.51	0.20	-0.29	-0.70
1.50	Y	0.50	50	0.001	0.01	0.00	-2.09	-2.52
1.50	Y	1.00	1000	0.001	*	0.07	*	-1.15
1.50	Y	1.00	2000	0.001	0.01	0.09	-2.20	-1.04
1.50	Y	1.00	50	0.001	*	0.00	*	-2.42
1.50	Y	2.00	1000	0.001	0.00	0.09	-2.52	-1.05
1.50	Y	2.00	2000	0.001	0.01	0.13	-2.03	-0.90
1.50	Y	2.00	50	0.001	*	0.00	*	-2.59
1.50	Y	4.00	1000	0.001	0.00	0.08	-2.52	-1.09
1.50	Y	4.00	2000	0.001	0.01	0.14	-2.03	-0.86
1.50	Y	4.00	50	0.001	*	0.00	*	-2.58
1.50	Y	8.00	1000	0.001	0.01	0.09	-2.22	-1.03
1.50	Y	8.00	2000	0.001	0.02	0.53	-1.82	-0.27
1.50	Y	8.00	50	0.001	*	0.00	*	-2.56
1.50	EH	0.50	1000	0.01	4.38	13.40	0.64	1.13
1.50	EH	0.50	2000	0.01	2.71	19.91	0.43	1.30
1.50	EH	0.50	50	0.01	0.22	0.08	-0.67	-1.12
1.50	EH	1.00	1000	0.01	0.20	0.40	-0.70	-0.40
1.50	EH	1.00	2000	0.01	6.10	5.56	0.79	0.74
1.50	EH	1.00	50	0.01	0.01	0.13	-1.89	-0.88
1.50	EH	2.00	1000	0.01	0.18	0.76	-0.75	-0.12
1.50	EH	2.00	2000	0.01	1.77	12.22	0.25	1.09
1.50	EH	2.00	50	0.01	0.01	0.22	-2.10	-0.66
1.50	EH	4.00	1000	0.01	0.19	8.78	-0.73	0.94
1.50	EH	4.00	2000	0.01	2.83	*	0.45	*
1.50	EH	4.00	50	0.01	0.01	0.29	-2.04	-0.54
1.50	EH	8.00	1000	0.01	2.81	6.11	0.45	0.79
1.50	EH	8.00	2000	0.01	0.41	18.63	-0.38	1.27
1.50	EH	8.00	50	0.01	0.01	0.53	-2.19	-0.27
1.50	T	0.50	1000	0.01	0.91	14.45	-0.04	1.16
1.50	T	0.50	2000	0.01	3.76	14.85	0.58	1.17
1.50	T	0.50	50	0.01	0.51	0.10	-0.29	-1.00
1.50	T	1.00	1000	0.01	6.79	15.43	0.83	1.19

Q_{sed}	F	G_{bed}	q	S	Scour RMSE	Deposition RMSE	\log_{10} Scour RMSE	\log_{10} Deposition RMSE
1.50	T	1.00	2000	0.01	4.09	4.42	0.61	0.64
1.50	T	1.00	50	0.01	0.02	0.18	-1.78	-0.75
1.50	T	2.00	1000	0.01	2.52	11.69	0.40	1.07
1.50	T	2.00	2000	0.01	2.62	2.00	0.42	0.30
1.50	T	2.00	50	0.01	0.01	0.23	-2.21	-0.63
1.50	T	4.00	1000	0.01	2.65	10.94	0.42	1.04
1.50	T	4.00	2000	0.01	2.62	2.21	0.42	0.34
1.50	T	4.00	50	0.01	0.01	0.34	-2.26	-0.47
1.50	T	8.00	1000	0.01	0.29	10.12	-0.54	1.01
1.50	T	8.00	2000	0.01	1.40	3.07	0.14	0.49
1.50	T	8.00	50	0.01	0.00	0.22	-2.52	-0.66
1.50	Y	0.50	1000	0.01	3.93	1.94	0.59	0.29
1.50	Y	0.50	2000	0.01	6.66	15.00	0.82	1.18
1.50	Y	0.50	50	0.01	0.24	0.09	-0.62	-1.05
1.50	Y	1.00	1000	0.01	0.18	2.75	-0.76	0.44
1.50	Y	1.00	2000	0.01	3.28	*	0.52	*
1.50	Y	1.00	50	0.01	0.01	0.07	-1.89	-1.15
1.50	Y	2.00	1000	0.01	1.36	4.61	0.13	0.66
1.50	Y	2.00	2000	0.01	2.83	6.01	0.45	0.78
1.50	Y	2.00	50	0.01	0.01	0.21	-2.13	-0.67
1.50	Y	4.00	1000	0.01	2.01	7.39	0.30	0.87
1.50	Y	4.00	2000	0.01	1.44	17.67	0.16	1.25
1.50	Y	4.00	50	0.01	0.01	0.50	-2.16	-0.30
1.50	Y	8.00	1000	0.01	0.25	6.94	-0.61	0.84
1.50	Y	8.00	2000	0.01	0.56	3.79	-0.25	0.58
1.50	Y	8.00	50	0.01	0.00	0.43	-2.47	-0.36

Table F-2 Zero scour test case runs removed from the analysis

Sediment Loading Case	Transport Function	Bed Sediment Gradation Case	Flow (cfs)	Slope (ft/ft)
0.5Qs	EH	8G	1000	0.0005
0.5Qs	EH	8G	2000	0.0005
0.5Qs	T	0.5G	50	0.0005
0.5Qs	T	1G	1000	0.0005
0.5Qs	T	1G	2000	0.0005
0.5Qs	T	1G	50	0.0005
0.5Qs	T	2G	1000	0.0005
0.5Qs	T	2G	2000	0.0005
0.5Qs	T	2G	50	0.0005
0.5Qs	T	4G	50	0.0005
0.5Qs	T	8G	1000	0.0005
0.5Qs	T	8G	50	0.0005
0.5Qs	Y	1G	50	0.0005
0.5Qs	Y	2G	50	0.0005
0.5Qs	Y	4G	50	0.0005
0.5Qs	Y	8G	1000	0.0005
0.5Qs	Y	8G	2000	0.0005
0.5Qs	Y	8G	50	0.0005
0.5Qs	EH	8G	1000	0.001
0.5Qs	EH	8G	50	0.001
0.5Qs	T	0.5G	50	0.001
0.5Qs	T	1G	1000	0.001
0.5Qs	T	1G	50	0.001
0.5Qs	T	2G	50	0.001
0.5Qs	T	4G	50	0.001
0.5Qs	T	8G	50	0.001
0.5Qs	Y	2G	50	0.001
0.5Qs	Y	4G	50	0.001
0.5Qs	Y	8G	50	0.001
1.0Qs	EH	2G	1000	0.0005
1.0Qs	EH	2G	2000	0.0005
1.0Qs	EH	2G	50	0.0005
1.0Qs	EH	4G	1000	0.0005
1.0Qs	EH	4G	2000	0.0005
1.0Qs	EH	4G	50	0.0005
1.0Qs	EH	8G	1000	0.0005
1.0Qs	EH	8G	50	0.0005

1.0Qs	T	0.5G	50	0.0005
1.0Qs	T	1G	1000	0.0005
1.0Qs	T	1G	50	0.0005

Table F-2 Zero scour test case runs removed from the analysis (cont'd)

Sediment Loading Case	Transport Function	Bed Sediment Gradation Case	Flow (cfs)	Slope (ft/ft)
1.0Qs	T	2G	1000	0.0005
1.0Qs	T	2G	50	0.0005
1.0Qs	T	4G	50	0.0005
1.0Qs	T	8G	1000	0.0005
1.0Qs	T	8G	50	0.0005
1.0Qs	Y	0.5G	50	0.0005
1.0Qs	Y	1G	50	0.0005
1.0Qs	Y	2G	1000	0.0005
1.0Qs	Y	2G	2000	0.0005
1.0Qs	Y	2G	50	0.0005
1.0Qs	Y	4G	1000	0.0005
1.0Qs	Y	4G	2000	0.0005
1.0Qs	Y	4G	50	0.0005
1.0Qs	Y	8G	1000	0.0005
1.0Qs	Y	8G	50	0.0005
1.0Qs	EH	2G	1000	0.001
1.0Qs	EH	4G	50	0.001
1.0Qs	EH	8G	50	0.001
1.0Qs	T	0.5G	50	0.001
1.0Qs	T	1G	50	0.001
1.0Qs	T	2G	50	0.001
1.0Qs	T	4G	50	0.001
1.0Qs	T	8G	50	0.001
1.0Qs	Y	1G	50	0.001
1.0Qs	Y	2G	1000	0.001
1.0Qs	Y	2G	50	0.001
1.0Qs	Y	4G	1000	0.001
1.0Qs	Y	4G	50	0.001
1.0Qs	Y	8G	50	0.001
1.5Qs	EH	2G	1000	0.0005
1.5Qs	EH	2G	50	0.0005
1.5Qs	EH	4G	1000	0.0005
1.5Qs	EH	4G	50	0.0005
1.5Qs	EH	8G	1000	0.0005

1.5Qs	EH	8G	50	0.0005
1.5Qs	T	0.5G	50	0.0005
1.5Qs	T	1G	1000	0.0005
1.5Qs	T	1G	50	0.0005
1.5Qs	T	2G	50	0.0005
1.5Qs	T	4G	50	0.0005

Table F-2 Zero scour test case runs removed from the analysis (cont'd)

Sediment Loading Case	Transport Function	Bed Sediment Gradation Case	Flow (cfs)	Slope (ft/ft)
1.5Qs	T	8G	50	0.0005
1.5Qs	Y	0.5G	50	0.0005
1.5Qs	Y	1G	1000	0.0005
1.5Qs	Y	1G	2000	0.0005
1.5Qs	Y	1G	50	0.0005
1.5Qs	Y	2G	1000	0.0005
1.5Qs	Y	2G	50	0.0005
1.5Qs	Y	4G	1000	0.0005
1.5Qs	Y	4G	50	0.0005
1.5Qs	Y	8G	50	0.0005
1.5Qs	EH	2G	50	0.001
1.5Qs	EH	4G	50	0.001
1.5Qs	EH	8G	50	0.001
1.5Qs	T	0.5G	50	0.001
1.5Qs	T	1G	50	0.001
1.5Qs	T	2G	50	0.001
1.5Qs	T	4G	50	0.001
1.5Qs	T	8G	50	0.001
1.5Qs	Y	1G	1000	0.001
1.5Qs	Y	1G	50	0.001
1.5Qs	Y	2G	50	0.001
1.5Qs	Y	4G	50	0.001
1.5Qs	Y	8G	50	0.001

Table F-3 Zero deposition test case runs removed from the analysis

Sediment Loading Case	Transport Function	Bed Sediment Gradation Case	Flow (cfs)	Slope (ft/ft)
1.5Qs	EH	1G	50	0.0005
0.5Qs	Y	0.5G	50	0.0005
0.5Qs	EH	4G	50	0.0005
0.5Qs	EH	2G	50	0.0005
1.0Qs	EH	1G	50	0.0005
0.5Qs	EH	1G	50	0.0005
1.5Qs	EH	0.5G	50	0.0005
0.5Qs	EH	8G	50	0.0005
0.5Qs	EH	0.5G	50	0.0005
1.0Qs	EH	0.5G	50	0.0005
0.5Qs	Y	1G	50	0.0005
1.0Qs	EH	2G	50	0.0005
0.5Qs	EH	4G	1000	0.0005
1.0Qs	EH	1G	1000	0.0005
1.5Qs	EH	1G	1000	0.0005
0.5Qs	EH	2G	1000	0.0005
1.5Qs	EH	1G	1000	0.001
0.5Qs	EH	4G	1000	0.001
0.5Qs	EH	2G	1000	0.001
0.5Qs	EH	1G	1000	0.0005
0.5Qs	Y	4G	1000	0.0005
0.5Qs	Y	1G	1000	0.0005
0.5Qs	Y	2G	1000	0.0005
0.5Qs	Y	4G	1000	0.001
0.5Qs	Y	2G	1000	0.001
0.5Qs	EH	4G	2000	0.001
1.0Qs	Y	1G	2000	0.001
1.0Qs	EH	8G	2000	0.01
1.0Qs	Y	2G	2000	0.01
1.5Qs	EH	4G	2000	0.01
1.5Qs	Y	1G	2000	0.01

**Appendix G: FCDMC Final Review
Comment Technical Memorandum**



Flood Control District

of Maricopa County

MEMORANDUM

Date: August 23, 2011

To: Brian Wahlin, Ph.D., P.E., D.WRE, WEST Consultants, Inc.

From: Richard Waskowsky, P.E., Hydrologist, Flood Control District of Maricopa County

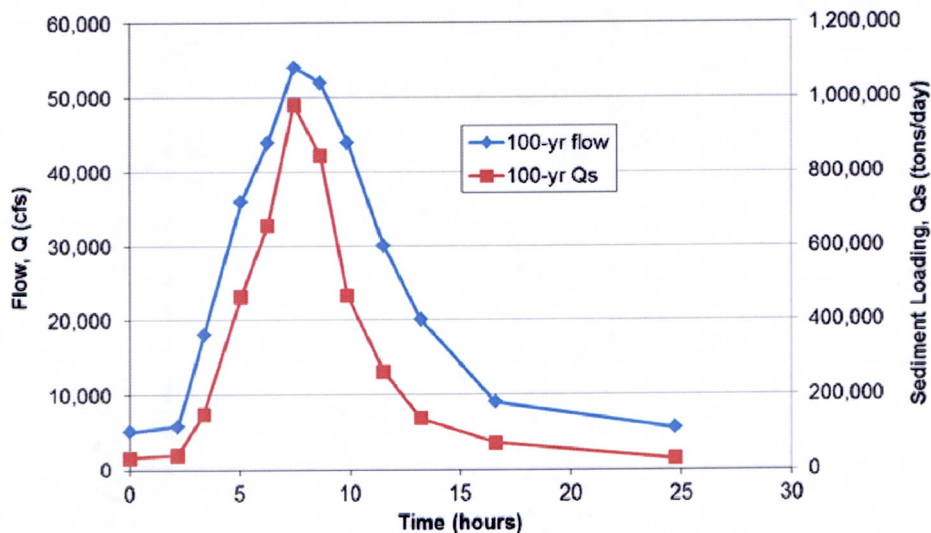
CC: Bing Zhao, Ph.D., P.E., Engineering Application Development and River Mechanics Branch Manager, Flood Control District of Maricopa County

Subject: Sediment Transport Model Comparison Draft Report prepared by WEST Consultants, Inc.

The Engineering Application Development and River Mechanics (EADRM) Branch received the revised report on August 4, 2011. The EADRM Branch has finished its review and has the following comments. The consultant should submit written responses (with digital copy) to these comments to the FCDMC. The comments that have been resolved have been shown in a gray font.

- 1) **FCD Comment (June 27, 2011):** In Table 2-4, the sediment load for 5500 cfs is 29661 tons/day. However, since the 100-year Agua Fria hydrograph has been expanded to cover 12 days, will this additional load affect the results? Should the load for the samples around 5500 cfs (in Table 2-4) be lowered to minimize any possible errors from the additional days of the Agua Fria hydrograph?

WEST Response (July 15, 2011): This loading was taken from the output of the Kimley-Horn HEC-6T sediment transport analysis at the end of a 100-year hydrograph. When analyzing a 100-year hydrograph for sediment conditions, hysteresis effects are commonly seen in the sediment loading conditions as the District pointed out. However, in the case of the Agua Fria hydrograph, the rising and falling limbs of the flow hydrograph correspond closely to the rising and falling limbs of the sediment loading discharge (as shown in the figure below). Kimley-Horn ran an initial 30-day constant flow simulation in their HEC-6T model before entering the 100-year hydrograph to approximate a steady-state sediment condition prior to the 100-year flow event. As can be seen from the figure below, the steady-state sediment loading at the beginning of the hydrograph (corresponding to a $Q = 5000$ cfs) is approximately the same as the loading at the end of the hydrograph (corresponding to a $Q = 5500$ cfs). Therefore, WEST assumed the 29,000 tons/day also approximated an equilibrium loading condition which should represent the physical processes of what the "base sediment loading" into the Gila should be.

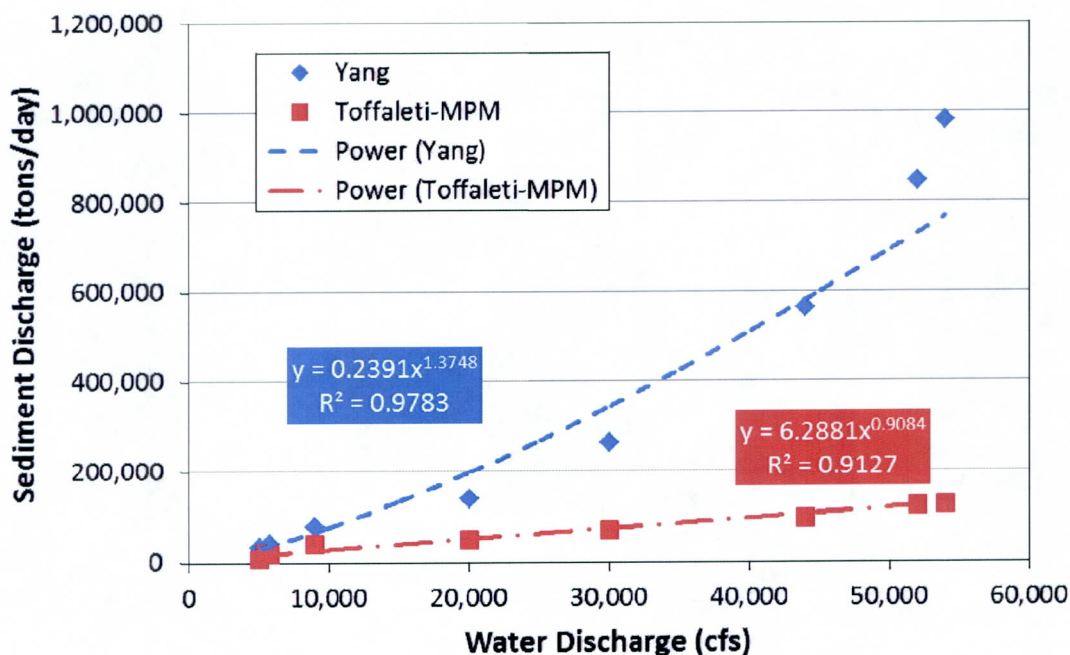


FCD Response (July 26, 2011): The District agrees with the above response. However, the original intent of the initial comment may have been misunderstood. Basically, the intent was to clarify that extending the Kimley-Horn 100-year hydrograph from 1 day to 12 days does not add an additional load that may skew the results. Even though the load is small for 5500 cfs, adding this load for 11 extra days does introduce a significant total load. If the load does skew the results, should the 5500 cfs (and 5100 cfs) sediment load be reduced since these flows only occur during the extra 11 days?

Additionally, it seems strange that the Agua Fria River provides more load at 54,000 cfs than the Salt River does at 200,000 cfs. Is this reasonable? Can the Agua Fria River load also be developed with the Toffaleti Meyer-Peter Muller equation?

WEST Response (August 4, 2011): Yes, this sediment loading can be reduced. However, this may introduce additional scour downstream of the confluence since the equilibrium loading from the Agua Fria will not be maintained for the duration of the hydrograph in the Gila River.

The Agua Fria model was developed, calibrated, and verified by Kimley-Horn with the chosen sediment transport equation. Changing the transport function solely would invalidate many of the model adjustments made by Kimley-Horn during their model development phase. That being said, the Kimley-Horn model was re-run using the Toffaleti-MPM equation as requested by the District. The rating curve developed for the outflowing sediment load from the Agua Fria River for the Toffaleti-MPM run was compared to the outflowing sediment load rating curve for the original model run with Yang's curve. The comparison of the outflowing sediment load rating curves from these two model runs can be seen in the figure below.



For the Yang sediment transport function, the loading from the Agua Fria River at the peak flow of 54,000 cfs is 981,454 tons/day. For the Toffaleti-MPM function, the loading from the Agua Fria River at the peak flow of 54,000 cfs is 123,917 tons/day. The Toffaleti-MPM results are approximately one order of magnitude lower than the results from the Yang model. This value seems reasonable, and further inspection of the model indicates numerical stability throughout the length of the study reach.

Based on these findings, re-running the Gila River model with this updated sediment inflow from the Agua Fria River does seem like a useful task. A future study could re-run each of the Gila River sediment transport models with this updated inflowing sediment load rating curve to investigate the results of this reduced load on the formation of pseudo-dams in the model (see the District's comment #12 below for more information on these pseudo-dams). However, to re-run each of the models developed for the Gila River in this study with an updated sediment load would only address one of the many pseudo-dams occurring in the models, and this task fell beyond the scope of the current study.

FCD Response (August 10, 2011): The above results for the sediment loading from the Agua Fria River do seem to indicate that the inflowing load should be revised for the current models. Since these revisions are beyond the scope of the current study, it is recommended that the final comment memorandum be included in the final report as an appendix in order to include this data in the report.

WEST Response (August 16, 2011): The final comment memorandum has been included in the final report as an appendix in order to include this discussion directly into the report.

- 2) **FCD Comment (June 27, 2011):** In the comparison of the Yang equation between models (Tables 3-2 and 3-3, Figures 3-2 and 3-5), a note should be added that highlights the fact the HEC-6T results do not use the 1984 Yang equation for gravels.

WEST Response (July 15, 2011): A note referencing the fact that 6T does not include the 1984 Yang equation for gravels has been added to several tables throughout the report.

FCD Response (July 26, 2011): Notes have been added to better highlight that HEC-6T does not use the Yang equation for gravels. Comment resolved.

- 3) **FCD Comment (June 27, 2011):** For the final report, will the Conclusions section be expanded?

WEST Response (July 15, 2011): The Conclusions section has been expanded significantly in the updated document.

FCD Response (July 26, 2011): The Conclusions section has been expanded. However, could some recommendations, which indicate how best to use the results, conclusions and the report in general, also be provided in the report?

WEST Response (August 4, 2011): WEST has added recommendations to the report based on our findings. However, these recommendations should be read in light of the limited number of test runs and sediment transport equations tested in this analysis. Any recommendations regarding a particular sediment transport model over another should consider that other transport functions or models applied to systems with differing dominant physical processes could be modeled more accurately using a sediment transport function or model not recommended herein.

FCD Response (August 10, 2011): Recommendations have been added to the report. However, could the phrase, "Based on the current results for the Gila River" (or something similar), be added at the beginning of the third recommendation in Section 4.2?

WEST Response (August 16, 2011): This comment is very similar to Dr. Bing Zhao's comment in email format to Dr. Brian Wahlin dated August 10, 2011. This comment has been reproduced below.

One revision would be to emphasize that the conclusions and recommendations are made only based on Gila River study. I noticed that conclusions and recommendations seem to be made for all rivers in Maricopa County. One particular discussion was about using HEC-RAS for sand and gravel permitting. It seems to me that the recommendations should be only limited to Gila River. For other rivers, we do not know. We may guess it is okay but we cannot make that kind of generalization. Another consultant working on a different river found out that

HEC-RAS should not be used for sand and gravel. I am not saying that consultant is correct. My suggestion is to make conclusions based on the rivers that were used.

Based on these comments, the conclusions and recommendations sections have been edited to ensure that overgeneralizations were not stated in the conclusions for all rivers in Maricopa County, and that it was emphasized that these conclusions and recommendations should be limited to the Lower Gila River System. Specifically, this discussion was added to the third recommendation in Section 4.2.

- 4) **FCD Comment (June 27, 2011):** On page 3-1 and the pages for Appendix B, an incorrect footer is shown.

WEST Response (July 15, 2011): Footers have been corrected in the updated document.

FCD Response (July 26, 2011): The incorrect footers have been removed. Comment resolved.

- 5) **FCD Comment (June 27, 2011):** On page ii, some figures do not have a page number.

WEST Response (July 15, 2011): Page numbers have been added to all figures in the TOC.

FCD Response (July 26, 2011): Page numbers have been added. However, the tables in Appendix F are not listed in the List of Tables, and these tables do not have a table number. Please make sure all tables are listed in the List of Tables and have numbers associated with them.

WEST Response (August 4, 2011): WEST has labeled these tables, added these tables to the master List of Tables, and updated all references in the text referring to these tables based on the updated naming convention.

FCD Response (August 10, 2011): The tables in Appendix F have been labeled and added to the List of Tables. Comment resolved.

- 6) **FCD Comment (June 27, 2011):** On page 4 of Appendix A, 98.33 should be 198.33.

WEST Response (July 15, 2011): This was changed to 198.33 in the updated document.

FCD Response (July 26, 2011): The number has been corrected. Comment resolved.

- 7) **FCD Comment (June 27, 2011):** In the third paragraph on page 2-1, form should be from.

WEST Response (July 15, 2011): This was changed to “from” in the updated document.

FCD Response (July 26, 2011): This has been corrected. Comment resolved.

- 8) **FCD Comment (July 26, 2011):** In Appendices C, D and E, the figures all show initial and final water surface elevations. Which model produced the elevations for those figures that have results for multiple models? The initial water surface should be very similar for all models, but the final water surface should be different since the final thalwegs are different. Please indicate which model produced the water surface elevations for these figures.

WEST Response (August 4, 2011): The water surface profile produced by HEC-RAS was used in the final figures comparing a single sediment transport function across various sediment transport models in the appendices. WEST chose to include this water surface elevation profile in the final figures because of the District’s preference for HEC-RAS as the preferred modeling tool for hydraulic studies and because of the general acceptance of HEC-RAS in the industry as trusted hydraulic modeling software. Additionally, although the hydraulic calculations drive the sediment transport computations, it was assumed in this study that the hydraulics would have been calculated similarly by each model, and the variance in hydraulic calculations was not included in the final statistical analysis of modeling results. Finally, additional water surface profiles would have added too many lines to the already-busy figures.

WEST added footnotes to these figures indicating that the water surface profiles shown in the figures comparing the same sediment transport function calculated using various sediment transport models were computed in HEC-RAS. Footnotes were also added to figures comparing the results of a single sediment transport model for multiple sediment transport functions (e.g., Yang, Toffaleti, and Engelund Hansen in HEC-6T) stating that the water surface elevations shown in these figures were computed by the sediment transport model for that figure.

FCD Response (August 10, 2011): Footnotes that indicate the source of the water surface elevation have been added to the figures. Comment resolved.

- 9) **FCD Comment (July 26, 2011):** From Bullard Avenue to El Mirage Road, the 2008 topography is available. However, on page 2-2, it is indicated that the topography from the Tres Rios model is representative of existing conditions, and the Tres Rios topography was used. On page 2-2, could some documentation that verifies this assumption be added to the report?

WEST Response (August 4, 2011): This comment was not supported well in the text of the document. WEST would like to thank the reviewer for pointing out this inconsistency. Based on WEST’s knowledge of the Tres Rios model from recent work

that WEST is performing for the District on a LOMR being completed to update the FEMA FIRM panels to remove the floodplain areas behind the Tres Rios North Levee, WEST is aware that the topography from the 2008 Gillespie topography is not significantly different from the topography that was used in the development of the Tres Rios HEC-6T model in 2004. Additionally, updating the topography in this area with the Gillespie topography would have required significant additional effort to verify the use of ineffective flow areas, moveable bed limits, bank stations, and levee alignments from the original Tres Rios HEC-6T model. WEST felt that this task fell beyond the scope of the current study. As long as the geometry was represented identically in the HEC-6T, HEC-RAS, and SRH-1D geometries, WEST felt that a reasonable comparison could be made between the models.

WEST added more supporting documentation to this portion of the text supporting this decision. Specifically, this sentence appeared in the original text: *“These data were considered to be representative of existing conditions and the geometry for these cross sections was not updated.”* This sentence was changed to the following in the final text:

“Since the Tres Rios Levee PED HEC-6T model was a fully calibrated sediment transport model that had previously verified many parameters of numerical modeling associated with model geometry through sensitivity analysis such as moveable bed limits, ineffective flow areas, and bank stations, the geometry of this model overlapping the Gillespie topography was not updated based on the newer topographic information. Additionally, a brief comparison of the topography in the overlapping region indicated that the 2008 topography was slightly lower than the original 2001 topography, but the cross sectional geometries would not have reflected significant differences. A future effort could include verification of the sediment transport model by comparing the results of the Tres Rios Levee PED model run with the 2008 topography as a validation and verification modeling effort.”

FCD Response (August 10, 2011): The text has been revised to include the supporting documentation. Comment resolved.

10) FCD Comment (July 26, 2011): A figure that shows the general locations of the ultimate gravel pits may be useful.

WEST Response (August 4, 2011): WEST has added an additional figure to the document, Figure 2-2, showing the general location of the sand and gravel pits.

FCD Response (August 10, 2011): A figure has been added. Comment resolved.

11) **FCD Comment (July 26, 2011):** Based on other plan sheets and permit stipulations, the pit contours for SG08-004 are shown in NAVD88.

WEST Response (August 4, 2011): WEST has updated the text of the final report to reflect that the pit contours for SG08-004 are shown in NAVD88.

FCD Response (August 10, 2011): The text has been revised. Comment resolved.

12) **FCD Comment (July 26, 2011):** In the profile plots in the appendices, there are multiple locations where sediment deposition produces a pseudo-dam. This scenario does not seem realistic and gives indicators that the model may be unreliable. Please add some discussion to the report about these areas, why they could be occurring and if any model should be precluded based on these results.

WEST Response (August 4, 2011): Based on the scope of work provided for this document, the comparison of the model results based on the exact same input was the ultimate goal of this task order. Therefore, WEST felt that significant levels of effort for model calibration and verification to avoid unrealistic model results were not warranted as this would change the input files as a function of the computer model being used.

To begin the discussion of pseudo-dams, WEST would like to define what a pseudo-dam is in reference to this study and the figures in Appendices C, D, and E. For the purposes of this discussion, pseudo-dams will only be defined based on the final thalweg elevation plots.

These pseudo-dams as defined above occurred at four primary locations in the study reach for the various models. First, a pseudo-dam formed at RS 196.08 (with less but still significant amounts of deposition occurring at the downstream cross section 195.98) for the HEC-RAS comparison models using the Yang function and the Toffaleti function. In the thalweg elevation profile plots from the HEC-6T model runs, it can be seen that pseudo-dams are formed at RS 195 and at the downstream end of the comparison model (approximately RS 179) for the Engelund Hansen function.

For the base conditions (i.e., with bridge) model runs, HEC-RAS showed a pseudo-dam at RS 196.08 based on the thalweg elevation profile plot. This is the same location where a pseudo-dam occurred for the Yang function for the HEC-RAS base condition models. However, another pseudo-dam appears to be forming at RS 180 in HEC-RAS. No pseudo-dams occur in HEC-6T model runs for the base model. It should be noted that the base conditions models only utilized Yang's function for sediment transport.

Finally, for the ultimate pit runs, HEC-6T showed a pseudo-dam at one cross section upstream of pit SG08-004 (RS 197.14). Also, the HEC-RAS final thalweg elevation profile showed another apparent pseudo-dam near RS 180. Again, the ultimate pit conditions models only utilized Yang's function for sediment transport.

The Agua Fria inflowing sediment point load enters the model at RS 196.08 in the HEC-RAS model. One of the primary pseudo-dam locations occurs at this site in HEC-RAS for the Yang and Toffaleti functions in the comparison model without bridges. However, a similar pseudo-dam does not occur within the model runs for HEC-6T or SRH-1D. This discrepancy could be due to the methodology employed by the various models to handle lateral sediment inflows. HEC-RAS allows the user to enter either a lateral sediment inflow at a point or a uniformly distributed lateral sediment inflow over a number of cross sections. HEC-6T only allows a lateral sediment inflow to be entered at a point between two cross sections. It could be that the original methodology in HEC-6T averaged the lateral sediment inflow over the two cross sections between which the lateral sediment inflow was entered. Since HEC-RAS has an option to have a uniformly distributed lateral inflow, this methodology may reflect the original HEC-6T methodology more directly, and the point inflow in HEC-RAS may be a different methodology that introduces the entire sediment load at a single cross section. This could possibly explain the large depositional feature at RS 196.08, the location of the point lateral inflow for the HEC-RAS model, for the Yang and Toffaleti functions. Unfortunately, the exact numerical techniques used to code these methodologies into the various models are not documented in the user's manuals directly. Therefore, this is only a hypothesis. However, the fact that the pseudo-dam is occurring immediately at the cross section of the lateral sediment inflow from the Agua Fria River implies that the formation of this pseudo-dam has to do with the inflowing sediment load and not a physical phenomenon occurring in the river system.

The pseudo-dams occurring in the comparison model for HEC-6T using the Engelund Hansen function near RS 179 appear to be due to numerical instabilities in the model. This area has several significant variations in scour and deposition from one cross section to the next, which creates an apparent zigzag pattern in the thalweg elevation profile plot. This is often attributed to numerical instabilities in one-dimensional sediment transport modeling, and this erroneous result is often combated by decreasing computational time steps or increasing cross sectional spacing in the model. Additionally, a model that creates numerical instabilities in the sediment calculations and develops a zigzag pattern in thalweg elevations near the downstream boundary condition for the hydraulic calculations will ultimately create significant instabilities throughout the study reach, especially when the downstream boundary condition is specified as a known water surface elevation as was the case for the models herein. Therefore, the pseudo-dam at RS 195 in this model should be ignored as a product of numerical instabilities elsewhere in the model. The reason for these instabilities is unclear. Based on discussion with the developer of HEC-6T, the Engelund Hansen equation was not implemented fully in the version of HEC-6T utilized herein, and the most recent version of HEC-6T seemed to have a bug associated with the Engelund Hansen function. Therefore, WEST is assuming that the continued development and improvement of the implementation of the Engelund Hansen function in HEC-6T would possibly remove this pseudo-dam issue from this run.

The pseudo-dam that occurs in the base conditions model for HEC-RAS near RS 180 is due to the bridge structure at RS 180.025 (bridge over Arizona State Route 85). This bridge is creating a backwater effect that allows sediment to drop out of the water column

upstream of this bridge, thereby creating a slight pseudo-dam in the modeling output. However, it should be noted that this pseudo-dam is smaller than the others discussed herein and could be an accurate representation of the physical processes controlling sediment flow through this bridge structure. The decrease in bed slope near the downstream end of the model coupled with the additional losses associated with the bridge in the model with the most piers (21, see Table 2-1 in the report) and the highest gross pier width (189 feet) would provide significant backwater which creates a depositional situation in a riverine system.

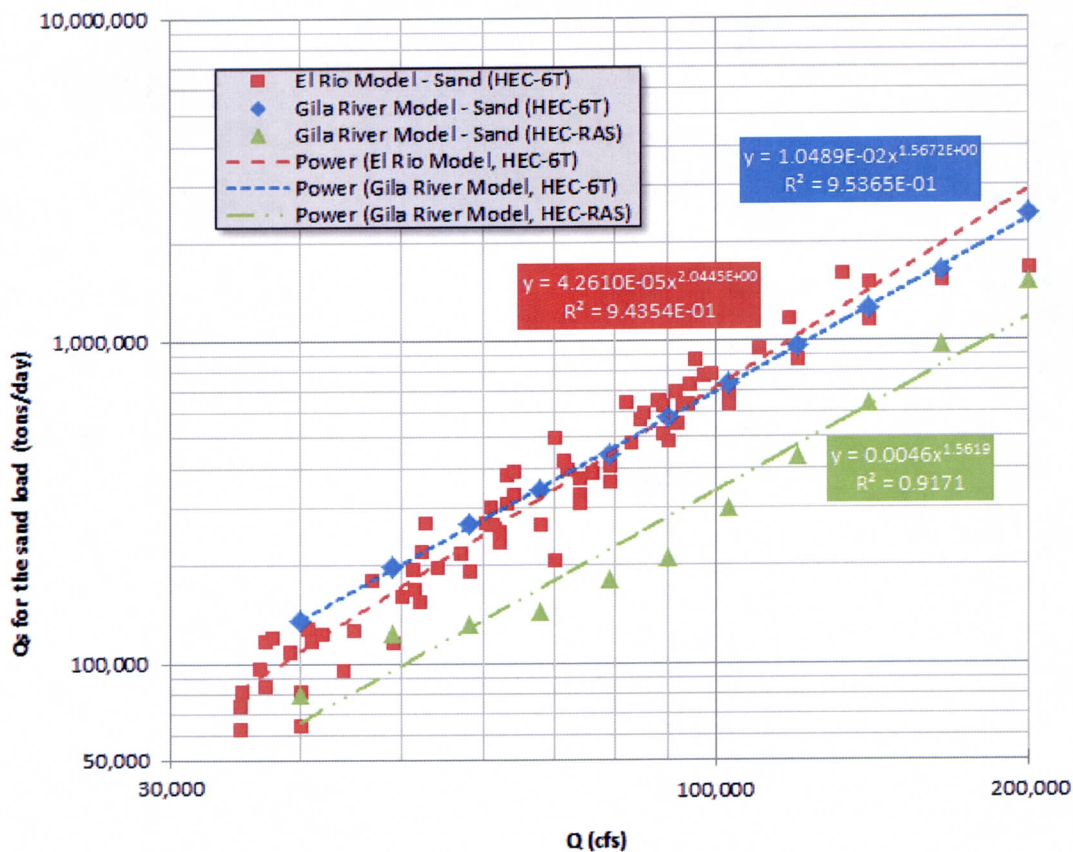
Finally, the pseudo-dam occurring in HEC-6T upstream of the gravel pit in the ultimate gravel pit run is likely the result of a numerical instability associated with the shock of such a drastic change in cross sectional area from the cross section upstream of the pit to the fully developed pit cross section. In a complete model calibration, WEST would consider tweaking the weighting factors for numerical integration on the I4 record as a mechanism to fine-tune the numerical stability in this location.

Although possible reasons that the pseudo-dams have formed are presented above, a more applicable question for typical sediment transport applications is whether or not the pseudo-dams should be removed from the modeling results. Obviously, if a sediment transport modeling study is intended to be used for the design of a project along a small portion of the study reach, and a pseudo-dam that appears to be entirely physically impossible occurs at the location of the project, model adjustment should be conducted until this numerical instability is removed from the modeling results. More generally, though, these phenomena in the modeling results may be local effects of the numerical sediment transport calculations that do not affect the global results of the sediment transport model significantly. For example, the outflowing sediment load from the downstream most cross section of the comparison model (i.e., not including bridges in the model) from this study using the Yang transport function in HEC-RAS (which had pseudo-dams) and in HEC-6T (which did not have pseudo-dams) were compared to the results of the El Rio model study (which also used the Yang function). Based on the Outflowing Sand Load Comparison figure below, the outflowing sand load trend lines for the HEC-6T from this study and the El Rio HEC-6T models are very similar even though they have different inflowing sediment loads. However, the HEC-RAS trend line is lower than other two. For high flows such as 200,000 cfs, the HEC-RAS and El Rio HEC-6T have similar results. The differences in the outflowing sand load could be due to different modeling assumptions and topographic data. The HEC-RAS and HEC-6T models in this study are based on the latest topographic data while the El Rio HEC-6T model is based on topographic data collected in the early 1990's. The inflowing sediment load for the El Rio HEC-6T model is based on measured data at the downstream USGS gage because the study reach was considered to be at an equilibrium condition. The inflowing sediment load in this study (for both HEC-6T and HEC-RAS) is not based on measured sediment data. Instead, it is based on the outflowing sediment load from previous studies at the upstream reach and tributaries. However, for the purposes of model comparison, this approach is sufficient because the same inflowing sediment loads are used for both the HEC-6T and HEC-RAS models. For the purposes of estimating the outflowing sediment load, the El Rio HEC-6T model will probably provide more accurate results. Although

there is a difference in outflow sand load between HEC-RAS and HEC-6T in this study, the results can still be considered comparable from the practical point of view. However, further study may be needed to find out the cause of this difference.

One should keep in mind that the sediment loading at the downstream end of the El Rio model only represents the sand portion of the outflowing load from that study's HEC-6T modeling effort. The El Rio study considered cohesive sediment transport, which was not considered for this study using HEC-6T and HEC-RAS. Therefore, comparing total load from the El Rio study which would have included the cohesive fraction would not have been directly comparable to the results of the modeling runs for this study.

Outflowing Sand Load Comparison



FCD Response (August 10, 2011): In order to include this discussion in the report, it is recommended that the final comment memorandum be included in the final report as an appendix.

WEST Response (August 16, 2011): The final comment memorandum has been included in the final report as an appendix in order to include this discussion directly into the report.

13) **FCD Comment (July 26, 2011):** The note for Table 3-2 is unclear. Does the note mean that only the Yang equation was used to develop the sediment inflow?

WEST Response (August 4, 2011): The note for Table 3-2 was previously incorrect. This note has been rewritten as follows:

“Note that these inflowing sediment load rating curves were developed using the “equilibrium sediment load” boundary condition option in HEC-RAS. This option automatically calculates an equilibrium sediment load for the associated transport function. Differences in equilibrium load computation algorithms between HEC-RAS and the other sediment transport models were not considered.”

FCD Response (August 10, 2011): The note for Table 3-2 has been revised and clarified. Comment resolved.

14) **FCD Comment (July 26, 2011):** On page 3-5, the maximum deposition was actually 24,004 feet?

WEST Response (August 4, 2011): Yes, this number is reported correctly; over twenty thousand feet of deposition occurs at this cross section. HEC-6T did not have a limit for the maximum amount of deposition that could occur at a cross section. This would be the result of a numerical instability in the model, not a true solution of the physical processes occurring in the system reflected by the empirical development of the various sediment transport functions. The obvious physical impossibility of this occurrence was not considered in the HEC-6T output, and this is the reason for the unrealistic results. The text of the report in this area has been updated slightly to cast less doubt on the results of these models based on such unrealistic results. Additionally, this further highlights the need for engineering judgment and familiarity with the limitations and inherent problems (e.g., numerical instabilities creating unrealistic results or zigzag patterns in the profile elevations) with sediment transport modeling.

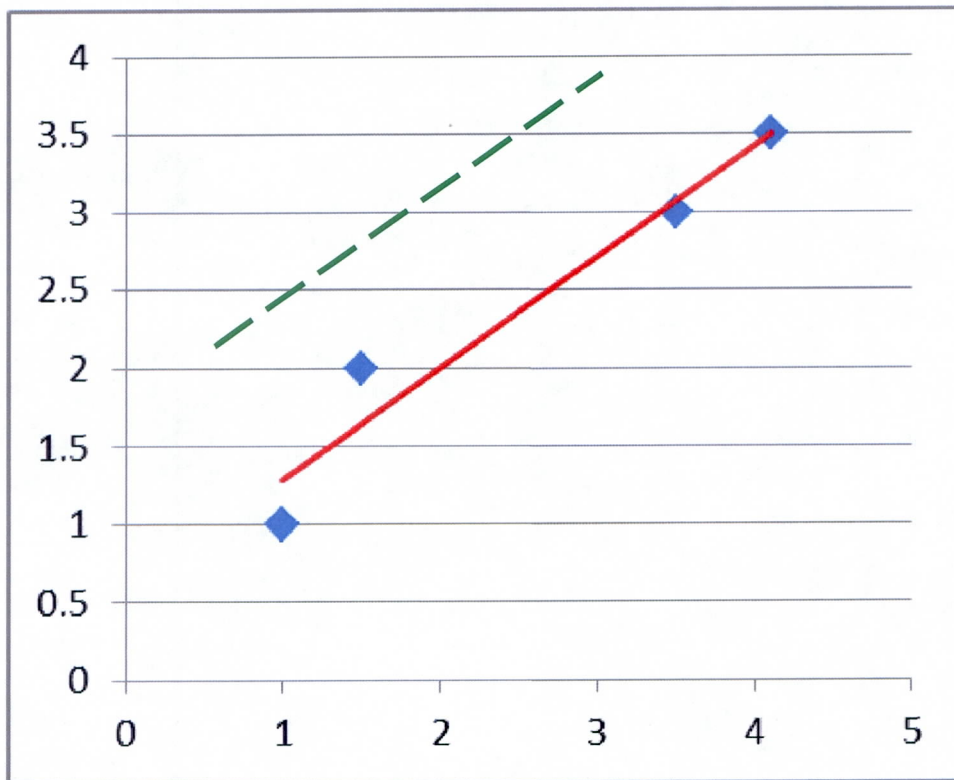
FCD Response (August 10, 2011): The text has been revised to clarify the 24,004 feet of deposition. However, the discussion in section 3.4 on page 3-6 is somewhat confusing. For example, in the third paragraph, it is indicated that HEC-6T did not encounter fatal errors; but in the previous paragraph, it is indicated that HEC-6T had the erroneous results of 24,004 feet. Thus, in some places it is unclear which model is being discussed. It is recommended that this section be modified to clearly indicate which model and its corresponding errors (or results) are being discussed.

WEST Response (August 16, 2011): WEST was not clear in our initial description of fatal errors. In this context, a fatal error is described as an error that causes the model to stop computing before the end of the prescribed simulation period. While HEC-6T did encounter highly unrealistic results, the model never ceased its computations before the end of the prescribed simulation period. In an attempt to clarify the differences in fatal errors and unrealistic results, the third paragraph of section 3.4 on page 3-6 has been rewritten as follows:

For the present applications, wherein deposits of less than 10 feet are expected, all model runs that produced depositions of 20 feet or more were considered highly unrealistic and erroneous, caused by model instabilities or other errors. Additionally, numerical instabilities can cause fatal errors in the calculations causing the model to crash. Unlike the HEC-RAS results, fatal errors were not encountered in HEC-6T (i.e., the model never ceased the sediment transport computations before the prescribed end of the simulation period). However, highly unrealistic results still occurred; for instance, 34 cross sections showed deposition of greater than 50 feet, 24 cross sections show deposition of greater than 100 feet, and 8 cross sections show deposition greater than 1,000 feet. All of these unrealistic results occurred in test case runs with the bed slope equal to 0.01 ft/ft.

15) FCD Comment (July 26, 2011): How were the Huybrechts enveloped determined. Were they determined from Figures 3-8 through 3-10? Were the data that is plotted on these figures taken from Table 3-1 of Huybrechts' dissertation?

WEST Response (August 4, 2011): The Huybrechts envelopes were determined by offsetting a best-fit regression line through the Huybrechts data (i.e., maintaining the same empirical regression coefficients, or maintaining the same slope as the regression line) to pass through the outlier or near-outlier point of the dataset. For example, in the figure below, the red line is the best fit linear regression of the data. The dotted green line is what would be termed the "envelope curve."



The data plotted on these figures was taken from Table 3-1 in the appendix of Huybrechts' dissertation.

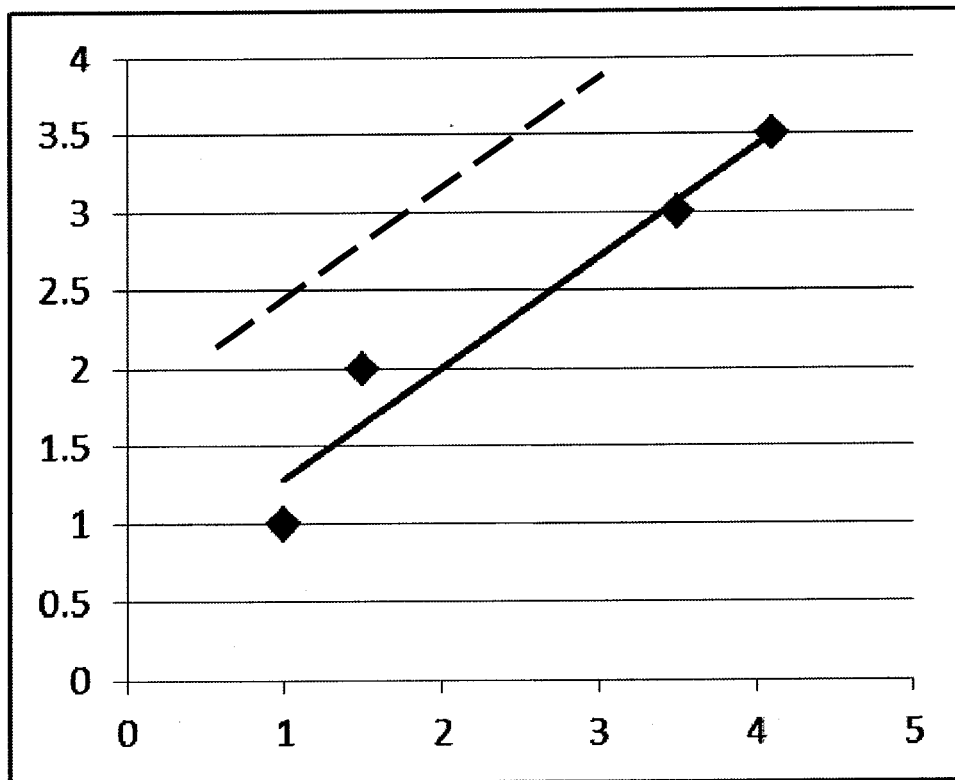
FCD Response (August 10, 2011): The development of Huybrechts envelope curves has been explained in the report. Comment resolved.

- 16) **FCD Comment (July 26, 2011):** If the model results fall between the Huybrechts envelopes, does this situation serve as an indicator of reasonable results? If so, please add more discussion that highlights this indicator to the report.

WEST Response (August 4, 2011): The overarching goal of the scatter plot comparisons of the test case data with the Huybrechts envelopes was to verify that the results were reasonable. WEST clarified this in the body of the text of the report.

FCD Response (August 10, 2011): The goal of the Huybrechts envelopes has been clarified. However, at the bottom of page 3-15, Huybrechts is misspelled.

WEST Response (August 16, 2011): This spelling error has been corrected in the final version of the report.



The data plotted on these figures was taken from Table 3-1 in the appendix of Huybrechts' dissertation.

FCD Response (August 10, 2011): The development of Huybrechts envelope curves has been explained in the report. Comment resolved.

- 16) **FCD Comment (July 26, 2011):** If the model results fall between the Huybrechts envelopes, does this situation serve as an indicator of reasonable results? If so, please add more discussion that highlights this indicator to the report.

WEST Response (August 4, 2011): The overarching goal of the scatter plot comparisons of the test case data with the Huybrechts envelopes was to verify that the results were reasonable. WEST clarified this in the body of the text of the report.

FCD Response (August 10, 2011): The goal of the Huybrechts envelopes has been clarified. However, at the bottom of page 3-15, Huybrechts is misspelled.

WEST Response (August 16, 2011): This spelling error has been corrected in the final version of the report.